Archean to recent komatiites and basalts

Igor S Puchtel[a] **and Nicholas T Arndt**[b], [a]Department of Geology, University of Maryland, College Park, MD, United States; [b]ISTerre, Maison des Géosciences, University of Grenoble, Grenoble, France

This chapter has been reviewed by the section editor Catherine Chauvel.

Abstract

Komatiites, the hottest known magmas, were abundant in the Archean and rare thereafter. They commonly erupted as lava flows with characteristic spinifex texture. Al-depleted komatiites with low Al_2O_3/TiO_2 and Gd/Yb formed at depths >300 km. Al-undepleted komatiites with near-chondritic Al_2O_3/TiO_2 and Gd/Yb formed at shallower depths via a fractional melting process. High MgO contents and high inferred potential temperatures indicate that both types formed in hot mantle plumes. Their isotopic compositions point to variably depleted mantle sources. Spatially associated komatiitic and tholeiitic basalts erupted in analogs of recent oceanic plateaus, while calc-alkaline basalts were generated at Archean convergent margins.

Keywords

Komatiites; Komatiitic basalts; Tholeiites; Calc-alkaline basalts; Oceanic plateaus; Mantle plumes; Spinifex texture; Trace elements; Isotope systematics

Key points:

- Komatiites are the hottest magmas on Earth. They formed in deep mantle plumes derived from variably depleted sources.
- Komatiites were common in the Archean and increasingly rare thereafter.
- Geochemical data point to komatiite generation at different mantle depths via different melting processes.
- Archean komatiitic and tholeiitic basalts erupted in oceanic plateaus, whereas calc-alkaline mafic to felsic lavas were generated at subduction settings.

Introduction

Archean magmas are different from modern magmas. Komatiites are thought to have erupted at temperatures several hundred degrees above those of common basalts, from sources that were far hotter than the modern mantle (Nisbet et al., 1993; Herzberg et al., 2007; Arndt et al., 2008). It is not clear, however, how the temperatures of komatiite sources relate to those of the ambient mantle. Certain petrological and chemical features of komatiites point to an origin deep in the mantle, with melting near the base of the transition zone of a source that rose from the core-mantle boundary. These rocks, therefore, provide a unique record of melting and physical conditions, as well as chemical compositions, of these, otherwise inaccessible, parts of the mantle.

Basalts are the most common type of mantle-derived rock, both during the Archean (e.g., De Wit and Ashwal, 1997; Condie, 1994) and at present. Some Archean basalts are spatially associated with komatiites and probably are genetically related to them, either by fractional crystallization or by derivation from a common source. Other Archean basalts share certain petrological and geochemical characteristics with modern oceanic plateau or subduction-related basalts, but whether they formed in similar tectonic settings is a subject of debate. Likewise, it is by no means clear whether the equivalents of modern mid-ocean ridge basalts are preserved in Archean terranes. The origin of komatiites and basalts and their tectonic settings are some of the issues that will be discussed in this chapter.

Komatiites

Definitions

Komatiites are defined as rocks with field relations and/or textures indicating a volcanic origin, and mineral and chemical compositions indicative of an ultramafic composition. Examples of features that point to a volcanic origin include the presence of upper chilled margins, breccias, and hyaloclastite. The limit between komatiite and basalt is set at 18 wt% MgO (Arndt and Nisbet, 1982). This value, although rather arbitrary, corresponds to a minimum in the abundances of komatiitic rocks in the majority of volcanic sequences. Volcanic rocks with 9–18 wt% MgO that can be linked to komatiites using textural or chemical features are termed komatiitic basalts.

Many komatiites contain spinifex texture, the most spectacular and characteristic texture in komatiites (Nesbitt, 1971; Kerr and Arndt, 2001). The presence of spinifex texture distinguishes komatiites from other ultramafic lavas, such as picrites, boninites, and meimechites.

Structural, textural, and volcanological characteristics of komatiites

A textural classification of komatiite lava flows was proposed on the basis of studies at the Pyke Hill locality in Munro Township, Canada (Pyke et al., 1973; Arndt et al., 1977), where relatively thin lava flows are exposed. Here, the most common lava flow type is differentiated into an upper spinifex-textured layer and a lower cumulate layer. A second type of komatiite lava flow is undifferentiated and polyhedrally jointed. These two types represent endmembers, with intermediate members containing a weakly developed, thin upper spinifex layer and a lower cumulate layer containing loosely packed olivine grains. Subsequent studies revealed the existence of much thicker lava flows such as those at Kambalda in Western Australia (e.g., Lesher and Arndt, 1995; Barnes et al., 1988; Hill et al., 1995). These units are dominated by olivine cumulates and spinifex texture is rare. This observation led to a more elaborate classification of komatiite lava flows that is based mostly on physical volcanology of komatiites (Hill et al., 1995; Barnes, 2006). Other relatively rare types include pillowed and volcaniclastic komatiites.

The thickness of komatiite lava flows varies significantly. At one end of the spectrum are flows only $<$50 cm thick, sometimes fully differentiated, such as those described at Munro Township and the Barberton greenstone belt (Pyke et al., 1973; Arndt et al., 1977; Smith et al., 1980; Viljoen et al., 1983). On the other end are differentiated flows $>$100 m, and sometimes up to 500 m, thick, such as those in parts of the Yilgarn Craton (Gresham and Loftus-Hills, 1981; Lesher et al., 1984; Perring et al., 1995; Hill et al., 1995), the Abitibi belt (Houlé et al., 2001), and the Barberton greenstone belt (Kareem, 2005; Stiegler et al., 2012; Hofmann et al., 2021). The thickest komatiite flows were likely not emplaced in a single pulse of magma but were ponded in depressions or advanced as a series of thinner flows that continued to be inflated by influx of new batches of melt (e.g., Arndt, 1982; Perring et al., 1995; Hill et al., 1995; Dann, 2000, 2001).

The relative thicknesses of spinifex vs cumulate layers in komatiite lava flows also vary. In thin flows, the two layers have approximately the same thickness, whereas in thicker flows, the cumulate zone is much thicker (e.g., Lesher, 1989). And some flows, such as those on the Gorgona Island, are composed almost entirely of spinifex-textured lava (Echeverria, 1980).

The lateral extent of komatiite lava flows is difficult to assess due to limited outcrop and the deformation that affected most komatiite sequences, but can be as large as hundreds of kilometers. The komatiites in the 2720 Ma Kidd-Munro volcanic assemblage in Ontario are correlative over a distance of $\geq$400 km (Ayer et al., 2002), and individual flow fields in the 2692 Ma Reliance Formation of the Belingwe greenstone belt can be correlated using lithological features and geochronology for $\sim$700 km across the Rhodesian Craton (Prendergast, 2003). Individual komatiite assemblages with similar ages and compositions in the Yilgarn Craton of Western Australia can be correlated for up to 500 km (Hill et al., 1995). However, given that the Archean komatiites sequences represent only remnants of volcanic provinces that survived multiple accretion and deformation events during the evolution of granite-greenstone terrains, their original extent was most likely far greater, covering vast areas on the Earth's surface. Clues to the

extent of Archean volcanic sequences are provided by the >1000 km dimensions of Phanerozoic continental flood basalt provinces such as the Siberian Traps, and oceanic plateaus such as Ontong Java.

A differentiated komatiite lava flow usually contains a spinifex zone (A) at the top and an olivine cumulate zone (B) at the base (Pyke et al., 1973; Arndt et al., 1977; Nisbet et al., 1977). The spinifex zone is subdivided into a chilled margin and aphanitic flowtop (subzone A_1) and subzone of random (A_2) and oriented spinifex (A_3). The cumulate zone is subdivided into a subzone of foliated skeletal olivine (B_1), a subzone of olivine cumulate (B_{2-4}) and a lower chilled margin. Not all flows conform to the simple differentiation pattern of the Pyke Hill flows. Variants include flows whose upper portions consist of multiple alternating layers of spinifex-textured and massive lava (e.g., Wilson, 2019).

The term "spinifex texture," introduced by Nesbitt (1971), comes from the grass *Triodia spinifex*, which is endemic to Western Australia where komatiites were identified as ultramafic lavas soon after the discovery of the rock type in South Africa (Viljoen and Viljoen, 1969). Spinifex texture is characterized by large, skeletal, platy blades of olivine or acicular needles of pyroxene in the upper parts of komatiitic flows or at margins of sills and dikes.

In oriented olivine spinifex texture, olivine has a platy or lattice habit and forms complex grains made up of many individual plates arranged roughly parallel to one another in "books" of grains. The books commonly are oriented near-perpendicular to flow boundaries or margins of a sill. The plates can be up to 1 m long, but are only 0.5–2 mm thick (e.g., Pyke et al., 1973; Arndt et al., 1977). The interstitial material is composed of skeletal, dendritic, or spherulitic pyroxene, cruciform or dendritic chromite, and devitrified glass. Plagioclase may be present in the matrix of some komatiites (e.g., Gorgona Island: Aitken and Echeverría, 1984). Random olivine spinifex texture contains shorter, less elongate, randomly oriented plates.

Platy spinifex is thought to form during moderately rapid cooling in thermal gradients at the margins of lava flows or shallow intrusions. Faure et al. (2006), building on the ideas of Donaldson (1982), Turner et al. (1986), and Shore and Fowler (1999), demonstrated experimentally that these conditions led to the build-up of olivine-depleted melt at the tips of downward-growing crystals, causing the development of skeletal or dendritic morphologies. Random spinifex forms during more rapid cooling closer to the flow margin (Faure et al., 2006; Sossi and O'Neill, 2016).

Pyroxene spinifex texture contains skeletal needles (Nesbitt, 1971; Arndt and Fleet, 1979; Puchtel et al., 1996), or rarely plates (Wilson et al., 2003; Lowrey et al., 2017), that are arranged in sheaths that are sub-perpendicular to flow margins or randomly oriented. Individual needles can be up to 5 cm long but only 0.5 mm wide, and are submerged in a matrix of fine augite needles, plagioclase, quartz, and devitrified glass. The larger needles or plates are zoned, with cores of orthopyroxene or pigeonite surrounded by mantles of augite. Primary mineral phases are usually replaced by serpentine, chlorite, tremolite, talc, epidote, and albite. The term spinifex is reserved for macroscopic textures that grow at the margins of komatiitic flows and sills.

Massive lava flows are far more common than layered flows, making up as much as 80% of komatiite sequences (Hill et al., 1995; Dann, 2000). These flows are undifferentiated and have a uniform olivine porphyritic texture throughout. They are usually cut by polyhedral joints, which increase in size from 2 to 5 cm near the contact to 20–30 cm near the center of the flows. Massive flows are generally thicker, but not as laterally extensive as layered flows. They are texturally relatively uniform containing polyhedral solid olivine grains and sparse, minute euhedral chromite grains in the usual augite-glass matrix. Some flows contain platy, hopper olivine grains. The abundance of olivine phenocrysts varies little throughout the flows, although some flows exhibit an increase toward the base, with a maximum amount reached two-thirds of the way. Olivine usually forms clusters of multiple grains separated by areas with much lower modal olivine abundance.

Thick dunitic bodies, such as the 220 m thick Honeymoon Well ultramafic body and the >700 m thick Perseverance, Six Mile, and Mt. Keith bodies in the Yilgarn Craton of Western Australia (e.g., Naldrett and Turner, 1977; Barnes et al., 1988, 2011; Lesher and Keays, 2002), can be traced along strike for tens of kilometers. These units are usually zoned, with massive olivine adcumulates in the center and olivine-pyroxene meso- and orthocumulates at the margins. Layered pyroxenites and gabbros may overlie the lower dunite layer. The olivine adcumulates are nearly monomineralic, being made up of up to 99% coarse-grained (up to 2 cm), mosaic-textured, highly magnesian olivine with interstitial chromite and Ni-sulfides. In meso- and orthocumulates, smaller, equant to elongate, euhedral olivine grains are surrounded by poikilitic pyroxene grains. In the upper marginal zones, layers of coarse branching and skeletal olivine grains (the so-called harrisitic olivine) may be present. The large dunitic bodies have been interpreted to represent lava rivers (Barnes et al., 1988) or intrusive units (Naldrett and Turner, 1977; Rosengren et al., 2005).

Finally, rare textural types of komatiitic lavas are pillowed (e.g., Pyke et al., 1973; Arndt et al., 1977) or fragmental (e.g., Gélinas et al., 1977; Barnes and Often, 1990; Saverikko, 1985; Aitken and Echeverría, 1984). In most Archean greenstone belts, fragmental ultramafic volcanic rocks are limited to thin flowtop breccias and hyaloclastites, such as those on top of the Alexo and Fred's Flows (Arndt, 1977b, 1986) or Tony's Flow (Nisbet et al., 1987). In the Quebec portion of the Abitibi greenstone belt, ultramafic volcaniclastics occur as thin tuffaceous units interlayered with komatiite flows (Gélinas et al., 1977), but these units represent very minor proportion of the volcanic sequences. Abundant volcaniclastic komatiites, represented by ultramafic tuffs and breccias, have been described in the Sattasvaara area in northern Finland (Saverikko, 1985), in several parts of the Superior Province of Canada (e.g., Schaefer and Morton, 1991), in the Dachine region in French Guiana (Capdevila et al., 1999), and on Gorgona Island (Echeverria and Aitken, 1986). These units are most likely epiclastic or hydroclastic in origin.

Mineralogy and mineral compositions of komatiites

The mineralogy of komatiites is relatively simple. Olivine is the most abundant mineral, making up 40–80% of massive and differentiated lava flows, respectively, and close to 100% in the cores of large dunitic units.

The morphology of olivine crystals in komatiites depends on the composition of the komatiite liquid and the cooling rate during their crystallization. At a given cooling rate, the higher the MgO content of the liquid, the less skeletal the olivine morphology (Donaldson, 1982). The cooling rate is influenced by the position in the lava flow. The mostly polyhedral olivine crystals in the lower cumulate parts of differentiated flows formed during relatively slow cooling. The thermal gradient in the upper part of differentiated lava flows has a strong effect on the morphology of olivine crystals, with fine, highly skeletal dendritic crystals forming during rapid cooling and unconstrained growth near the flow tops, and larger, platy olivine crystals forming during constrained growth and slower cooling deeper in the flow (Faure et al., 2003, 2006).

The composition of olivine also varies systematically from top to base of komatiite lava flows. The highest Fo content is usually found in the upper chilled margins and in the olivine cumulate (Pyke et al., 1973; Arndt, 1986). In differentiated flows, the Fo content of olivine remains nearly constant in cumulate zones (Arndt et al., 1977; Renner et al., 1994), but progressively decreases from top to bottom of the spinifex zone.

Major element compositions of liquidus olivine in most komatiites range between Fo_{90} and Fo_{94}, being linked to the MgO content of the parent komatiite liquid. Values as high as $Fo_{96.6}$ are reported in komatiites from the Weltevreden (Kareem, 2005; Connolly et al., 2011; Stiegler et al., 2012) and Commondale (Wilson and Bolhar, 2022) localities in South Africa. In both spinifex and cumulate zones, olivine grains are continuously zoned from core to rim as a result of the evolution of the composition of the liquid from which they grew (e.g., Arndt, 1986). Variations of Fo contents within single olivine grains can be as large as 9 mol% (Renner et al., 1994) due to a combination of factors specific to komatiites, such as rapid cooling and the large temperature and compositional interval over which olivine crystallized.

The Ni contents in komatiitic olivine also varies as a function of the MgO content of the liquid they crystallized from, reaching a maximum of ~4000 ppm in olivines with composition ~Fo_{92}. Values are lower in olivines with higher or lower Fo contents due to an interplay between variations in the Ni partition coefficient and the MgO content of the liquid (Arndt, 1986; Renner et al., 1994; Matzen et al., 2013; Sossi and O'Neill, 2016; Sobolev et al., 2016).

The Cr content of olivine in komatiites ranges between ~1000 and 3500 ppm, with the highest Cr contents found in olivines that crystallized rapidly and early (Barnes, 1998). These concentrations are up to 20 times higher than those in olivine from typical basalts, likely due to a number of factors. These include much higher Cr content in the komatiite liquid compared to basalts as a result of much higher degrees of partial melting that formed komatiites, higher $D_{Cr}^{Ol\text{-}liq}$ at higher temperatures, and the delayed onset of chromite crystallization in komatiites (Shore and Fowler, 1999; Barnes and Roeder, 2001).

The CaO content of olivine in komatiites ranges between 0.20 and 0.35 wt%, consistent with a higher Ca partition coefficient at the elevated temperatures of komatiitic liquids (Kinzler and Grove, 1985; Libourel, 1999; Shejwalkar and Coogan, 2013).

Chromite is found as dendritic or cruciform skeletal grains in spinifex-textured komatiites, and cubic or octahedral crystals in cumulate and porphyritic komatiite lavas. Its modal abundance rarely exceeds 1% by volume, with spinifex lavas containing more chromite than olivine cumulates, probably because of the late onset of chromite crystallization in highly-magnesian komatiitic liquids (Murck and Campbell, 1986). An exception is the high chromite concentrations documented in B_1 layers of some differentiated komatiite lava flows in Finland (e.g., Hanski, 1980).

The composition of chromite in komatiites (e.g., high Cr/(Cr + Al)) is consistent with crystallization from high-temperature ultramafic magma with higher Cr and lower Al contents compared to basalt.

Pyroxene in komatiites ranges in composition from augite to pigeonite to orthopyroxene. In pyroxene spinifex-textured komatiitic basalts, it occurs as needle- or, less commonly, blade-like megacrysts; in the groundmass of spinifex-textured and cumulate komatiites, it forms subhedral to euhedral, solid prismatic grains or needles, dendrites, and feathery aggregates (Viljoen and Viljoen, 1969; Arndt and Fleet, 1979; Puchtel et al., 1996; Lowrey et al., 2017; Wilson, 2019).

Most pyroxene megacrysts are large, individual or composite needles, 0.1–1.0 mm across and several cm in length, hollow in cross-section, commonly with pigeonite cores and augite mantles. The needles are arranged in sheaths or columns, either parallel to one another or slightly branching. Sheaths are oriented sub-perpendicular to the flowtop, often splaying out downwards. In finer-grained pyroxene spinifex texture, the pigeonite-augite needles are only 1–5 mm long and are randomly oriented. Pigeonite in the cores of the needles is highly magnesian, with Mg# = 0.81–0.85. Clinopyroxene in the mantles is subcalcic augite. Pigeonite contains 2–3 wt% Al_2O_3 and augite contains 3–10 wt% Al_2O_3. The habits of pyroxene in cumulate zones vary from stubby, solid or skeletal prisms and needles to fan-like and feathery grains. The coarser interstitial pyroxenes are subcalcic augite with up to 8 wt% Al_2O_3.

In the cumulate portions of komatiitic basalt lava flows, pyroxene has compositions and habits similar to those of mafic lava flows. Most grains are subhedral to euhedral, with prismatic habits, and vary in size from a few mm to up to 1 cm. The cumulates of layered mafic lava flows in the Abitibi and Belingwe greenstone belts (Arndt, 1977b; Nisbet et al., 1977) are composed predominantly of augite and subordinate bronzite with compositions similar to those of pyroxenes from mafic plutonic rocks. Orthopyroxene dominates in the cumulates from Commondale in South Africa (Wilson, 2019).

Plagioclase in komatiites is restricted to the groundmass of platy olivine spinifex layers and cumulate portions of some layered lavas flows, most notably in the komatiites from Gorgona Island (Aitken and Echeverría, 1984). Plagioclase has composition of ~An_{75} and is intergrown with interstitial augite.

Glass, invariably devitrified and variably altered, occurs in the groundmass between olivine and pyroxene grains. Fresh glass is restricted to inclusions in olivine and chromite grains (Nisbet et al., 1987; Puchtel et al., 1996; Shimizu et al., 2001; Sobolev et al., 2016, 2019; Asafov et al., 2018). The glass contains 2–11 wt% MgO, 50–58 wt% SiO_2, 11–16 wt% Al_2O_3, 14–20 wt% CaO and 0.7–1.6 wt% Na_2O, representing evolved liquid compositions derived from extreme olivine fractionation.

Geochemistry

Introduction

An essential characteristic of komatiites is their high MgO content, which, by definition, is greater than 18 wt% (Arndt and Nisbet, 1982). In practice, some caution is required if the MgO content is to be used to decide whether a rock is or is not a komatiite. Implicit in the definition of komatiite is the notion that the rock formed from a melt with an ultramafic composition. The problem is that many olivine porphyries and cumulates with high MgO contents are derived from melts with basaltic or picritic compositions—their elevated MgO are caused by the presence of excess olivine. When the rocks are little altered, and particularly when fresh olivine is preserved, it is possible to determine the composition of the parental liquid using procedures described in a later section. However, when primary textures and minerals have been destroyed during metamorphism, it is often difficult, if not impossible, to clearly identify a sample as komatiite.

Another problem is the distinction that must be made between komatiite and volcanic rocks such as picrites and meimechites, which have MgO contents greater than 18 wt% and far higher contents of alkali elements and titanium. To address this issue, Le Bas (2000) proposed the use of MgO and $Na_2O + K_2O$ contents (Fig. 1a), and Hanski et al. (2001) developed the [MgO] and [TiO_2] diagram shown in Fig. 1b.

Major and trace elements

The chemical compositions of typical komatiites considered in this review are presented in Table 1. These compositions are commonly illustrated in MgO variation diagrams, such as those in Fig. 2. In these diagrams, MgO is plotted on the X-axis and used as a differentiation index, because fractional crystallization or accumulation of olivine exerts a major control on the compositions of erupted komatiites and has a major impact on the concentration of MgO in the residual liquid. In such diagrams, elements such as Al, Ti, the rare earth elements (REE), and the high-field-strength elements (HFSE) commonly plot on tight linear arrays with negative slopes. These elements are incompatible with olivine, i.e., they do not enter the olivine crystal lattice and removal of this mineral causes their concentrations in the residual melt to increase, while accumulation leads to lower concentrations in the cumulates. When elements plot on tight arrays, this can be taken as evidence that their concentrations were not measurably affected by the alteration and metamorphism experienced to a greater or lesser extent by all komatiites. The term "immobile" is used to describe the behavior of such elements.

In contrast, elements such as Ca, Na, K, and the large-ion lithophile trace elements (LILE, e.g., Cs, Rb, Ba, Sr) either scatter about linear arrays or show no correlation with MgO contents. The concentrations of these elements are known to change during seafloor alteration and metamorphism; they are said to be "mobile." When using geochemistry to study the origin and evolution of komatiites, only the immobile elements are employed (e.g., Nesbitt and Sun, 1976; Nisbet et al., 1977; Jahn et al., 1982; Jochum et al., 1991).

The situation is more complicated for three important major elements, Si, Fe, and Mg. The tight correlations often displayed when immobile elements such as Al, Ti or the REE are plotted against MgO can be taken as evidence that the latter normally behaves as an immobile element, but there are exceptions. Lahaye and Arndt (1996) showed that completely serpentinized samples from the flowtop breccia and cumulate zones of the Alexo Flow in the Abitibi belt of Canada had gained/lost a few percent of MgO. Demonstrable mobility of most major and trace elements, including MgO, was found in the komatiites from the Crixás belt in Brazil (Arndt et al., 1989) and Tipasjarvi and Kuhmo belts in eastern Finland (Tourpin et al., 1991; Gruau et al., 1992).

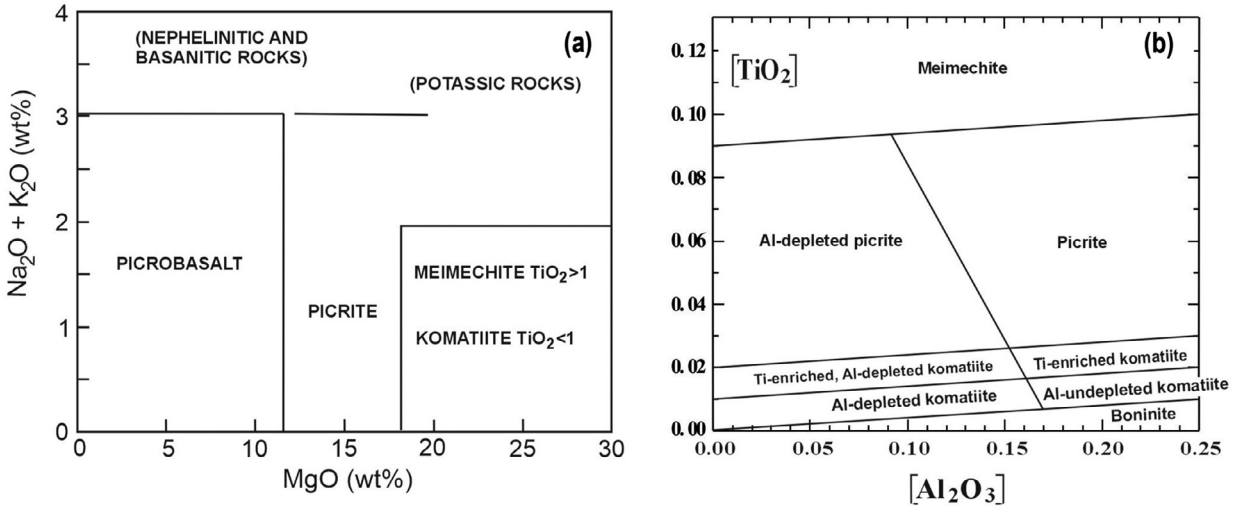

Fig. 1 (a) The classification scheme of komatiites and related low-silica rocks proposed by Le Bas (2000). (b) The classification scheme of Hanski et al. (2001). From Le Bas MJ (2000). IUGS reclassification of the high-Mg and picritic volcanic rocks. *Journal of Petrology* 41: 1467–1470. Hanski E, Huhma H, Rastas P, and Kamenetsky VS (2001). The Palaeoproterozoic komatiite-picrite association of Finnish Lapland. *Journal of Petrology* 42(5): 855–876.

Table 1 Summary of ages, physical characteristics, and chemical features of selected komatiite suites.

Komatiite suite	*Age, Ga*	*MgO_{liq}*	*T_{liq}°C*	*T_p°C*	*$D_{melt\ init,\ km}$*	*Al_2O_3/TiO_2*	*$(La/Sm)_N$*	*$(Gd/Yb)_N$*	*Nb/Nb**	*Th/U*[a]
Kaapvaal Craton, South Africa										
Schapenburg	3.55	29.1 ± 2.8	1580	1810	440	10.0 ± 0.8	0.93 ± 0.04	1.57 ± 0.10	1.2 ± 0.1	
Komati	3.48	29.9 ± 0.5	1590	1820	490	10.1 ± 0.7	0.97 ± 0.24	1.39 ± 0.05	1.1 ± 0.2	4.08 ± 0.29
Weltevreden	3.26	31.4 ± 0.9	1610	1840	610	29.2 ± 1.1	0.68 ± 0.06	0.84 ± 0.03	1.4 ± 0.1	
Commondale	3.33	36.1 ± 1.0	1650	1890	>600	81 ± 14	0.24 ± 0.20	0.29 ± 0.07		
Pilbara Craton, Western Australia										
Coonterunah	3.53	23.0 ± 0.3	1500	1710	200	23.8 ± 1.7	0.80 ± 0.04	0.96 ± 0.04	1.08 ± 0.02	
Kelly	3.34	27.4 ± 1.0	1560	1790	350	22.1 ± 1.7	0.65 ± 0.02	0.91 ± 0.04	1.03 ± 0.04	
Ruth Well	3.18	29.3 ± 0.7	1580	1810	460	11.0 ± 0.5	0.55 ± 0.09[b]	1.31 ± 0.04	1.0 ± 0.1[b]	
Regal	3.18	29.3 ± 0.7	1580	1810	460	11.9 ± 0.8	0.61 ± 0.11[b]	1.28 ± 0.12	1.0 ± 0.1[b]	
Fennoscandian Shield, northern Europe										
Sumozero-Kenozero	2.90	29.5 ± 1.0	1570	1800	410	19.3 ± 0.2	0.70 ± 0.02	1.00 ± 0.10	1.2 ± 0.2	3.43 ± 0.24
Kostomuksha	2.82	27.6 ± 1.0	1560	1790	360	17.2 ± 1.2	0.48 ± 0.13	1.16 ± 0.02	1.2 ± 0.1	2.99 ± 0.19
Vetreny	2.41	27.0 ± 1.0	1560	1780	330	19.7 ± 0.5	0.41 ± 0.10[b]	1.20 ± 0.10	1.0 ± 0.1[b]	4.45 ± 0.12
Lapland	2.05	25.2 ± 0.5	1530	1750	260	13.9 ± 0.4	0.14 ± 0.02[b]	1.48 ± 0.02	1.0 ± 0.1[b]	
Superior Craton, Canada										
Boston Creek	2.72	23.6 ± 0.5				5.1 ± 0.8	1.9 ± 0.3	2.0 ± 0.2	1.2 ± 0.2	
Pyke Hill-Alexo	2.72	28.2 ± 0.5	1570	1790	390	20.4 ± 0.6	0.53 ± 0.16	0.98 ± 0.03	1.0 ± 0.1	3.00 ± 0.10
Winnipegosis	1.87	23.6 ± 1.0	1510	1720	220	17.2 ± 0.4	0.76 ± 0.07	1.13 ± 0.04	1.1 ± 0.1	
Rhodesian Craton, Zimbabwe										
Belingwe	2.69	25.6 ± 0.5	1540	1760	280	19.8 ± 0.6	0.68 ± 0.02	1.02 ± 0.04	0.97 ± 0.05	2.95 ± 0.17
Caribbean Large Igneous Province										
Gorgona komatiite	0.089	20 ± 2	1460	1650	160	18.4 ± 0.7	0.28 ± 0.03	1.2 ± 0.1	1.0 ± 0.2	
Gorgona picrite	0.089	25 ± 2	1520	1730	240	33 ± 7	0.15 ± 0.04	0.68 ± 0.13	0.86 ± 0.34	

MgO_{liq}—the MgO content of the original emplaced komatiite magma for each komatiite system compiled from Nicklas et al. (2018, 2019), Puchtel et al. (2022b) and references therein. **T_{liq}°C, T_p°C**—estimates of liquidus temperatures of the emplaced komatiite magmas and mantle potential temperatures for the studied komatiite systems at 1 bar pressure. $D_{melt\ init}$—estimates for depths of melting initiation. These estimates were generally derived from the studies for the particular komatiite systems referenced in Table 2 and updated by Puchtel et al. (2022b) on the basis of data from Nicklas et al. (2018, 2019), where available, coupled with the previous and more recent mantle melting parameterization models of McKenzie and Bickle (1988), Herzberg and O'Hara (2002), Herzberg and Asimow (2008), and Herzberg and Gazel (2009). Details of the methodology used for calculating these parameters were provided by Puchtel et al. (2022b). $Nb/Nb^* = Nb_N/\sqrt{(Th_N \times La_N)}$. N here and in the table are the Bulk Silicate Earth (BSE) normalizing values from Hofmann (1988). For the sources of the data, see Table 2.

[a]Calculated from the Pb-Pb isotope data. All uncertainties are 2SD of the mean.

[b]Values corrected for AFC.

Element mobility in komatiites can also be detected by monitoring elemental ratios (e.g., Nesbitt and Sun, 1976). A strong correlation between two elements that behave in a similar manner during magmatic processes can be regarded as evidence of immobile behavior of these elements. It should be kept in mind, however, that if two mobile elements are affected by alteration in a similar manner (e.g., Rb and Sr), they can produce good correlation when plotted against each other. This correlation can be misinterpreted as evidence for immobile behavior.

High values of loss-on-ignition (LOI), the sum of measured H_2O and CO_2 contents, can also be taken as an indication of potential element mobility, but this parameter, too, can be misleading. The main problem is that during alteration, LOI in komatiites is dominantly controlled by the modal abundance of olivine. Komatiites with MgO >25% have olivine that alters to H_2O-rich serpentine and typically have LOI >8 wt%, while those with lower MgO content have olivine that alters to chlorite or talc that have lower structural H_2O and, hence, lower LOI. Serpentinization can be a near-isochemical process, whereas chloritization commonly involves mobility of major elements (Lahaye and Arndt, 1996). Talc forms when the fluids contain CO_2 and this leads to significant element mobility. In such cases, the real indicator of alteration, when LOI is considered, is the CO_2 content, but this is rarely measured separately from H_2O.

Classification of komatiites

When Pyke et al. (1973) described komatiites from Pyke Hill, the classic locality in Munro Township, they realized that these rocks did not have the high CaO/Al_2O_3 ratios of >1.0 that Viljoen and Viljoen (1969) had proposed as a defining chemical characteristic of komatiites, based on their study of Barberton lavas. It subsequently became clear that there are several geochemically different types of komatiite. When it was realized that CaO behaves as a mobile element during alteration of komatiites, especially in cumulate zones of differentiated lava flows, the distinctive characteristic of the Barberton komatiites was quantified using the ratio of two relatively immobile elements, Al_2O_3 and TiO_2. Nesbitt and Sun (1976) introduced the term "Al-depleted" for the Barberton komatiites, and "Al-undepleted" for those from Pyke Hill and other parts of the Abitibi belt. These terms have stuck, abbreviated as

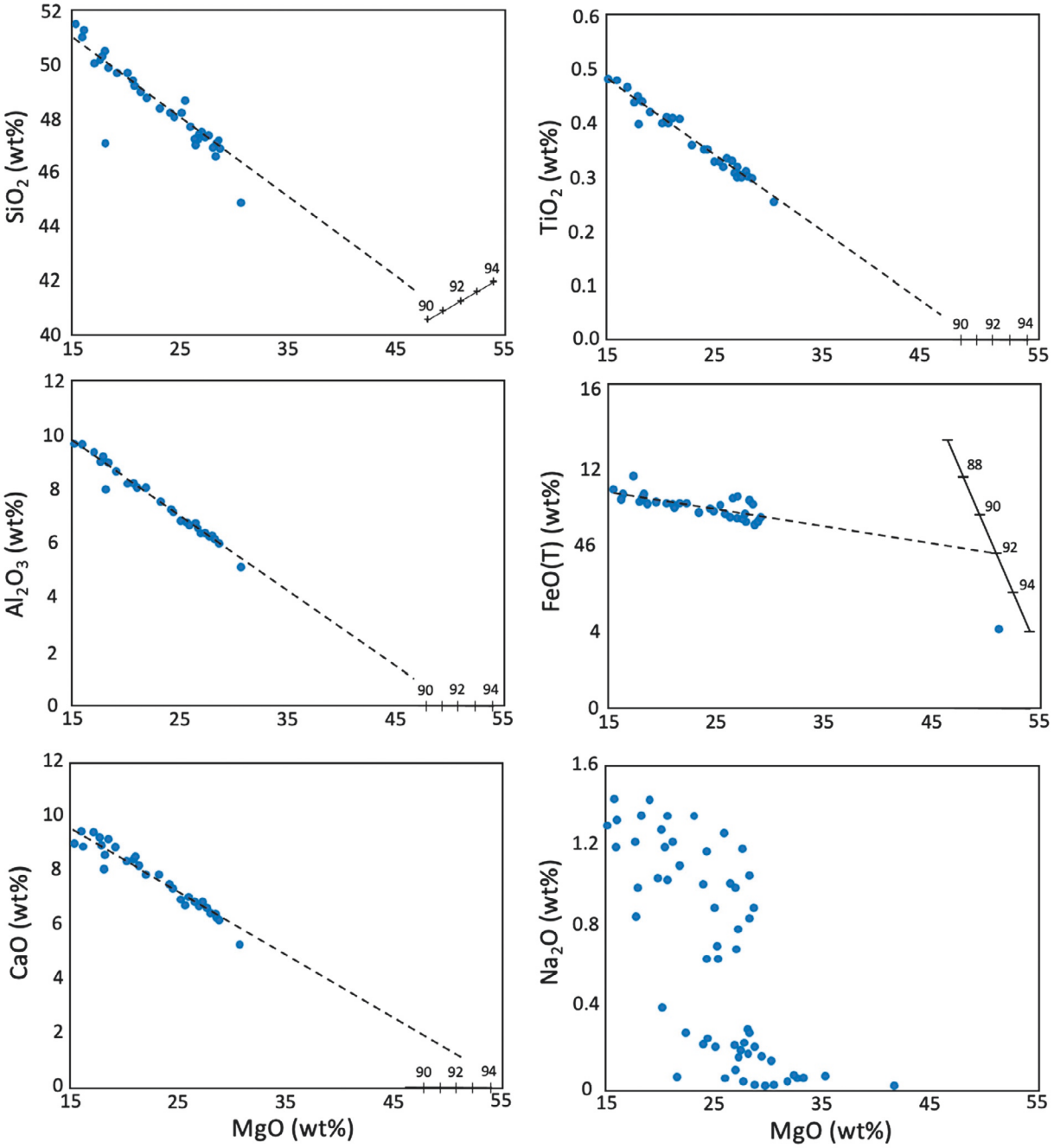

Fig. 2 MgO vs selected major elements in komatiites from the Belingwe greenstone belt in Zimbabwe. From Arndt NT, Lesher CM, and Barnes SJ (2008) *Komatiite*. Cambridge, UK: Cambridge University Press, 467 pp.

ADK and AUK in many publications (e.g., Nesbitt et al., 1979). Sun (1984) then somewhat confused the issue by proposing the terms "Barberton-type" for Al-depleted komatiites and "Munro-type" for Al-undepleted komatiites. In this chapter, fueled by a dislike of acronyms, we will eschew ADK and AUK and will spell out in full the terms Al-depleted and Al-undepleted.

The Al_2O_3/TiO_2 ratio is employed in Fig. 3, which shows the two main types of komatiites, together with a third type called "Al-enriched" komatiite. This diagram illustrates that in most cases, a low Al_2O_3/TiO_2 is accompanied by high Gd/Yb, the latter ratio being a measure of the slope of the heavy REE in Bulk Silicate Earth (BSE)-normalized trace element diagrams such as those plotted in Figs. 4 and 5 (see also Sun and Nesbitt, 1978; Jahn et al., 1982). In the Al_2O_3/TiO_2 vs Gd/Yb diagram, we have chosen not to plot the compositions of the many thousands of analyses of komatiites that are now available on several sites such as GEOROC, because doing so gives a rather confusing picture. Instead, we plot just the average compositions from a small number of localities to illustrate the main geochemical characteristics of komatiites.

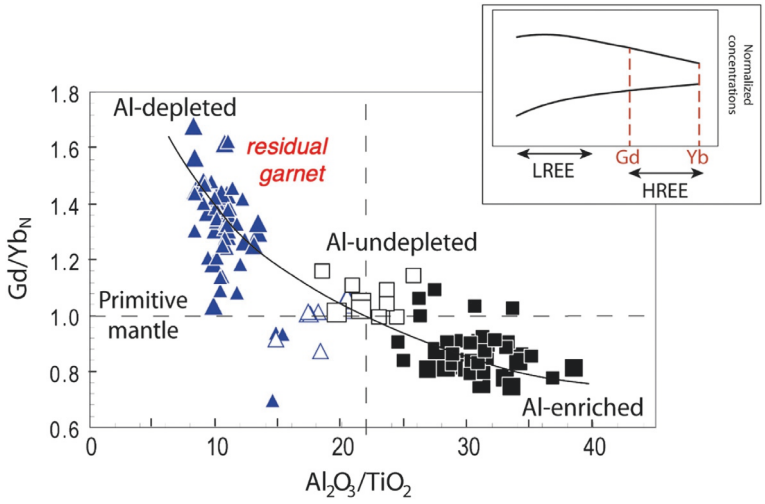

Fig. 3 Diagram of Al_2O_3/TiO_2 (wt%) vs Gd/Yb_N (BSE-normalized using values from Hofmann, 1988) ratios illustrating the three main types of komatiite: Al-depleted, Al-undepleted, and Al-enriched.

Incompatible trace elements

Two important aspects of the chemical compositions of komatiites are not captured in the Al_2O_3/TiO_2 vs Gd/Yb diagram: (1) the extent of depletion or enrichment of the more incompatible elements such as the light REE relative to the middle REE, and (2) the concentrations of moderately incompatible elements such as Ti or the middle REE. The first trait is illustrated in the $(La/Sm)_N$ vs $(Gd/Yb)_N$ diagram (Fig. 6; the subscript "N" indicates that the concentrations are normalized to the Bulk Silicate Earth (BSE) values of Hofmann, 1988). This diagram shows that komatiites with high Gd/Yb tend to have high La/Sm, reflecting overall enrichment of highly incompatible compared to moderately incompatible elements. There are, however, several exceptions, such as the komatiites from Lapland (Hanski et al., 2001) and from Ruth Well in Western Australia (Nisbet and Chinner, 1981), which have hump-shaped REE patterns due to relative depletion of both the light and heavy REE compared to the middle REE. Also notable in this diagram is the extreme depletion of incompatible elements in the komatiites from Commondale (Wilson, 2019) and more moderate depletion in all Al-undepleted komatiites.

The overall level of moderately incompatible elements is captured to some degree in the $[Al_2O_3]$ vs $[TiO_2]$ diagram (Hanski et al., 2001), reproduced in Fig. 1b. This diagram clearly illustrates the differences in Ti contents of komatiites, picrites, and meimechites, but it does not appear to be widely used.

In Fig. 7, we propose another approach. In this diagram, we plot $(Al_2O_3)_{25}$ vs $(TiO_2)_{25}$, where the subscript "25" indicates that the Al_2O_3 and TiO_2 contents are those estimated for a melt containing 25 wt% MgO. This approach is very similar to that used by Klein and Langmuir (1987) to correct for fractional crystallization in modern mid-ocean ridge basalts. In komatiites, normalization to a given MgO content is required to eliminate the changes in chemical composition caused by the fractionation or accumulation of olivine that occurs in all komatiite flows to a greater or lesser extent. The value of 25 wt% MgO was chosen because it is close to the median value in Archean komatiites (Barnes et al., 2021). In some cases, this value is lower, and in others, it is higher than those of the parental komatiite melts. Sossi et al. (2016) used a similar diagram, but instead of using 25 wt%, the oxides were normalized to the MgO content of the inferred primary melt. We prefer to use 25 wt% MgO because it is often impossible to determine the composition of the primary komatiite melt.

Our method for estimating the concentrations of major or trace elements at 25 wt% MgO is illustrated in Fig. 8. We applied it only to those suites in which there is a tight correlation between the concentration of the element and that of MgO; in such cases, it is a simple procedure to estimate the element concentration, either numerically or graphically.

The utility of the normalizing procedure is illustrated in Fig. 7, which shows how the concentrations of Al_2O_3 and TiO_2 change from suite to suite. For example, the high Al_2O_3/TiO_2 of the "Al-enriched" Commondale komatiites is due mainly to low TiO_2, rather than to high Al_2O_3, and the low Al_2O_3/TiO_2 in Barberton Al-depleted komatiites is due in part to moderately high TiO_2. In addition, the diagram shows that, while all the Al-undepleted komatiites share a chondrite-like Al_2O_3/TiO_2 ratio of ~20, they have very different concentrations of both elements, from very high in Gorgona komatiites, to strikingly low in the enigmatic Barberton Al-undepleted komatiites (e.g., Chavagnac, 2004; Robin-Popieul et al., 2012; Sossi et al., 2016).

Immobile incompatible lithophile trace elements generally follow REE in their behavior, and on the BSE-normalized trace element diagrams exhibit a relatively smooth progression from highly incompatible elements such as Th, Nb, and La, to moderately incompatible such as Y, Ti, and Lu (Fig. 4).

Effects of crustal contamination

Owing to their high liquidus temperatures and low viscosities, komatiitic liquids are highly susceptible to contamination during their passage through or emplacement onto the continental crust (Huppert et al., 1984; Huppert and Sparks, 1985).

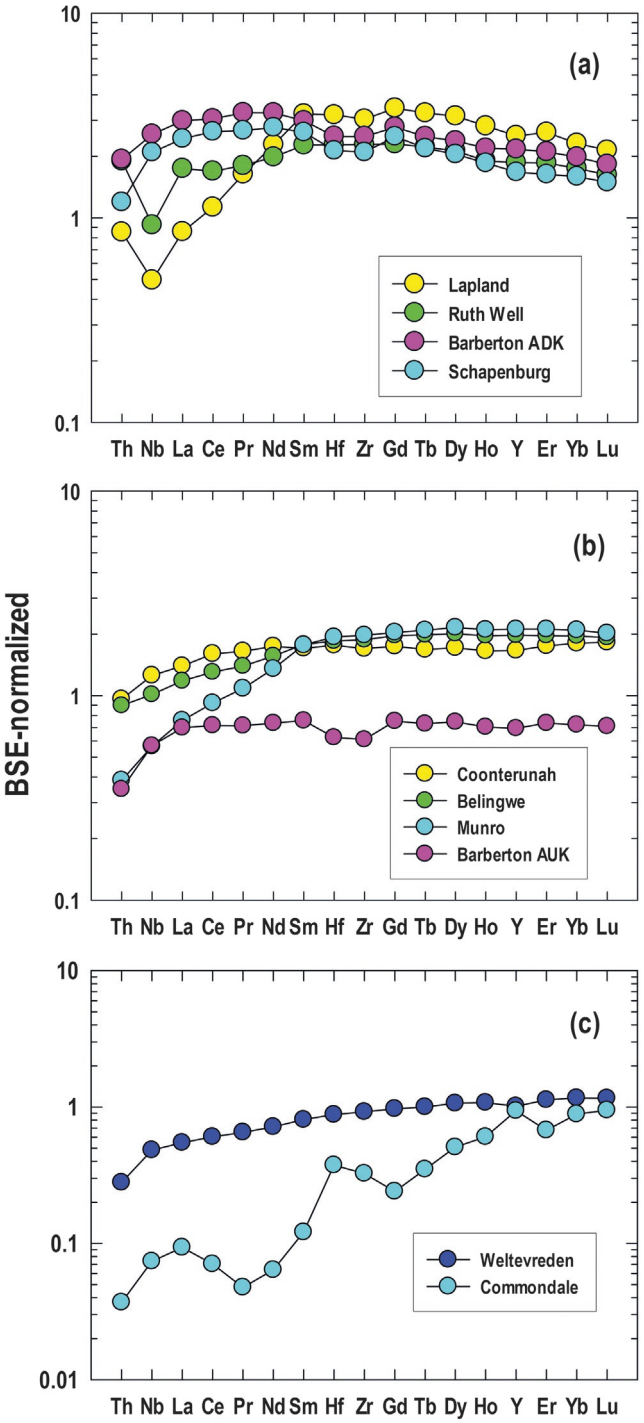

Fig. 4 BSE-normalized trace element diagrams with the compositions of representative examples of komatiite. Only immobile elements are plotted and each profile represents composition of emplaced komatiite lava. Principle sources of data (a–c): Barberton Al-depleted komatiite: (Puchtel et al., 2013); Coonterunah, Ruth Well: (Puchtel et al., 2022a); Lapland: (Puchtel et al., 2020); Munro: (Puchtel et al., 2009a; Sossi et al., 2016); Belingwe: (Puchtel et al., 2009a); Barberton Al-undepleted komatiite (Robin-Popieul et al., 2012); Weltevreden: (Puchtel et al., 2013); Commondale (Hoffmann and Wilson, 2017).

Upper crustal rocks are strongly enriched in Th, U, and light REE, and relatively depleted in Nb (Rudnick and Gao, 2014) as a result of subduction zone processes involving preferential removal of Nb-poor fluids and retention of Nb-rich rutile in the eclogitic residue (Foley et al., 2000; Rudnick et al., 2000). Because of this, upper crustal rocks are characterized by Nb concentrations that are low relative to elements with similar incompatibility during mantle melting (Th and La), i.e., $Nb/Nb^* \ll 1.0$ (where $Nb/Nb^* = Nb_N/\sqrt{(Th_N \times La_N)}$). By contrast, primary komatiitic magmas are expected to have $Nb/Nb^* \geq 1.0$ (e.g., Hofmann et al., 1986; Jochum et al., 1991). Due to large differences in the concentrations of incompatible trace elements between the

Type	Characteristics	Origin	REE diagram
Barberton ADK	Low Al_2O_3/TiO_2, depletion of HREE, slight depletion of LREE	Batch melting above top of mantle transition zone; garnet left in residue; slight depletion of source	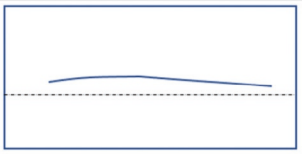
Munro AUK	Chondritic Al_2O_3/TiO_2, no depletion of HREE, strong depletion of LREE	Fractional melting of source strongly depleted by prior extraction of low-degree melt	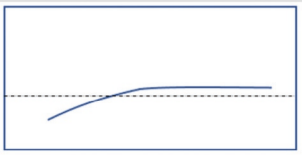
Barberton AUK	Chondritic Al_2O_3/TiO_2, no depletion of HREE or LREE; very low concentrations of incompatibole trace elements	High-degree melting undepleted source	
Lapland	Low Al_2O_3/TiO_2, high concentreation of TiO_2; depletion of HREE, strong depletion of LREE	Moderate degree of melting; garnet left in residue; source depleted by prior extraction of melt	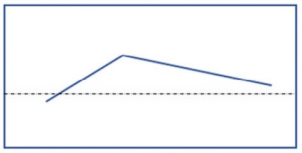
Boston Creek	Low $Al_2O_3/TiO2$, high TiO_2, high Al_2O_3; depletion of HREE, enrichment of LREE	Low-degree melting at high pressure where garnet is left in residue	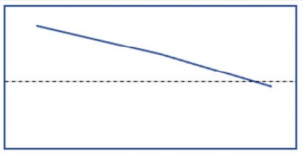
Commondale	High Al_2O_3/TiO_2; very low TiO_2 and other incompatible elements; extreme depletion of LREE	High-degree melting of a source extremely depleted by prior extraction of low-degree melt	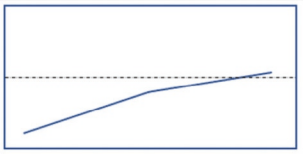

Fig. 5 Summary of the geochemical characteristics and some ideas about the origin of komatiites from several key locations.

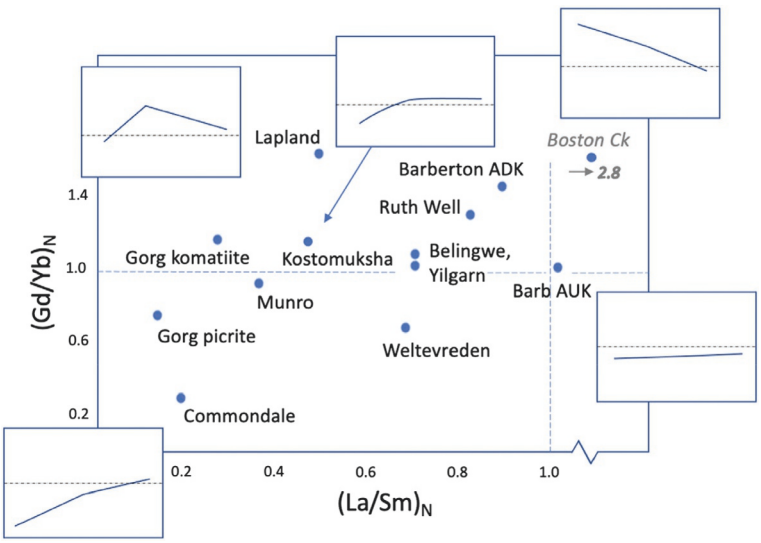

Fig. 6 Diagram illustrating variations in the ratios of light and heavy REE in selected komatiites. Data sources as in Fig. 4 with the following additions. Gorgona picrite and komatiite—Révillon et al. (2000); Belingwe—Shimizu et al. (2001); Yilgarn—Lesher and Arndt (1995); Kostomuksha—Puchtel et al. (1998a); Boston Creek—Stone et al. (1987).

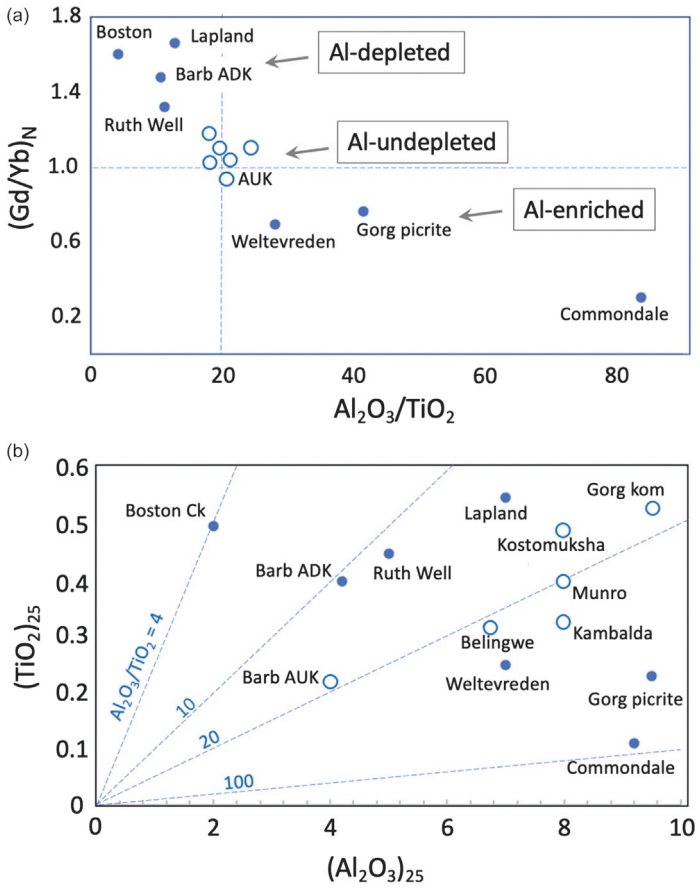

Fig. 7 (a) Al_2O_3/TiO_2 vs $(Gd/Yb)_N$ diagram with the compositions of selected komatiite samples. (b) $(Al_2O_3)_{25}$ vs $(TiO_2)_{25}$ diagram, where the subscript "25" indicates that the oxide percentage is normalized to 25 wt% MgO using the procedure illustrated in Fig. 8.

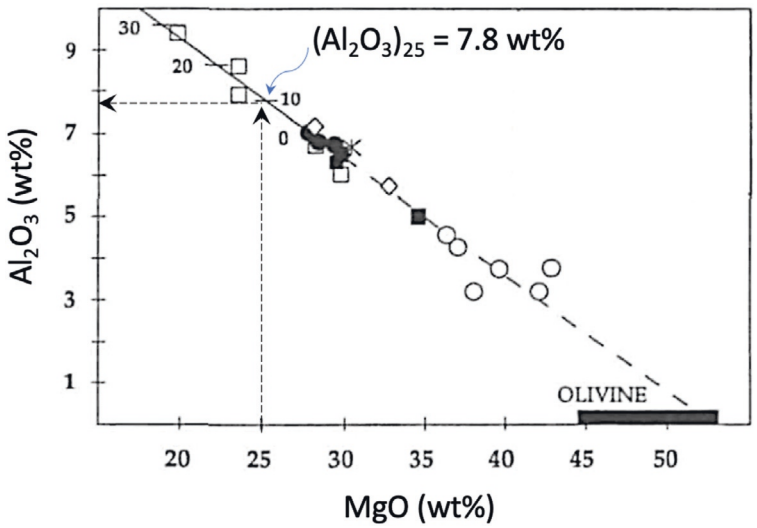

Fig. 8 Diagram illustrating the procedure used to normalize major and trace element data to 25 wt% MgO. Modified from Arndt NT, Lesher CM, and Barnes SJ (2008). Komatiite. Cambridge, UK: Cambridge University Press, 467 pp.

upper crustal rocks and komatiitic melts, crustal contamination usually leads to a sharp increase in the abundances of Th, U, and LREE, but much less so of Nb. The contaminated melts acquire negative Nb anomalies ($Nb/Nb^* < 1.0$) in this process, and the Nb/Nb^* ratio represents a diagnostic tool that has been utilized to identify and mathematically correct for crustal contamination (e.g., Jochum et al., 1991; Sobolev et al., 2016; Puchtel et al., 1997, 2016b, 2020, 2022a).

Pronounced negative Nb anomalies accompanied by enrichment of incompatible elements and continental crust-like Nd and Pb isotope compositions have been found in komatiites and komatiitic basalts from the Yilgarn Craton (Arndt and Jenner, 1986; Barley, 1986; Barnes et al., 2021), Superior Craton (Cattell, 1987; Xie et al., 1993; Sproule et al., 2002), Pilbara Craton (Sun et al., 1989; Smithies et al., 2007; Puchtel et al., 2022a), and Fennoscandian Shield (Puchtel et al., 1997). These authors attribute the negative Nb anomalies to crustal contamination.

Compatible elements

Nickel abundances in komatiites positively correlate with MgO content due to compatibility of Ni in olivine. The olivine-melt partition coefficient increases as the liquid composition changes from komatiite to basalt and as the temperature drops from ~1600 °C to ~1200 °C (Hart and Davis, 1978; Smith and Erlank, 1982; Kinzler et al., 1990; Matzen et al., 2013).

Chromium is moderately incompatible in olivine and highly compatible in chromite (e.g., Barnes, 1986; Sossi and O'Neill, 2016). Under normal conditions of komatiite crystallization at the oxygen fugacity of the FMQ buffer, chromite does not start to crystallize until the MgO content of the liquid drops below ~24 wt%. This leads to an unusual hump-shaped pattern with a maximum at ~24 wt% MgO when Cr is plotted against MgO (Murck and Campbell, 1986; Barnes, 1998, 2000).

Vanadium is incompatible in olivine, but its incompatibility is redox-sensitive. Canil (1997, 1999, 2002), Canil and Fedortchouk (2001), and Mallmann and O'Neill (2009) showed that the major factor controlling the distribution of V between olivine and komatiitic melt ($D_V^{ol/liq}$) was oxygen fugacity (fO_2), and used V partitioning between liquidus olivine and komatiite liquid as a redox indicator. More oxidized, water-rich island arc magmas (higher fO_2) are invariably characterized by ($D_V^{ol/liq}$) < 0.01, whereas less oxidized, anhydrous magmas (e.g., OIB and MORB) exhibit ($D_V^{ol/liq}$) = 0.025 – 0.10. Nicklas et al. (2018, 2019) used this indicator and calculated MgO contents of the emplaced lavas for a global set of komatiites and picrites ranging in age from 3.5 Ga to recent to show that the redox state of the mantle gradually increased by ~1.3 ΔFMQ log units between 3.5 and 2.0 Ga and then remained nearly constant from 2.0 Ga until the present day.

The abundances of the platinum-group elements (PGE: Os, Ir, Ru, Rh, Pt, and Pd) in komatiites and other mantle-derived magmas strongly depend on the nature of the residue that remains after the partial melting that produced these lavas. The PGE are both highly chalcophile and siderophile ($D^{sulf\text{-}silicate} = 10^4$–$10^5$, $D^{metal\text{-}silicate} = 10^5$–$10^6$: Peach et al., 1994; O'Neill et al., 1995; Fleet et al., 1996). The PPGE (Pt, Rh, and Pd: Barnes et al., 1985) are hosted mainly by low-temperature Cu-Ni sulfides (e.g., Keays, 1995; Alard et al., 2000; Lorand and Alard, 2001; Luguet et al., 2007), whereas the IPGE (Os, Ir, and Ru) are hosted mainly by high-temperature Os-Ir-Ru-rich Fe-Ni monosulfide solid solution and Os-Ir-Ru alloys. During low degrees of partial melting of mantle peridotite, Cu-Ni sulfides enter the melt as the degree of melting increases, while the monosulfide solid solution remains trapped in the melting residue. Because of this, the resultant basaltic melts acquire high PPGE and low IPGE contents. It takes ~20% partial melting to exhaust the low-temperature Cu-Ni sulfides, at which point the PPGE reach their highest levels in the melt (Keays, 1995; Luguet et al., 2007; Mungall and Naldrett, 2008; Naldrett, 2010; Fonseca et al., 2011, 2012; Kiseeva et al., 2017). As the degree of melting increases and the magma becomes komatiitic in composition, the monosulfide solid solution enters the melt and the proportion of PPGE to IPGE in the melt decreases and approaches that of the source.

Fig. 9 shows CI chondrite-normalized PGE abundances of komatiite lavas from several localities, normalized to 25 wt% MgO using the procedure outlined in the section on lithophile trace elements. Generally, the PGE contents in komatiites are high indicating that these magmas formed via high degrees of partial melting. Maier et al. (2009) recognized a broad inverse correlation between the age of the lavas and the degree of enrichment in Pt and Ru, and attributed this phenomenon to progressive mixing of "late veneer" into the mantle. However, Puchtel et al. (2016a, 2020, 2022a,b) pointed out that this simple interpretation is complicated by several additional processes that may have affected the PGE abundances in komatiite mantle sources, such as metal-silicate fractionation, grainy late accretion, and core-mantle interaction.

During differentiation of komatiite lavas, Pt, Pd, and Rh are incompatible with the liquidus mineral assemblage, whereas Os, Ir, and Ru are usually compatible, largely due to co-precipitation of olivine and Os-Ir alloys (Brügman et al., 1987; Barnes et al., 1985; Rehkämper et al., 1999; Puchtel and Humayun, 2000, 2001; Puchtel et al., 2004b). There are some notable exceptions, however, in which Os and Ir also behaved incompatibly, likely due in part to complete exhaustion of IPGE hosts in the mantle source of these komatiites during partial melting (Puchtel and Humayun, 2005; Puchtel et al., 2009b, 2014, 2016a).

Isotopes

Isotopic systems of the lithophile elements (Sm-Nd, Lu-Hf)

Komatiites were recognized as a new class of volcanic rock shortly before the development of the ^{147}Sm-^{143}Nd and ^{176}Lu-^{176}Hf isotopic systems as geochronological tools and tracers of the chemical composition of the mantle. As a result, komatiites were the target of many studies involving these isotopic systems. Early studies, especially those that used the ^{147}Sm-^{143}Nd system (e.g., Hamilton et al., 1977, 1978, 1979, 1983; Jahn et al., 1982; McCulloch and Compston, 1981; Zhuravlev et al., 1987, 1989; Walker et al., 1988), were initially aimed at determining the ages of the volcanic sequences and evolution of the time-integrated Sm/Nd ratios of their mantle sources. Emphasis was placed on this system because of the relative immobility of Sm and Nd during alteration and metamorphism. However, it soon became clear that Sm and Nd and, to a lesser extent, Lu and Hf, can be significantly affected by contamination with crustal materials, which have much higher concentrations of REE and Hf and, if older than the

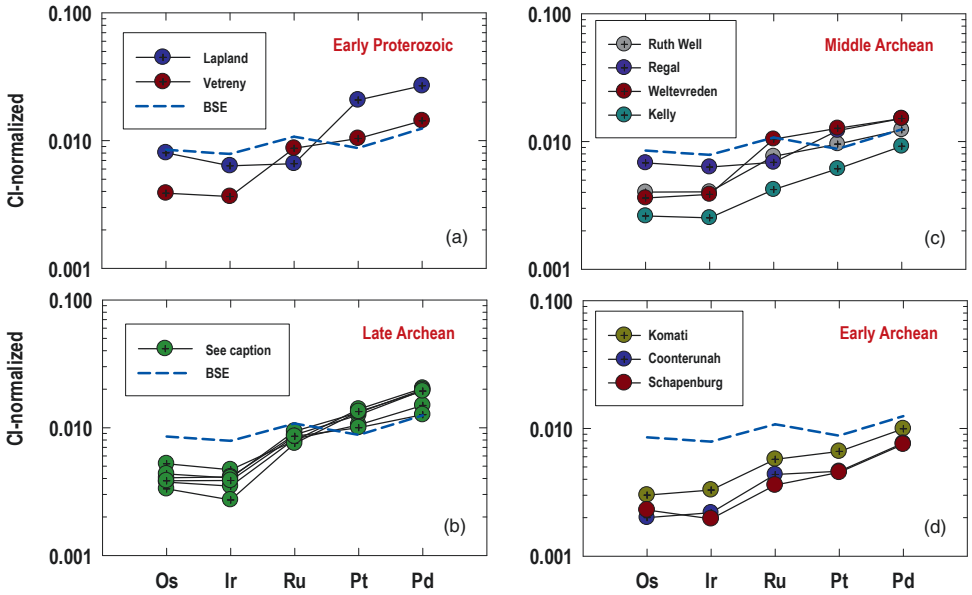

Fig. 9 Cl chondrite-normalized PGE abundances in emplaced early Proterozoic (a) to Archean (b–d) komatiite lavas. The abundances are normalized to 25 wt% MgO following the procedure described earlier. The chondrite-normalizing abundances used are those for the average Orguiel Cl-chondrite from Horan et al. (2003). Data are from Puchtel et al. (2022a and references therein) and Puchtel (2022). In panel (b), the overlapping profiles of late Archean lavas represent komatiites from Belingwe, Pyke Hill, Alexo, Kostomuksha, and Sumozero-Kenozero. The BSE values are from Becker et al. (2006).

komatiites, would be isotopically distinct (e.g., Claoué-Long et al., 1984; Cattell et al., 1984; Chauvel et al., 1985; Lesher and Arndt, 1995; Puchtel et al., 1997). In addition, Rosing (1990), Tourpin et al. (1991), and Gruau et al. (1992, 1996) pointed out that calculated initial isotope ratios were incorrect if secondary alteration or metamorphism had changed the Sm/Nd and Lu/Hf ratios of the rocks several hundred Ma after emplacement. On the other hand, DePaolo and Wasserburg (1979), Walker et al. (1988), Puchtel and Zhuravlev (1993), Blichert-Toft and Puchtel (2010), Puchtel et al. (1998a,b, 1999, 2013, 2016b, 2018, 2020, 2022a) and Tympel et al. (2021) demonstrated that correct ages and initial isotope ratios can be obtained using the Sm-Nd or Lu-Hf systems, particularly if whole rocks from individual differentiated flows or intrusions, or mixtures of whole rocks and mineral separates, were used. The long-lived Sm-Nd and Lu-Hf isotopic systems have been and remain some of the most robust tracers of the composition and depletion/enrichment history of the mantle.

Table 2 presents initial ε^{143}Nd and ε^{176}Hf values that record the compositions of the mantle sources of several komatiite suites. These values were derived from the Sm-Nd and Lu-Hf isochrons obtained for each suite, corrected, where appropriate, for crustal contamination using the lithophile trace element systematics (Puchtel et al., 2022b). The initial ε^{143}Nd and ε^{176}Hf values are all positive, ranging between +0.5 ± 0.4 and + 10 ± 1 and between +1.7 ± 0.6 and + 17.0 ± 0.6, respectively, indicating that all these komatiite suites were derived from sources with long-term trace-element depletion, with fractionation in Lu/Hf much larger than that for Sm/Nd (Fig. 10).

Time-integrated, model-specific Sm/Nd and Lu/Hf ratios in the mantle sources of komatiite suites are plotted in Fig. 11. The individual models assume a minimum-degree fractionation of Sm/Nd and Lu/Hf in the particular mantle domains from either the chondritic values or values defined by the combined ^{142,143}Nd/^{144}Nd systematics to those required to bring the ε^{143}Nd and ε^{176}Hf in the mantle sources to the initial ε^{143}Nd and ε^{176}Hf by the times of the respective komatiite formation.

All komatiites were derived from mantle sources with suprachondritic time-integrated ^{147}Sm/^{144}Nd and ^{176}Lu/^{177}Hf ratios between those of CHUR and DMM (Fig. 11). An important observation is that, while all komatiite suites with ages <3.0 Ga follow the terrestrial Nd-Hf mantle evolution array, indicating long-term "coupled," or congruent, behavior of the Nd and Hf isotope systematics, some suites with ages >3.0 Ga plot above the terrestrial evolution curve, indicating long-term "decoupled" behavior (Puchtel et al., 2022a). This is the case for all komatiites from the Kaapvaal Craton in South Africa, but not for those from the Pilbara Craton in Australia. Proposed reasons for such decoupling are case-specific and include the effects of early magma ocean crystallization (e.g., Caro et al., 2005; Rizo et al., 2011; Puchtel et al., 2013, 2016b; Boyet et al., 2021), recycling of pelagic sediments into the source of the komatiites (Blichert-Toft et al., 2015), long-term storage and re-melting of Hadean proto-crust (Tusch et al., 2022), or, on one occasion, post-emplacement disturbance of one or both isotope systems (Blichert-Toft et al., 2015).

The fact that the isotope data for the majority of late Archean and younger komatiite systems plot on the Nd-Hf mantle evolution curve, whereas those for the early Archean komatiite systems from, e.g., the Kaapvaal Craton, do not, likely indicate that the chemical heterogeneities created by the early magma ocean differentiation processes and recorded by the short-lived isotope systems have been largely erased by vigorous mantle convection by ~2.7 Ga (Tusch et al., 2021, 2022; Puchtel, 2022; Puchtel et al., 2022b; Nakanishi et al., 2023). These data require that survival times of the early heterogeneities within the mantle, before near-complete homogenization, were on average around 1.7 Ga. This estimate represents a constraint on the average mixing rates of the terrestrial mantle in terms of the lithophile elements in the Hadean and Archean.

Table 2 Summary of isotopic features of selected komatiite suites.

Komatiite system	$\varepsilon^{143}Nd(T)$	$\varepsilon^{176}Hf(T)$	$\mu^{142}Nd$	$\mu^{182}W$	$\gamma^{187}Os(T)$	$\mu^{186}Os(T)$	μ_1[a]	*Data sources*
Kaapvaal Craton, South Africa								
Schapenburg	+2.4 ± 0.5	+5.8 ± 0.8	−5.0 ± 2.8	−8.4 ± 4.1	+3.7 ± 0.3			[1–2]
Komati	+0.46 ± 0.39	+1.9 ± 1.0	−0.9 ± 2.7	+2.7 ± 4.5	+0.3 ± 0.3	−12 ± 8	8.78 ± 0.58	[3–6]
Weltevreden	+0.54 ± 0.40	+4.7 ± 2.1	+2.5 ± 3.8		−0.1 ± 0.2	+22 ± 7		[3–4]
Commondale	+2.0 ± 0.5	+6.3 ± 0.7			+0.80 ± 1.8			[7–10]
Pilbara Craton, Western Australia								
Coonterunah	+2.4 ± 0.5	+4.4 ± 0.3		+11.4 ± 4.6				[11]
Kelly	+0.5 ± 0.6	+1.7 ± 0.6		+8.2 ± 3.3	+0.8 ± 0.4			[11]
Ruth Well	+1.3 ± 0.7[b]	+2.4 ± 0.4[b]	−1.8 ± 3.8	+7.7 ± 5.0	−0.4 ± 0.4			[11]
Regal	+1.9 ± 0.3[b]	+4.6 ± 0.8[b]		+7.7 ± 5.0	+0.9 ± 0.3			[11]
Fennoscandian Shield, northern Europe								
Sumozero-Kenozero	+2.7 ± 0.3				+0.5 ± 0.2		8.73 ± 0.20	[12–13]
Kostomuksha	+3.0 ± 0.4	+4.9 ± 0.3	+0.4 ± 0.9	+15.0 ± 4.8	+2.5 ± 0.6	+22 ± 6	8.77 ± 0.10	[5, 14–17]
Vetreny	+3.7 ± 0.4[b]	+6.3 ± 0.9[b]	+0.5 ± 2.1	−0.5 ± 5.2[b]	+1.3 ± 0.2[b]	+3.2 ± 1.7	9.06 ± 0.05	[18–19]
Lapland	+4.9 ± 0.3[b]	+10.2 ± 0.7[b]		−10.0 ± 5.0[b]	−0.2 ± 0.3	+29 ± 2		[20]
Superior Craton, Canada								
Boston Creek	+2.5 ± 0.2	+4.3 ± 0.9	−3.8 ± 2.8	+11.7 ± 4.5	+0.1 ± 0.3			[21]
Pyke Hill-Alexo	+3.0 ± 0.5	+5.5 ± 0.6	+6.8 ± 2.5		+0.4 ± 0.1	−0.1 ± 4.2	8.59 ± 0.18	[22–28]
Winnipegosis					+1.3 ± 1.1			[29–30]
Rhodesian Craton, Zimbabwe								
Belingwe	+2.9 ± 0.2		+3.7 ± 7.0		+0.1 ± 0.2	+0.6 ± 2.5	8.74 ± 0.03	[27, 31–33]
Caribbean Large Igneous Province								
Gorgona komatiites	+9.7 ± 1.2	+17.0 ± 0.6			+0.90 ± 0.60	+97 ± 59		[34–38]
Gorgona picrites	+9.7 ± 1.4				+1.0 ± 1.1			[34, 36, 38]

Data sources are as follows: [1]—Puchtel et al. (2009a); [2]—Puchtel et al. (2016a); [3]—Puchtel et al. (2013); [4]—Puchtel et al. (2014); [5]—Touboul et al. (2012); [6]—Brévart et al. (1986); [7]—Wilson and Carlson (1989); [8]—Wilson et al. (2003); [9]—Hoffmann and Wilson (2017); [10]—Wilson (2019); [11]—Puchtel et al. (2022a); [12]—Puchtel et al. (1999); [13]—Puchtel (2022); [14]—Puchtel et al. (1998a); [15]—Boyet and Carlson (2006); [16]—Puchtel et al. (2005); [17]—Puchtel and Humayun (2005); [18]—Puchtel et al. (1997); [19]—Puchtel et al. (2016b); [20]—Puchtel et al. (2020); [21]—Puchtel et al. (2018); [22]—Dupré et al. (1984); [23]—Carignan et al. (1995); [24]—Blichert-Toft and Arndt (1999); [25]—Puchtel et al. (2004a); [26]—Puchtel et al. (2004b); [27]—Puchtel et al. (2009b); [28]—Debaille et al. (2013); [29]—Waterton et al. (2017); [30]—Waterton et al. (2020); [31]—Boyet and Carlson (2006); [32]—Dupré and Arndt (1990); [33]—Chauvel et al. (1993); [34]—Révillon et al. (2000); [35]—Thompson et al. (2003); [36]—Walker et al. (1999); [37]—Brandon et al. (2003); [38]—Walker et al. (2023).

$\varepsilon^{143}Nd$, $\varepsilon^{176}Hf$—deviations in parts per 10,000 of initial $^{143}Nd/^{144}Nd$ and $^{176}Hf/^{177}Hf$ in a given sample from those in CHUR at the time of lava emplacement. $\mu^{142}Nd$, $\mu^{182}W$—deviations in parts per million of $^{142}Nd/^{144}Nd$ and $^{182}W/^{184}W$ in a given sample from the laboratory reference materials. $\gamma^{187}Os$—percent deviation of $^{187}Os/^{188}Os$ in a given sample from a chondritic reference value at the time of lava emplacement. $\mu^{186}Os$—deviation in part per million of $^{186}Os/^{188}Os$ in a given sample from a chondritic reference value at the time of lava emplacement.

[a]The time-integrated $^{238}U/^{204}Pb$ ratio calculated from the Pb-Pb isotope data. All uncertainties are 2SD of the mean.

[b]Values corrected for AFC.

The short-lived ^{146}Sm-^{142}Nd isotopic system has improved the temporal resolution of the ^{147}Sm-^{143}Nd isotopic system; the two systems have been used in combination to decipher the timing and mechanisms of the earliest mantle differentiation events (Goldstein and Galer, 1992; Harper and Jacobsen, 1992; McCulloch and Bennett, 1993; Sharma et al., 1996; Boyet et al., 2003; Caro et al., 2003, 2006; Boyet and Carlson, 2005, 2006). However, relatively few ^{142}Nd data are available for komatiites (Table 2) and most of these exhibit $\mu^{142}Nd$ values that are indistinguishable from the standard reference value. Exceptions are the komatiites from the Schapenburg and Komati locations, which have small $\mu^{142}Nd$ deficits, averaging −5.0 ± 2.8 (Puchtel et al., 2016b) and −4.0 ± 4.1 (Boyet et al., 2021), respectively, and Theo's Flow, a layered tholeiitic unit from the Abitibi greenstone belt, which has a positive ^{142}Nd anomaly of +6.8 ± 2.5 ppm (Debaille et al., 2013). These data suggest that certain mantle domains sampled by komatiites formed within the first 500 Ma of the Solar System history and survived for at least 1.5 Ga, before being tapped by the respective mantle plumes.

Tungsten isotopic systematics

The short-lived ($t_{½}$ = 8.9 Ma) ^{182}Hf-^{182}W isotope system can be used to trace the early fractionation of a lithophile trace element Hf from a moderately siderophile element W. This system also records processes that occurred within the first ~50 Ma of Solar System history.

The available ^{182}W data for komatiite suites (Table 2) are listed in $\mu^{182}W$ terms. In contrast to ^{142}Nd, the majority exhibit either positive (Pilbara, Kostomuksha, and Boston Creek), or negative (Schapenburg and Lapland) ^{182}W anomalies, with only Komati and Vetreny komatiites having $\mu^{182}W$ values of around 0. These anomalies have been interpreted to result from early magma ocean

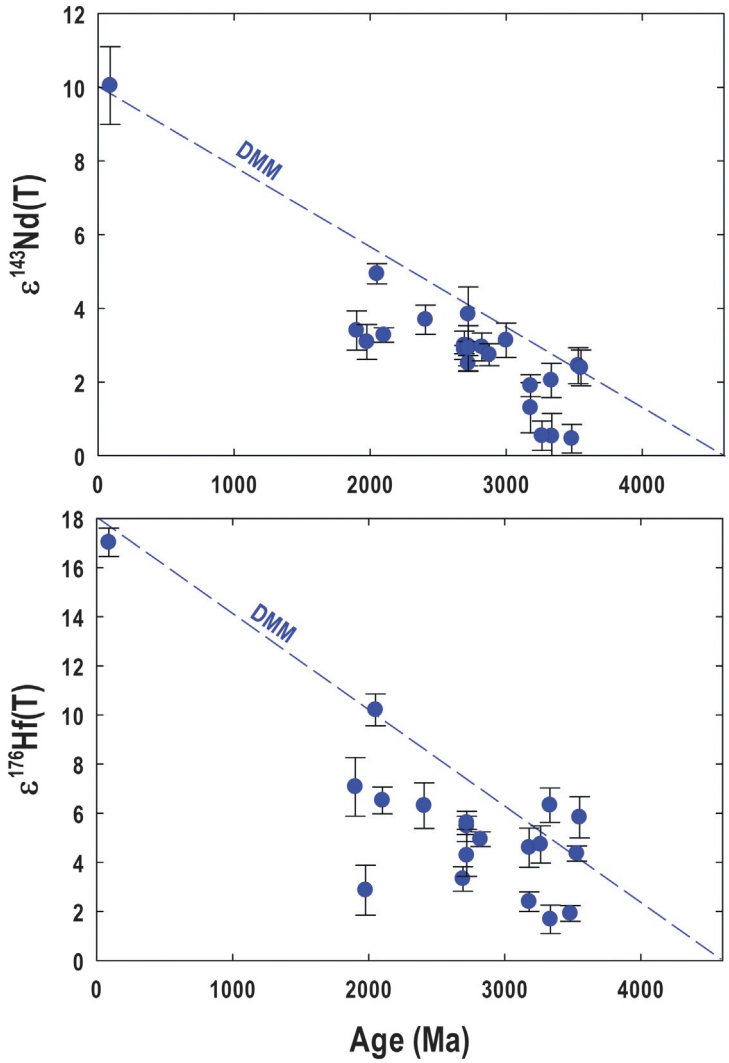

Fig. 10 Diagram illustrating variations of initial ε^{143}Nd and ε^{176}Hf in the mantle sources of komatiite and basalt systems. Data from Puchtel IS, Nicklas RW, Slagle J, Horan M, Walker RJ, Nisbet EG, and Locmelis M (2022a). Early global mantle chemical and isotope heterogeneity revealed by the komatiite-basalt record: The Western Australia connection. *Geochimica et Cosmochimica Acta* 320: 238–278; Puchtel IS, Blichert-Toft J, Horan M, Touboul M, and Walker RJ (2022b). The komatiite testimony to ancient mantle heterogeneity. *Chemical Geology* 594: 120776. Invited Review Article.

crystallization processes (Touboul et al., 2012; Puchtel et al., 2016b), grainy late accretion (Puchtel et al., 2018, 2020, 2022a), recycling of Hadean protocrust (Tusch et al., 2022) or core–mantle interaction (Puchtel et al., 2020).

Osmium isotopic systematics

The ^{187}Re-^{187}Os and ^{190}Pt-^{186}Os isotopic systematics of komatiites provide important information about the composition and depletion history of their mantle sources (e.g., Walker et al., 1988; Brandon et al., 2003; Puchtel et al., 2004a, 2005, 2009a,b). Behaviors of Re, Pt, and Os are governed by their variable, but generally strong, partitioning into metal or sulfide liquid relative to silicate melt (e.g., Crocket et al., 1997; Righter and Drake, 1997). During mantle melting, Os is typically compatible with the melting residue, whereas Pt and Re are incompatible (e.g., Barnes et al., 1985; Rehkämper et al., 1999). The initial ^{186,187}Os/^{188}Os ratios in komatiites record long-term evolution of Pt/Os and Re/Os in the mantle (e.g., Walker et al., 1988, 1991, 1999; Hanski et al., 2001, 2004; Puchtel et al., 2004a, 2005, 2009a,b, 2014, 2020).

The ^{186,187}Os data are listed in Table 2 and plotted in Fig. 12. Most komatiites have γ^{187}Os values within the chondritic range, indicating evolution of mantle sources with time-integrated near-chondritic Re/Os ratios (Fig. 12a). The only exceptions are the Schapenburg and Kostomuksha komatiites, which have more radiogenic γ^{187}Os values of +3.7 and +2.5, respectively, implying that their mantle sources evolved with long-term suprachondritic Re/Os ratios.

Relatively limited ^{186}Os data indicate that, out of the seven komatiite suites in Fig. 12b, only three (Pyke Hill, Belingwe, and Vetreny) have initial μ^{186}Os values that plot within the chondritic range. Sources of the other four komatiite suites evolved with either suprachondritic (Weltevreden, Kostomuksha, Lapland) or subchondritic (Komati) time-integrated Pt/Os ratios. Importantly,

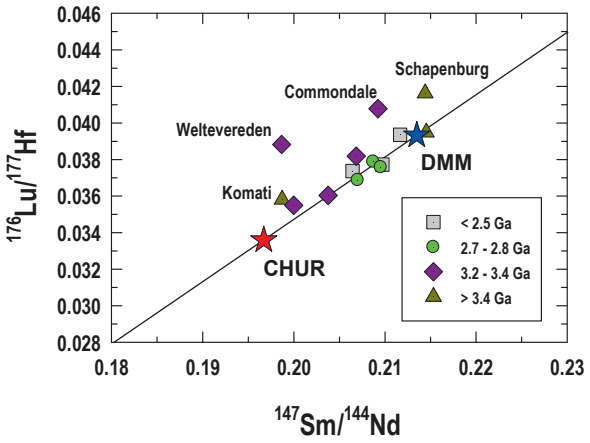

Fig. 11 Variations of time-integrated, model-specific Sm/Nd and Lu/Hf ratios in the mantle sources of komatiite and basalt systems. The individual models assume a minimum-degree fractionation of Sm/Nd and Lu/Hf in the particular mantle domains from either the chondritic values or values defined by the combined $^{142,143}Nd/^{144}Nd$ systematics (where available) to those required to bring the $\varepsilon^{143}Nd$ and $\varepsilon^{176}Hf$ in the mantle sources to the initial $\varepsilon^{143}Nd$ and $\varepsilon^{176}Hf$ by the times of the respective komatiite formation. The solid line connects Sm/Nd and Lu/Hf ratios inferred for the chondritic uniform reservoir (CHUR) and modern depleted mantle (DMM). The CHUR and DMM parameters used are from Jacobsen and Wasserburg (1980), Hamilton et al. (1983), Goldstein et al. (1984), Vervoort and Blichert-Toft (1999), and Bouvier et al. (2008) and are as follows. CHUR: $^{147}Sm/^{144}Nd = 0.1967$, $^{176}Lu/^{177}Hf = 0.03360$, $^{143}Nd/^{144}Nd = 0.512638$, $^{176}Hf/^{177}Hf = 0.282785$; DMM: $^{147}Sm/^{144}Nd = 0.2135$, $^{176}Lu/^{177}Hf = 0.03933$, $^{143}Nd/^{144}Nd = 0.513151$, $^{176}Hf/^{177}Hf = 0.283294$. Figure modified from Puchtel IS, Nicklas RW, Slagle J, Horan M, Walker RJ, Nisbet EG, and Locmelis M (2022a). Early global mantle chemical and isotope heterogeneity revealed by the komatiite-basalt record: The Western Australia connection. *Geochimica et Cosmochimica Acta* 320: 238–278; Puchtel IS, Blichert-Toft J, Horan M, Touboul M, and Walker RJ (2022b). The komatiite testimony to ancient mantle heterogeneity. *Chemical Geology* 594: 120776. Invited Review Article.

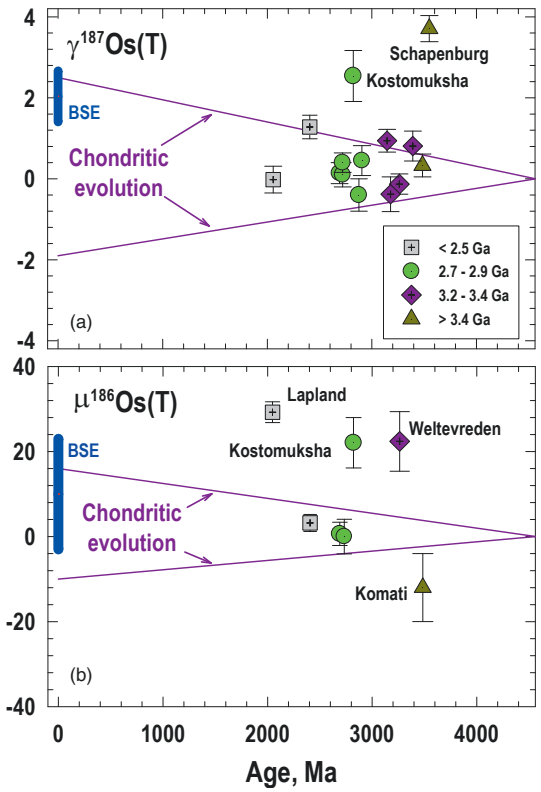

Fig. 12 (a) Initial $\gamma^{187}Os$ and (b) initial $\mu^{186}Os$ of Archean and Proterozoic komatiite systems plotted as a function of their age. The blue bars for the modern BSE estimates represent the 2SD of the mean from Meisel et al. (2001) and Brandon et al. (2006) for (a) and (b), respectively. The data for chondritic meteorites are compiled from Walker et al. (2002), Horan et al. (2003), Brandon et al. (2005, 2006), and Fischer-Gödde et al. (2010) and are plotted as an envelope enclosed between the slanting purple lines and corresponding to the entire range of calculated modern $\gamma^{187}Os$ and $\mu^{186}Os$ values projected back to the Solar System initial ratios. Figure modified from Puchtel IS, Nicklas RW, Slagle J, Horan M, Walker RJ, Nisbet EG, and Locmelis M (2022a). Early global mantle chemical and isotope heterogeneity revealed by the komatiite-basalt record: The Western Australia connection. *Geochimica et Cosmochimica Acta* 320: 238–278; Puchtel IS, Blichert-Toft J, Horan M, Touboul M, and Walker RJ (2022b). The komatiite testimony to ancient mantle heterogeneity. *Chemical Geology* 594: 120776. Invited Review Article and Puchtel IS (2022). Re-Os isotope and HSE abundance systematics of the 2.9 Ga komatiites and basalts from the Sumozero-Kenozero greenstone belt, SE Fennoscandian Shield: Implications for the mixing rates of the mantle. *Petrology* 30(6): 548–566.

of the mantle sources with non-chondritic Re-Os and/or Pt-Os systematics, only in the Kostomuksha source these isotope systems were coupled, i.e., behaved congruently. The processes responsible for the decoupled, or incongruent, behaviors of these systems in the sources of the Komati, Weltevreden, and Lapland komatiites have been argued to include early magma ocean processes (Puchtel et al., 2014), grainy late accretion, and/or core–mantle interaction (Puchtel et al., 2020).

In addition to serving as a tracer of chemical evolution of the mantle, the Re-Os isotope system is a valuable geochronological tool due to the contrasting behaviors or Re and Os during differentiation of mafic and ultramafic magmas after emplacement (e.g., Walker et al., 1988, 1991, 1999; Puchtel et al., 2001, 2005, 2004a, 2009a,b). Because Re is usually concentrated in the residual melt, while Os tends to enter the early crystallizing phases such as Os-Ir alloys (often as inclusions in olivine) and chromite, a large range of Re/Os ratios can be obtained for samples collected across a single differentiated komatiite unit, rendering the Re-Os system the only geochronometer that allows for direct determination of the komatiite emplacement ages. As a result, precise and accurate Re-Os isochrons have been obtained for the Archean and Proterozoic komatiites (Table 2), including Komati, Weltevreden, and Schapenburg in the Kaapvaal Craton (Puchtel et al., 2009b, 2014, 2016a), Alexo, Pyke Hill, and Boston Creek in the Superior Craton (Walker et al., 1988; Lahaye et al., 2001; Gangopadhyay and Walker, 2003; Puchtel et al., 2004a, 2009a, 2018), Belingwe in the Rhodesian Craton (Puchtel et al., 2009a), Kostomuksha, Sumozero-Kenozero, Vetreny, and Lapland in the Fennoscandian Shield (Puchtel et al., 2001, 2005, 2016b, 2020; Gangopadhyay et al., 2006; Moilanen et al., 2019; Puchtel, 2022), and Kelly, Regal, and Ruth Well in Western Australia (Puchtel et al., 2022a), as well as for the 89 Ma Gorgona komatiites (Walker et al., 1991, 1999, 2023).

Lead isotopic systematics

The Pb-Pb isotopic method has been used to date komatiites and to evaluate the time-integrated U/Pb and Th/U ratios of their mantle sources since early 1980s, but with very mixed results. The initial attempts to determine emplacement ages of mafic-ultramafic lavas were promising. These included studies at the Alexo and Pyke Hill localities in the Abitibi belt (Dupré et al., 1984; Brévart et al., 1986; Carignan et al., 1995), Komati Formation in the Barberton belt, Kaapvaal Craton (Brévart et al., 1986), Belingwe belt in the Rhodesian Craton (Chauvel et al., 1993), and Vetreny Belt in Fennoscandia (Puchtel et al., 1997). However, these studies also revealed that the Pb-Pb method can produce ages that are several hundred Ma younger than emplacement ages (e.g., Brévart et al., 1986; Dupré and Arndt, 1990).

As with the other radiogenic isotope systems, such as Sm-Nd, Lu-Hf or Re-Os, obtaining a precise age requires that the samples analyzed had a sufficiently large range of parent/daughter ratios at the time the isotopic system closed. Normally, this large range is achieved via magmatic fractionation of the parent–daughter isotope ratio. Unlike with the Re-Os system, however, U-Pb ratios are not expected to significantly fractionate during differentiation of komatiitic magmas and, therefore, whole-rock samples of unaltered rocks should have the same U/Pb ratios across even strongly differentiated units. Hence, if a Pb-Pb isochron is obtained and it yields a correct emplacement age, the spread in the U/Pb ratios must be due to non-magmatic processes that occurred very close to the time of lava emplacement. Dupré and Arndt (1990) obtained several seemingly correct ages that they attributed to disturbance of the U-Pb system shortly after lava emplacement, likely during seafloor alteration. In all other cases, the U-Pb system was reset later, often as a result of metamorphism, and the Pb-Pb isochron ages were too young. As such, the only way to establish whether a Pb-Pb isochron age is correct is to compare it with the emplacement age obtained using an independent method, which rather defeats the purpose of the exercise.

The initial Pb isotopic compositions of komatiites can be obtained directly by measuring associated magmatic sulfides, which normally contain negligible U and Th abundances. In most cases, however, when sulfides are not available, the initial Pb isotopic composition of a komatiite source can be calculated from $^{207}Pb/^{204}Pb$ vs $^{206}Pb/^{204}Pb$ correlations for a series of samples collected from genetically related komatiites, by making assumptions about the initial Pb isotopic composition of the bulk Earth, its age, and a single-stage evolution until the time of lava emplacement. Using this protocol, a model μ_1 value, or a time-integrated $^{238}U/^{204}Pb$ ratio of the source, is obtained. The time-integrated Th/U ratio of the source of a komatiite can be calculated from the $^{208}Pb/^{204}Pb$ vs $^{206}Pb/^{204}Pb$ correlations using an algorithm similar to that used for calculating the model μ_1 value.

The limited Pb-Pb isotopic data obtained using the procedures outlined above are listed in Table 2. Due to the difficulties in correcting for crustal contamination, the Pb-Pb isotopic data are presented as measured for all localities, including those where crustal contamination has been established using trace element data. The μ_1 values and Th/U ratios for uncontaminated komatiite suites vary in a narrow range, between 8.6–8.8 and 4.1–3.0, respectively, whereas in the crustally contaminated Vetreny Belt lavas, these values are higher, at 9.1 and 4.5, respectively, reflecting Pb isotopic composition dominated by that of the older continental crust (Puchtel et al., 1997). This is also the case for the crustally contaminated komatiites from Kambalda (Dupré and Arndt, 1990) and Belingwe (Chauvel et al., 1993), although the calculated μ_1 values are somewhat lower.

Stable isotopes

Oxygen Studies of oxygen isotopes in komatiites from the Barberton greenstone belt in the 1980s confirmed that the compositions of whole-rock samples are dominated by oxygen introduced during interaction with seawater (e.g., Beaty and Taylor, 1982; Smith et al., 1984). However, analyses of fresh olivine and pyroxene in Archean komatiites from the Yilgarn Craton in Western Australia (Hoefs and Binns, 1978) and the Abitibi belt in Canada (e.g., Lahaye and Arndt, 1996) returned mantle-like $\delta^{18}O$ values between +4.6 and +5.5 relative to VSMOW (the $^{18}O/^{16}O$ of Vienna Standard Mean Ocean Water). More recently, Gurenko et al. (2016) analyzed oxygen isotopes in olivine in komatiites from Gorgona Island and also found mantle-like values, which they advanced as

evidence that the elevated abundances of water and other volatiles in these rocks had a deep-mantle origin. Byerly et al. (2017) found relatively light oxygen isotopic compositions ($\delta^{18}O = +3.81 \pm 0.20$) in olivine in komatiites from Weltevreden in South Africa, which they attributed to mantle heterogeneities left over from a Hadean magma ocean. This interpretation has been questioned by Wang et al. (2023), who attributed the low isotope ratios to the presence of secondary serpentine and magnetite in the olivine fractions that were analyzed by Byerly et al. (2017). Finally, Zakharov and Bindeman (2019) used the results of triple oxygen isotopic analysis of komatiites from the Vetreny Belt in Fennoscandia to constrain the isotopic composition of Paleoproterozoic seawater.

Sulfur Recognition of mass-independent fractionation of sulfur isotopes (MIF-S) in the oxygen-poor Archean atmosphere by Farquhar et al. (2000) and Farquhar and Wing (2003) has provided an invaluable tool for tracing the origin and evolution of komatiites. Mass-independent fractionation of sulfur isotopes is restricted to the Archean, and this phanomenon has been employed in two ways. First, it has been used to confirm the role of assimilation of crustal sulfur during the formation of Archean komatiite-hosted NiS deposits. The distinctive sulfur isotope composition ($\delta^{34}S$) of sedimentary rocks has long been used as evidence for the assimilation of sedimentary sulfur during the formation of the ore deposits at Kambalda in Western Australia and elsewhere (e.g., Bavinton, 1981). This relationship was confirmed by more recent studies that demonstrated that the sulfides in these deposits have MIF-S signatures that are different from those of the mantle and close to those of sedimentary rocks intercalated with the komatiites (e.g., Bekker et al., 2009; Fiorentini et al., 2012; Hiebert et al., 2016).

A second application is illustrated by Kubota et al. (2022), who documented MIF sulfur anomalies in komatiites from the Belingwe belt in Zimbabwe. They use these results to propose that Archean oceanic crust had been recycled into the mantle and incorporated into the source of these komatiites.

Boron Gurenko et al. (2016) measured boron isotopes in olivine and melt inclusions in komatiites from Gorgona Island and found a range in $\delta^{11}B$ values from −11.5 to +15.6 that they attributed to the presence of hydrous fluids in the deep-mantle source of these rocks. Sobolev et al. (2016) found heavy B isotope ratios ($\delta^{11}B = -3.8 \pm 6.8‰$) in a sample of komatiite from the Alexo komatiite flow that had been contaminated with crustal rocks, and mantle-like ratios ($\delta^{11}B = -13 \pm 11‰$) in fresh olivine in a non-contaminated komatiite. For these authors, the mantle-like values in the non-contaminated komatiite indicated that the small amount of water in these komatiites (Shimizu et al., 2001; Sobolev et al., 2016) was acquired during interaction with hydrous material in the mantle transition zone.

Hydrogen Sobolev et al. (2019) analyzed hydrogen isotopes in inclusions in olivine from the Alexo komatiite and found δD (VSMOW) values that are positive and well above those reported for the crust and mantle. The proposed explanation for these data was contamination of the komatiite by hydrated rocks, such as sediments or serpentinites, during fractional crystallization of olivine. The calculated δD (VSMOW) of the parental komatiite magma is negative, providing additional evidence for a deep, hydrated mantle source.

Helium Two studies have documented unusually high $^3He/^4He$ ratios in Archean komatiites. Richard et al. (1996) and Matsumoto et al. (2002) obtained R/Ra values (where R is the measured $^3He/^4He$ ratio and Ra is the ratio in the present day atmosphere) between 30 and 70 in Alexo and Pyke Hill komatiites in the Abitibi belt. These elevated R/Ra values, which are attributed to the presence of primordial, undegassed material that had been stored deep in the mantle, provide additional evidence of a deep source of these komatiites.

Révillon et al. (2002) reported high R/Ra values (8–18 Ra) in olivines extracted from ~89 Ma komatiites of Gorgona Island, a result confirmed by Sumino et al. (2023) who found similar values in chromites from these komatiites. These results indicate derivation of the komatiites from a deep, incompletely degassed mantle source.

Transition elements Iron isotopes have been used to help understand the differentiation within a komatiite flow from Alexo in Ontario (Dauphas et al., 2010), while the similarity of Fe isotopic compositions in Archean and younger komatiites has been taken as evidence that the oxidation state of the Archean mantle was not significantly different from that of the modern mantle (Hibbert et al., 2012; Wagner et al., 2021).

Analyses of Mo (Greber et al., 2015), Ti (Greber et al., 2017), Sr (Amsellem et al., 2018), Zn (Sossi et al., 2018), Ca (Amsellem et al., 2019), Zr (Tian et al., 2020), and Cr (Jerram et al., 2020; Wagner et al., 2021) isotopes have helped define the isotopic composition of the Bulk Silicate Earth. Copper isotope data obtained by Savage et al. (2015) demonstrated that the fractionated Cu isotopic composition of the BSE relative to that inferred for the bulk Earth based on chondritic meteorites requires that a sufide-rich liquid segregated from the mantle and entered the core during early differentiation of the planet.

Geological/geodynamic setting of komatiite formation

Given our limited knowledge of the geodynamic regimes that existed in the Archean, significant uncertainty surrounds any reconstruction of the geological/geodynamic setting in which komatiite lavas erupted. For all komatiites, the geological environment can be best estimated from the nature of the rocks that are spatially and temporally associated with the lavas, as well as from the broader geological context. Any assessment of the komatiite eruptive setting must take into consideration the unique features of the Archean environment, including a hotter mantle (e.g., Richter, 1985, 1988; Takahashi, 1990; Nisbet et al., 1993; Abbott et al., 1994; Herzberg et al., 2010) and thicker oceanic crust (e.g., Sleep and Windley, 1982; McKenzie and Bickle, 1988). When these considerations are taken into account, it appears that komatiites erupted in a diversity of geodynamic settings, including ocean basins, island arcs, and continental platforms; these settings are briefly described below.

The usual habitat of Archean komatiites has been termed mafic plains, or oceanic plateaus (Condie, 1975; Dimroth et al., 1978, 1982; Card, 1990; Storey et al., 1991; Kusky and Kidd, 1992; Desrochers et al., 1993; Kimura et al., 1993; Abbott, 1996; Kent et al., 1996; Puchtel et al., 1998a; Arndt et al., 2001). Mafic plains are characterized by voluminous, laterally extensive, originally horizontally emplaced sequences of thick, mafic and ultramafic, pillowed or massive, lava flows. The volcanic units are interlayered with cherts and shallow-water terrigenous sediments and thin bands of felsic volcanic rock (Dann, 2000; De Wit and Ashwal, 1997; Bickle and Nisbet, 1993; Bickle et al., 1994; Cowden, 1988; Card, 1990; Dostal and Mueller, 1997). In this setting, sequences of mafic and ultramafic lava flows can be traced for tens to hundreds of kilometers along strike (e.g., Hill et al., 1995; Hill, 2001) indicating that large volumes of low-viscosity mafic-ultramafic lava erupted rapidly onto a near-horizontal surface to form an extensive submarine volcanic plain (Dimroth et al., 1982, 1985). The modern tectonic setting that most closely resembles that of Archean mafic plains is an oceanic plateau such as Ontong Java or Caribbean (e.g., Coffin and Gahagan, 1995; Kent et al., 1996; Kerr et al., 1997; Neal et al., 1997).

In some greenstone belts, komatiites are spatially associated with tholeiitic or calc-alkaline, mafic to felsic, lavas and pyroclastic rocks (e.g., Barnes et al., 1988; Dostal and Mueller, 1997; Wyman et al., 1998; Hollings et al., 1999; Puchtel et al., 1999; Hill et al., 2004). Many (e.g., Polat and Kerrich, 1999, 2001, 2002), but not all authors (e.g., Barnes et al., 2021) interpret the chemical compositions of the calc-alkaline rocks to indicate that they are related to subduction processes, as discussed in a later section.

Some komatiites appear to have erupted in a continental setting. For example, Nisbet et al. (1977) and Bickle et al. (1993, 1994) argued that the volcanic and sedimentary rocks of the Belingwe greenstone belt in the Rhodesian Craton were deposited on an older gneissic basement. The sequence in the type-area consists of a basal conglomerate containing clasts of granitic rocks from the basement, overlain by shallow water quartz sandstones associated with cherts and BIF. The overlying Reliance Formation consists almost entirely of komatiites and komatiitic basalts. Additional evidence for eruption of Belingwe komatiites onto a continental basement is afforded by the lithophile trace element and Sm-Nd and Pb-Pb isotope systematics (Chauvel et al., 1993), which indicate that the volcanic rocks were contaminated with older granitic crust en route to the surface, and discovery of xenoliths of crustal material in these komatiites (Shimizu et al., 2004).

At Kambalda in the Yilgarn Craton of Western Australia, the most convincing evidence for a continental setting of komatiite emplacement is geochemical. The lithophile trace element and Sm-Nd isotopic compositions indicate that these volcanic rocks assimilated up to 25% of granitic crust that was ~500 Ma older than the komatiites (Chauvel et al., 1985; Barley, 1986; Lesher and Arndt, 1995). Moreover, Compston et al. (1986) and Claoué-Long et al. (1988) separated zircon from the komatiites and showed that these minerals had ages up to 3.5 Ga and, thus, were xenocrysts from older granitic rocks that komatiitic magmas had assimilated on their way to the surface.

Furthermore, the Kambalda volcanic sequence contains cherts and pillow lavas indicating that the continental platform was submerged below sea level at the time of komatiite eruption, an occurrence that is very rare in modern geodynamic settings, but was common in the Archean (Arndt, 1999). This may indicate that sea levels were higher during periods of flood volcanism, perhaps because the ocean basins were filled with extensive, active, and high-standing oceanic ridges or oceanic plateaus, or because the oceans were more voluminous (e.g., Rosas and Korenaga, 2021).

The question of how komatiites could have erupted in such diverse tectonic settings can be answered if it is accepted that these magmas form in mantle plumes that originated deep in the mantle. If so, a mantle plume does not know what it will meet at the surface, be it an oceanic plateau, an island arc, or a continental plate, although the degree of decompression melting that can occur may be limited by the ability of a plume to upwell. For example, the plume's ascent can be impeded by thick continental roots (Davies et al., 2015), although most komatiite melts likely separate from their source well below the base of the lithosphere, as discussed in a later section.

Also relevant is the sheer volume of the mafic-ultramafic magmas that erupted onto the surface and what this implies for the volume and dynamics of the source. For example, Coffin and Eldholm (1993) estimated that the source of the Ontong Java oceanic plateau, based on the volume of the erupted lavas, had a diameter of as much as 1400 km and extended into the lower mantle. Adding the contemporaneous and spatially closely associated Manihiki and Hikurangi plateaus almost doubles this volume. A rising plume of that size, with a head of more than 1000 km in diameter, would either shove aside any tectonic plate that it would meet near the surface, or dramatically weaken the continental lithosphere and cause rifting and subsequent opening of ocean basins (Courtillot et al., 1999). If a starting mantle plume encountered a subducting slab of mantle lithosphere, it would likely disrupt or even terminate subduction at the site of impact. In that case, subduction-related volcanism will be followed by plume-derived lavas, as appears to have happened when the Triassic Wrangellia oceanic plateau erupted onto an older island arc (Lassiter et al., 1995; Greene et al., 2010), and most probably in parts of the Abitibi and Sumozero-Kenozero greenstone belts, where sequences of komatiites and basalts alternate with suites dominated by calc-alkaline volcanic rocks (Puchtel et al., 1999; Ayer et al., 2002; Wyman et al., 2002). As other parts of the slab continued to subduct, calc-alkaline volcanics intermingled with mafic-ultramafic lavas freely flowing from the site of plume impact. The association of komatiites with calc-alkaline and felsic volcanics, therefore, most likely reflects the conquest of part of a subduction zone by a plume, with the two magma types coming from completely separate sources.

Basalts and associated volcanic rocks

Low-K tholeiitic basalt is the most abundant component of the supracrustal sequences in Archean granite-greenstone belts. These, the so-called "monotonous Archean tholeiites" of Hallberg (1972), typically comprise 50–70% of all greenstone belt sequences,

the remainder being komatiites, calc-alkaline mafic to felsic volcanic rocks, and chemical or clastic sedimentary rocks. For descriptions of the tholeiites, we will initially draw on the work of the generations of field geologists who mapped in detail the exposures in the Abitibi belt of the Southern Superior Province of Canada. We made this choice because the region has many favorable characteristics compared to other regions of similar age: the volcanic rocks are commonly very well exposed in large glacially-polished outcrops, the metamorphic grade and degree of deformation are relatively low, and the rocks are not affected by tropical weathering. In addition, a large variety of volcanic rocks have been recognized and geochemically analyzed, and the stratigraphy is relatively well understood thanks to numerous detailed mapping and comprehensive geochronological studies. In the following sections, we summarize the field-based information before moving on to discuss the petrology and geochemistry. We then compare the compositions of the Abitibi rocks with those of some other Archean regions, notably those of the Yilgarn and Pilbara Cratons in Australia, and with some modern analogs, before speculating on the origin of the volcanic rocks and the tectonic settings in which they erupted.

Thurston et al. (2008) have summarized the stratigraphic relationships between the main volcanic and sedimentary units in the Abitibi belt. As shown in Table 3, seven major volcanic assemblages are recognized, most of which are separated by relatively thin sedimentary units. Although tholeiitic basalt is present in almost all these units, commonly as the dominant component, each of the units also contains other volcanic rock types. Komatiites are present in four units (Pacaud, Stoughton-Roquemaure, Kidd-Munro, and Tisdale) and two others are made up almost entirely of calc-alkaline mafic to felsic volcanics (e.g., Deloro and the upper Blake River Group). Successor basins filled with turbiditic or alluvial-fluvial sedimentary rocks overlie the volcano-sedimentary units.

Distinction between different basalt types

In addition to geochemical criteria, field and petrological criteria have been used to distinguish the three main basalt types in Archean greenstone belts. In the Abitibi belt, the different types are found in different volcanic assemblages and are indeed used to help define these assemblages. For example, komatiitic basalts are associated with komatiites and alternate with packages of tholeiitic basalts in the four assemblages listed above; tholeiitic basalt is the dominant component of the lower Tisdale and Blake River assemblages; and calc-alkaline basalts accompany intermediate to felsic volcanics in several other assemblages.

Komatiitic basalts

These rocks are the mafic members of the komatiitic magma series (Arndt and Brooks, 1980). Their MgO contents range between 9 and 18 wt%, the lower limit for komatiite, and the more evolved members have compositions similar to tholeiitic basalts. They are commonly, but not always, spatially associated with ultramafic komatiites. In some cases, their komatiitic character is signaled by the presence of pyroxene or olivine spinifex texture, which is their only definitive diagnostic feature (Sun and Nesbitt, 1978). Arndt et al. (1977) list several other criteria, such as color and grain size, that distinguish komatiitic and tholeiitic basalts, but these apply only to the volcanic rocks in the stratigraphically lower parts of the Abitibi belt, where the tholeiites are unusually rich in iron. In the younger parts of the Abitibi volcanic sequence, and in other greenstone belts, there is little to distinguish the two types of basalt.

Many komatiitic basalt flows are strongly differentiated into an upper spinifex-textured layer, an intermediate layer of fine-grained massive basalt, and lower portions composed of olivine and pyroxene cumulates. This is the case for thick (>100 m) layered flows, such as Fred's Flow in the Abitibi belt (Arndt, 1977b; Siégel et al., 2014), and similar units in the Belingwe belt (Nisbet et al., 1977), the Yilgarn Craton (Hill et al., 1995), and the Vetreny Belt in Fennoscandia (Puchtel et al., 1996). Other komatiitic basalt flows are massive throughout, or pillowed and brecciated. They tend to be thicker than Archean tholeiitic flows. Detailed descriptions of the field characteristics and petrography of komatiitic basalts are provided by Viljoen and Viljoen (1969), Nisbet et al. (1977), Arndt et al. (1977), Francis and Hynes (1979), Cameron and Nisbet (1982), Bickle and Nisbet (1993), Puchtel et al. (1996, 1997), Dann (2000), and Wilson (2019).

Table 3 Simplified stratigraphy of the Abitibi Belt.

Successor basins
- *Timiskaming 2677–2670 Ma*—fluvial and deltaic sandstones, conglomerates
- *Porcupine 2690–2685 Ma*—turbidites

Volcano-sedimentary assemblages
- *Upper Blake River 2701–2695 Ma*—tholeiitic and calc-alkaline mafic to felsic volcanics
- *Lower Blake River 2704–2701 Ma*—minor clastic metasediments overlain by Mg and Fe tholeiites with minor tholeiitic andesite, dacite, and rhyolite.
- *Upper Tisdale 2706–2704 Ma*—calc-alkaline felsic flows and volcanoclastics
- *Lower Tisdale 2710–2706 Ma*—tholeiitic basalts with minor komatiite and intermediate to felsic volcanics
- *Upper Kidd-Munro 2717–2711 Ma*—tholeiitic basalts with minor komatiite and intermediate to felsic volcanics
- *Lower Kidd-Munro 2719–2717 Ma*—calc-alkaline intermediate to felsic volcanics
- *Stoughton-Roquemaure 2723–2720 Ma*—tholeiitic basalts with komatiites and local felsic volcanic rocks
- *Deloro 2734–2724 Ma*—mafic to felsic calc-alkaline volcanic rocks with local tholeiitic basalts
- *Pacaud 2750–2735 Ma*—komatiite, tholeiitic basalt, felsic volcanics
- *Unnamed unit* ca. *2766 Ma*- intermediate to felsic pyroclastic rocks

Adapted from Thurston PC, Ayer JA, Goutier J, and Hamilton MA (2008) Depositional gaps in abitibi greenstone belt stratigraphy: A key to exploration for syngenetic mineralization. *Economic Geology* 103: 1097–1134.

Tholeiitic basalts

The best descriptions of the morphological features of these volcanic rocks are found in relatively old papers, such as Hargreaves and Ayres (1979), Wells et al. (1979), and Dimroth et al. (1982), who present excellent maps, sketches, and photos showing how the rocks appear in the field and in thin sections. The tholeiitic basalts erupted mainly as massive sheet flows that in places grade into, or are interlayered with, pillowed lava. Volcaniclastics are rare, being largely limited to intra-pillow hyaloclastite or thin interflow layers. Flow thickness varies from a few meters to several tens of meters for the biggest sheet flows. Maximum flow lengths are difficult to establish because of lack of continuous outcrop, but certain flows with distinctive characteristics, such as the variolitic units that are important marker horizons in the Timmins area in Ontario, have been traced for tens of kilometers. The orientation of drainage cavities in pillows have been used to infer that the ocean floor onto which the flows erupted was flat and monotonous, with slopes rarely exceeding 1–2°.

A notable feature of a tholeiitic basaltic sequence is the near absence of interflow sedimentary rocks (Thurston et al., 2008). Cherts, iron formations, and clastic sediments are present at contacts between different volcanic assemblages, but not between individual lava flows. Their absence, together with the large size and continuity of the sheet flows, is taken as evidence for high effusion rates of the lavas, with short or negligible times of repose between eruptions. The presence of pillowed lava and rare interflow sediment indicates that the eruptions were subaqueous, probably submarine. An absence of indicators of a shallow water setting, such as highly vesicular lava and current indicators in the sedimentary rocks, provides evidence of deep-water eruption for most basalts.

Mafic-ultramafic intrusions invade the volcanic sequences. Some consist entirely of gabbro, while others are differentiated into lower ultramafic cumulate portions and upper gabbro to diorite portions. In places, the upper contacts transition laterally from being clearly intrusive, as evidenced by cross-cutting contacts and chilled margins, to extrusive, as indicated by the presence of flow-top breccias intermingled with sedimentary rocks. These features demonstrate that at least some of the intrusions were contemporaneous with the volcanic rocks (Viljoen and Viljoen, 1969; Arndt, 1977b; Bickle and Nisbet, 1993). Although mafic dykes are common, they are usually less affected by metamorphism than the volcanic rocks they intrude and often can be shown to form parts of younger dyke swarms (e.g., Ernst and Bleeker, 2010; Stepanova et al., 2014, 2015).

The field characteristics of the tholeiitic basaltic sequences in Archean greenstone belts are strikingly similar to those of the basalts in Cretaceous oceanic plateaus. Common features are the predominance of massive sheet flows, the considerable thicknesses and lengths of these flows, eruption into deep water onto near-flat surfaces, and high effusion rates with little to no periods of repose. In contrast, certain features of modern mid-ocean ridge settings, such as a rugged topography with localized eruption centers and fault escarpments and contemporaneous dykes (e.g., Kennish and Lutz, 1998), are missing. However, it should be noted that the above features are common only at slow-spreading ridges and largely absent in modern fast-spreading centers.

A feature that distinguishes sequences of Archean tholeiites from their modern counterparts is the ubiquitous presence of felsic volcanic rock in the former. Even within the ca. 10-km-thick Lower Blake River assemblage in the Abitibi belt of Canada, which consists almost entirely of tholeiitic basalt and minor chemical sediments, thin (5–20 m), laterally persistent layers of rhyolitic or trachytic pyroclastic rock appear at regular intervals (Thurston et al., 2008). Such units are absent from more recent oceanic plateaus such as Ontong Java and Wrangellia (Neal et al., 1997; Greene et al., 2010), and their presence in the Archean sequences may signal differences in geodynamic setting.

The mineralogy, textures, and types of alteration of Archean tholeiites resemble those of their modern counterparts, particularly those in oceanic plateaus. Archean tholeiites have relatively evolved compositions compared to those of primary mantle melts and consist mainly of plagioclase, clinopyroxene, iron oxides, and volcanic glass, whose abundance depends on the position within the flow (Gélinas and Brooks, 1974; Hargreaves and Ayres, 1979; Wells et al., 1979; Dimroth et al., 1982). As in modern examples, glass is the dominant phase in hyaloclastites, common in the margins of pillows, and rare to absent in massive sheet flows. The morphologies of the main minerals also vary, from dendritic or skeletal where cooling rates were high, to coarser and more equant in slowly cooled flow interiors. Unlike modern MORB or ocean plateau basalts, in which olivine is a common phenocryst phase, this mineral appears to be largely absent from Archean tholeiites.

All Archean volcanic rocks are altered, initially on the seafloor and subsequently during the metamorphism and deformation that accompanied accretion of the greenstone sequences to the continents (Jolly, 1982; Cloete, 1999). The least affected samples display low-grade, prehnite-pumpellyite to greenschist facies assemblages that probably were acquired during circulation of hydrothermal fluids through the submarine volcanic pile (Jolly, 1982; Dupré et al., 1984). Superimposed on these are regional metamorphic upper greenschist to amphibolite facies assemblages. Still higher grades are observed in what are termed gneiss belts, i.e., continental crustal segments exhumed from deeper crustal levels. The volcanic rocks in these belts rarely retain their original petrological and geochemical characteristics and, as such, are not discussed in this chapter.

Calc-alkaline volcanics

There is little in the morphological features, petrography, and mineralogy to distinguish Archean calc-alkaline basalts from their tholeiitic or komatiitic counterparts. Large, laterally extensive sheet flows may be less common, but this may be due only to the more rugged topography onto which they erupted. The key distinguishing feature (apart from the geochemical criteria discussed in Section Geochemistry of Archean basalts) is the association with relatively rare andesitic flows and fragmental rocks, and more abundant dacitic to rhyolitic lava flows, domes, and volcaniclastic rocks. These assemblages occur in shield volcanoes that are built on the flat plains dominated by tholeiitic basalts. The volcanic structures are very similar to those in modern island arcs, as described by, e.g., De Rosen-Spence et al. (1980) and Mueller and Mortensen (2002). Evidence of subaerial eruption in the stratigraphically higher levels of these structures is provided by a higher vesicularity in the pillowed lavas and the presence of airfall tuffs.

One notable difference is the absence of strongly porphyritic Archean basalts and intermediate rocks. Andesites rich in feldspar phenocrysts are common in modern calc-alkaline suites but rare in the Archean.

Geochemistry of Archean basalts

Barnes et al. (2021) proposed a comprehensive classification of Archean basalts based on the relative proportions of the trace elements Th, La, and Nb. These elements were chosen because they are relatively impervious to alteration and because they allow the tectonic setting of the basalts to be identified (Sun and Nesbitt, 1978; Jochum et al., 1991). We have simplified their approach and have selected just three of their seven categories to represent the main types of Archean basalt, as shown in Fig. 13. The three types are (1) Low-La basalt ("Low and High-La" basalts of Barnes et al., 2021), which have nearly flat BSE-normalized trace element patterns without conspicuous anomalies. This type broadly corresponds to the monotonous Archean tholeiites that dominate many greenstone successions. (2) High-La basalt, which comprises both the "High-La" and "High-Th" types of Barnes et al. (2021). In these basalts, the incompatible trace elements are moderately to strongly enriched and negative Nb-Ta and Ti anomalies are pronounced. Included in this category are calc-alkaline basalts associated with intermediate to felsic volcanic rocks, and basalts with similar geochemical features that are interpreted as crust-contaminated komatiites. (3) The third type, high Nb/Th basalts, are also enriched in incompatible trace elements, but lack negative Nb-Ta anomalies. Also included in the Barnes et al. (2021) classification are Fe-rich picrites, a distinctive rock type with high MgO and FeO and strongly enriched incompatible elements and two others, "Low Nb/Yb" and "boninites," whose abundance and significance are difficult to evaluate.

The major element contents of Archean tholeiitic basalts (low-La) and calc-alkaline basalts (high-La) are similar in many respects to those of their modern counterparts. Most Archean basalts have relatively evolved compositions, with MgO contents between ~4 and 12 wt% and Mg# from ~40 to 57 (Figs. 14 and 15). The majority of tholeiites have relatively low concentrations of K and other incompatible elements and they plot on Fe-enrichment trends in MgO-FeO-alkali diagrams. As shown in Fig. 13, their REE and mantle-normalized trace-element patterns vary from almost flat to slightly depleted, or moderately enriched, in incompatible trace elements.

Contamination of mafic-ultramafic magmas with granitoids or sedimentary rocks from the continental crust results in an enrichment of incompatible trace elements and negative Nb-Ta anomalies. Sun et al. (1989) identified a population of basalts with moderate to high MgO contents (10–16 wt%) accompanied by elevated SiO_2 contents (51–55 wt%), the so-called "siliceous high-magnesian basalts." The more evolved members of this series have chemical compositions that are very similar to those

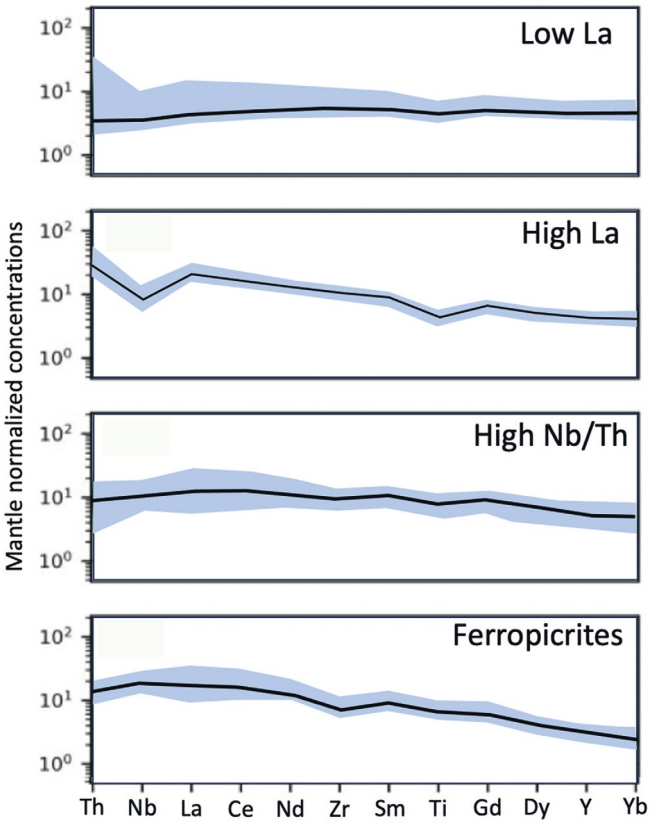

Fig. 13 BSE-normalized trace element patterns of four main types of Archean basalt. Modified from Barnes SJ, Williams M, Smithies RH, Hanski E, and Lowrey JR (2021). Trace element contents of mantle-derived magmas through time. Journal of Petrology 62(6): 1–38.

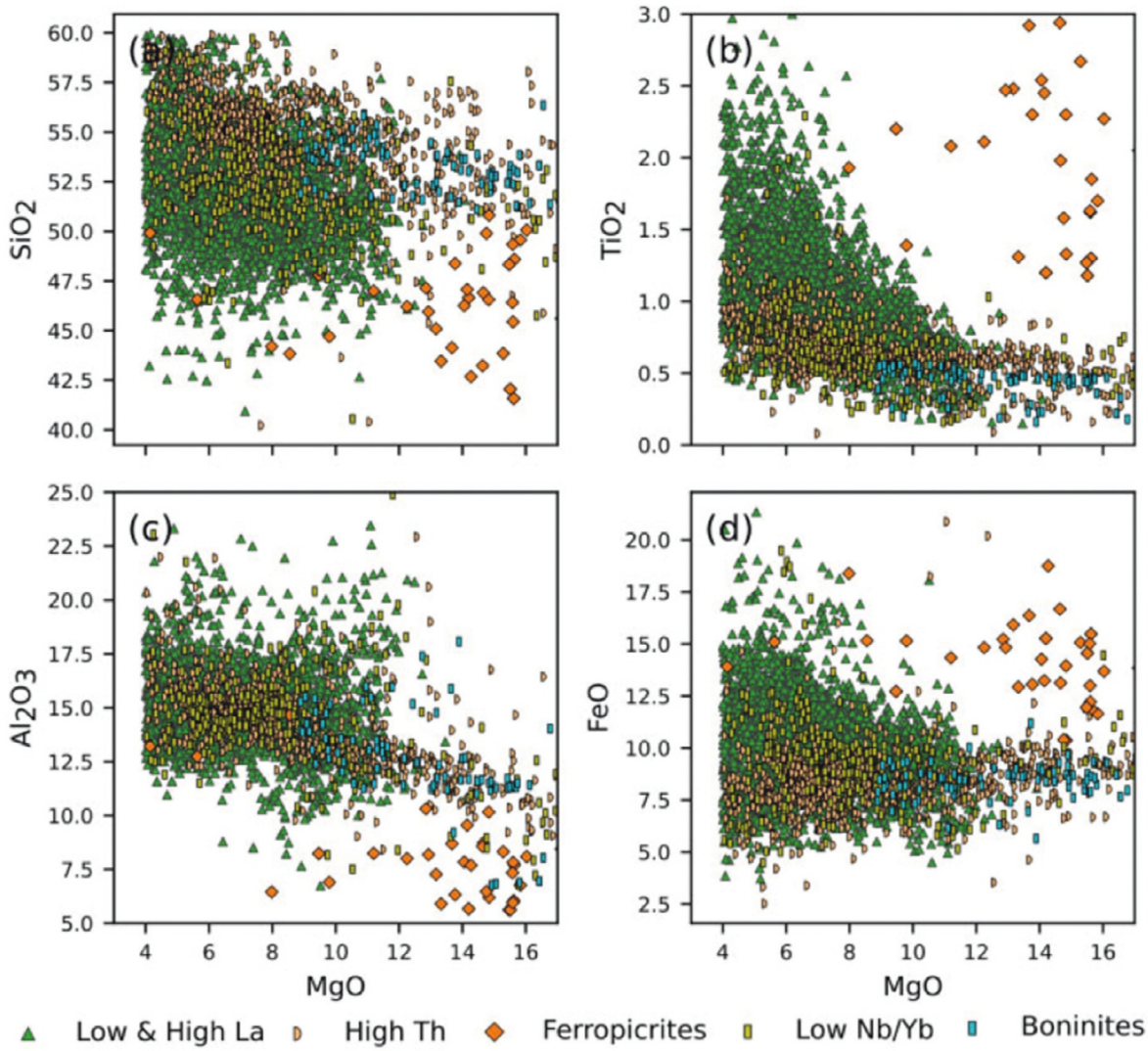

Fig. 14 Major element compositions of Archean basalts (a–d). From Barnes SJ, Williams M, Smithies RH, Hanski E, and Lowrey JR (2021). Trace element contents of mantle-derived magmas through time. *Journal of Petrology* 62(6): 1–38.

of the demonstrably calc-alkaline basalts, and, as discussed by Barnes et al. (2021), distinction between the two types is not straightforward (Fig. 16).

When their compositions are not dominated by the effects of crustal contamination, komatiitic basalts are geochemically similar to Archean tholeiites. MgO contents in layered mafic-ultramafic lava flows range from 15–18 wt% in flow-top breccias and spinifex layers, to about 5 wt% in central gabbroic portions. In the stratigraphically lower formations of the Abitibi belt, the mafic parts of layered flows, and associated thinner undifferentiated lava flows, have lower FeO and TiO_2 contents than associated tholeiites, but this distinction is not seen in other areas.

Comparisons with modern basalts

When Barnes et al. (2021) compared the compositions of Archean tholeiites with basalts from modern mid-ocean ridges and oceanic plateaus, they found that, while there was major overlap for most elements, there were also some significant differences. The Mg# (MgO/(MgO + FeO), mol. %, all Fe expressed as FeO^{total}) of Archean basalts (35–60) are lower than those of modern mid-ocean ridge basalts (55–67; Barnes et al., 2021), but similar to those in Phanerozoic oceanic plateau basalts. At a given Mg#, the TiO_2 and La contents of Archean basalts are much lower than in modern MORB and slightly lower than in modern oceanic plateau basalts, while SiO_2, Ni, and Cr contents are slightly higher.

The major and trace element characteristics of Archean calc-alkaline basalts resemble those of basalts in modern subduction settings. Certain trace-element ratios differ, however. Barnes and Arndt (2019) showed that in a large compilation of Archean basalts, very few samples had the combination of strong depletion of incompatible elements ($(La/Sm)_N \ll 1$) and large negative

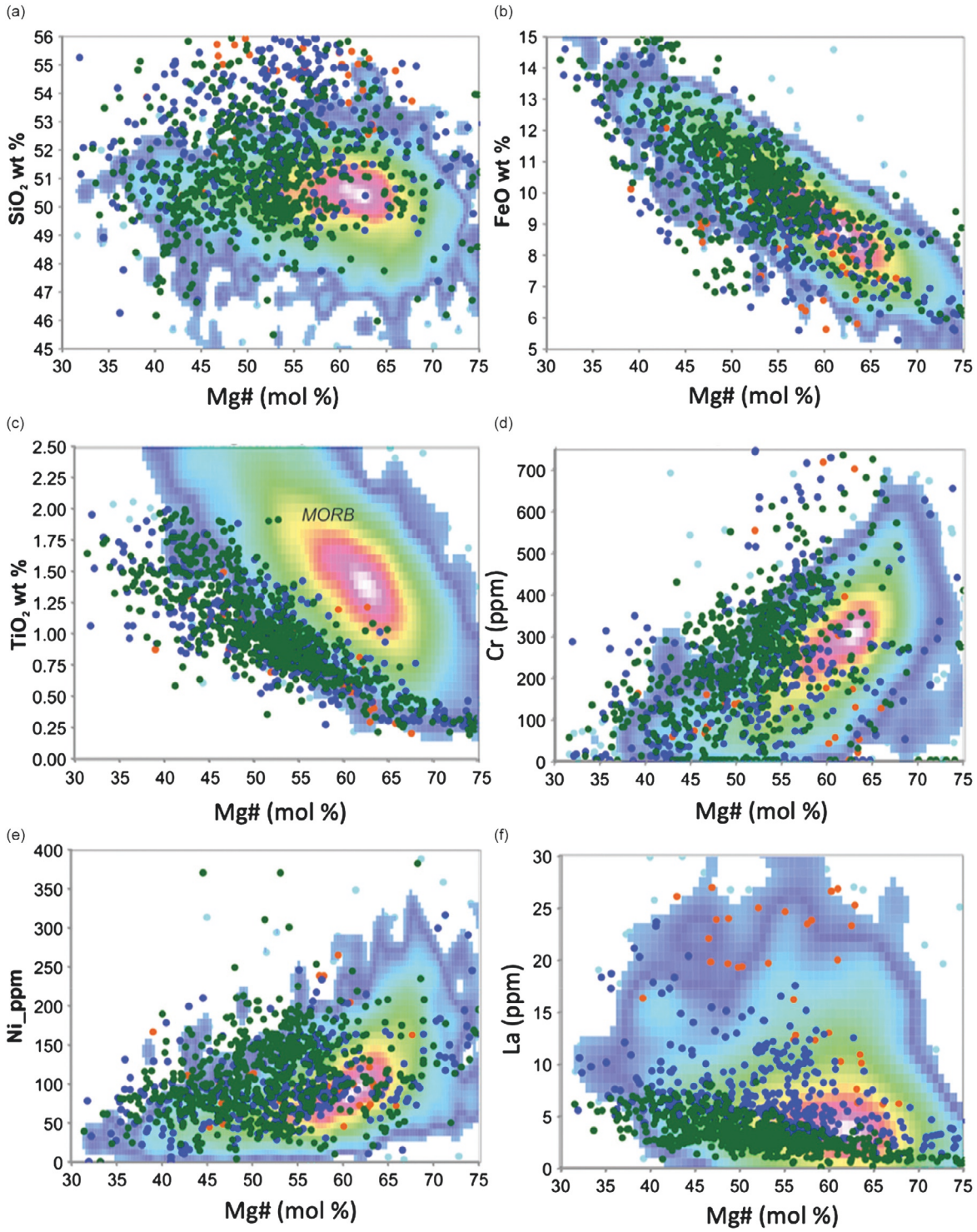

Fig. 15 Comparison between the compositions of Archean basalts with those of modern mid-ocean ridge basalts (a–f). From Barnes SJ and Arndt NT (2019). Distribution and geochemistry of komatiites and basalts through the Archean. In: Van Kranendonk MJ, Bennett VC, and Hoffmann E (eds.). *Earth's Oldest Rocks*, 2nd edn. pp. 103–132. Amsterdam: Elsevier.

Nb-Ta anomalies, a combination that is found in many basalts in modern subduction settings. Although moderate-sized Nb-Ta anomalies are present in most Archean calc-alkaline basalts, these anomalies are invariably accompanied by relative enrichment of the incompatible elements. A comparison can be made between those Archean basalts that are thought to have been contaminated with continental crustal material and basalts with similar origins in continental large igneous provinces. For example, the enrichment of incompatible elements and negative Nb-Ta anomalies of the low-Ti picrites and basalts from the Siberian Traps (Lightfoot et al., 1990) resemble those of the Archean volcanic rocks.

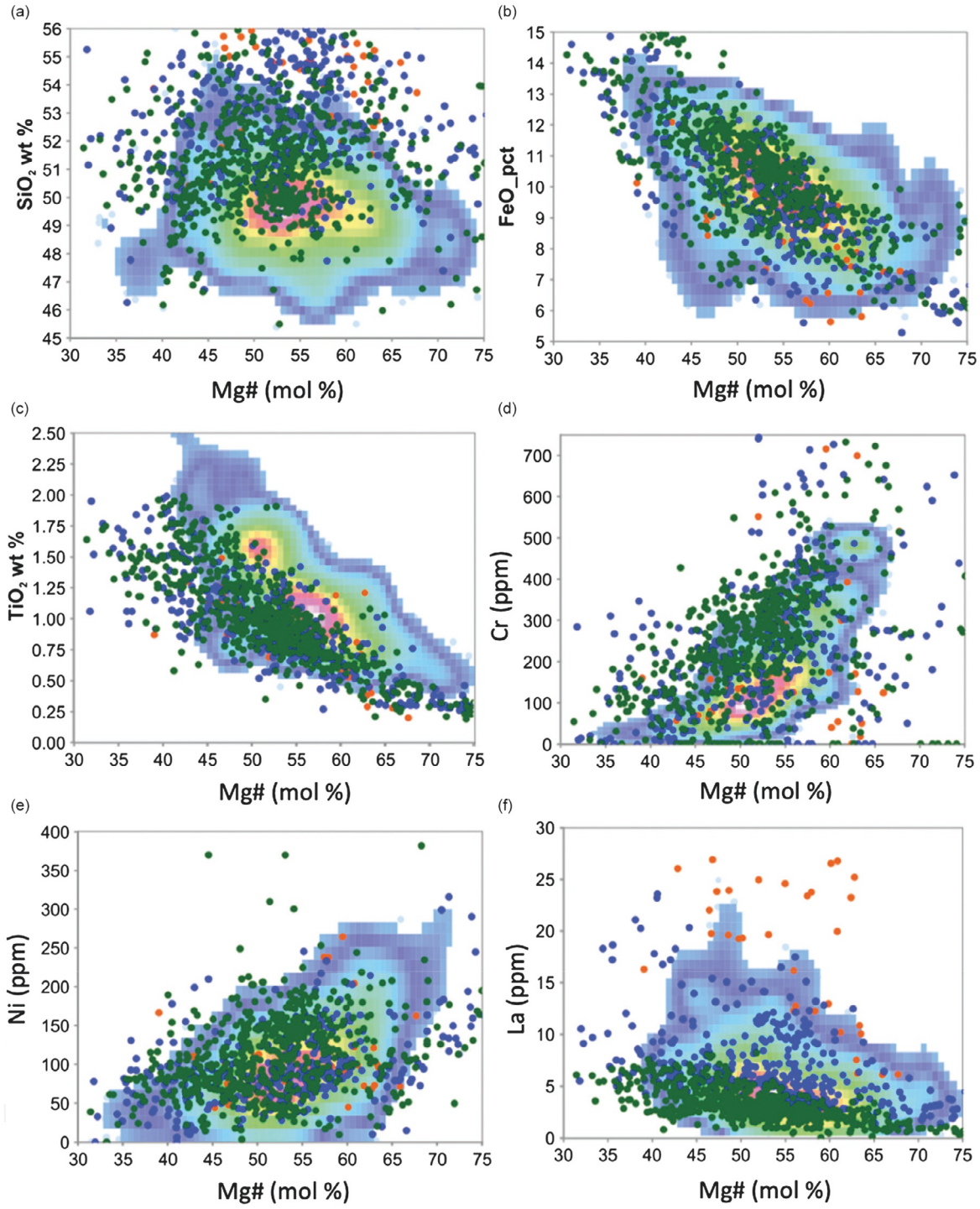

Fig. 16 Comparison between the compositions of Archean basalts with those of modern oceanic plateau basalts (a–f). From Barnes SJ and Arndt NT (2019). Distribution and geochemistry of komatiites and basalts through the Archean. In: Van Kranendonk MJ, Bennett VC, and Hoffmann E (eds.). *Earth's Oldest Rocks*, 2nd edn. pp. 103–132. Amsterdam: Elsevier.

The few Phanerozoic examples of komatiitic basalts have compositions that differ from those of the Archean rocks. The D-basalts from Gorgona Island have slightly depleted trace element patterns resembling those of modern mid-ocean ridge basalts and they share the relatively high Al_2O_3/TiO_2 ratios of Gorgona komatiites (Fig. 7; Kerr et al., 1996). The major and trace element patterns in Proterozoic komatiitic basalts from Gilmour Island in Canada resemble those of Al-undepleted komatiites, but for lower MgO contents and higher concentrations of all elements incompatible with olivine (Arndt et al., 1987) (Fig. 17).

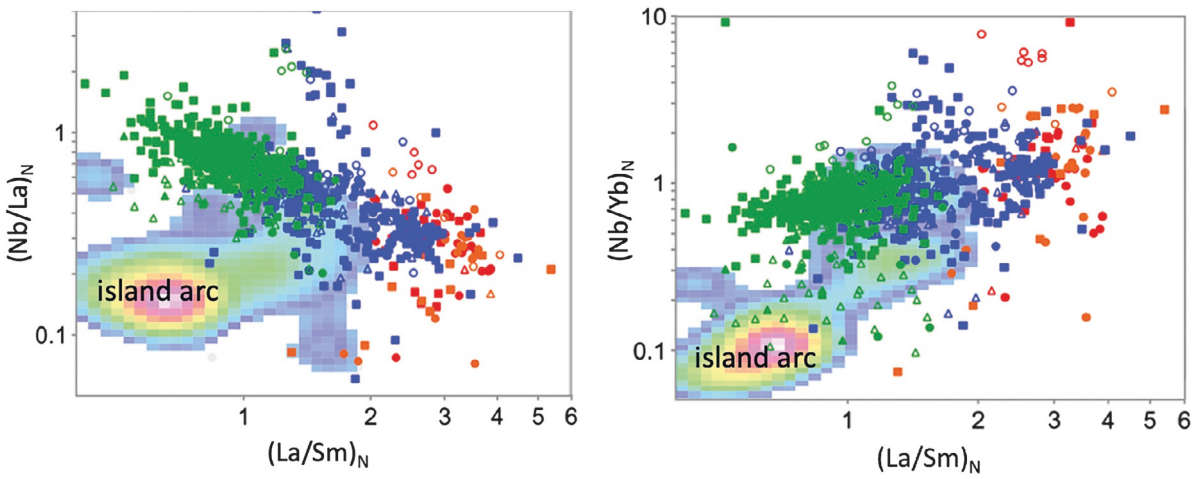

Fig. 17 Trace element ratios that illustrate some differences between the compositions of Archean basalts and those of basalts from modern subduction settings. From Barnes SJ and Arndt NT (2019). Distribution and geochemistry of komatiites and basalts through the Archean. In: Van Kranendonk MJ, Bennett VC, and Hoffmann E (eds.). *Earth's Oldest Rocks*, 2nd edn. pp. 103–132. Amsterdam: Elsevier.

Isotopic compositions

With very few exceptions (e.g., Shirey and Hanson, 1986), isotopic analyses of Archean basalts were carried out in conjunction with analyses of komatiites and in most cases, the initial Nd and Hf isotopic compositions of the basalts turned out to be very similar to those of their ultramafic counterparts. The compositions of basalts define a trajectory that monitors progressive departure from chondritic compositions of their mantle source (Fig. 10). There appear to be no systematic differences between the isotopic compositions of komatiitic and tholeiitic basalts. Neodymium isotopic analyses of whole-rock samples from differentiated flows and intrusions of both komatiitic and tholeiitic lineages, and clinopyroxenes from these samples, defined isochrons with correct ages and initial isotopic ratios that are also similar to those of associated komatiites and tholeiites (DePaolo and Wasserburg, 1979; Zindler, 1982; Chauvel et al., 1985; Machado et al., 1986; Barrie and Shirey, 1991; Puchtel et al., 1998a, 1999). Likewise, the few available Nd isotopic analyses of Archean calc-alkaline volcanic rocks, such as those from the Olondo greenstone belt in the Aldan Shield (Puchtel and Zhuravlev, 1993), Sura greenstone belt in the Ukrainian Shield (Zhuravlev et al., 1987), the Abitibi belt in Canada (Vervoort et al., 1994; Barrie et al., 1999), and the Belingwe and Barberton belts in South Africa (Hamilton et al., 1977, 1979) are identical, within uncertainties, to those of nearby tholeiiites and komatiites. As shown in Fig. 10, more radiogenic Nd isotopic compositions are only seen in Proterozoic basalts, such as those from the Cape Smith Belt of Canada (Arndt et al., 1987; Smith and Ludden, 1989). Basalts from the Eskimo Formation on the Belcher Islands and a layered sill intruding the Povungnituk Group have εNd(T) values down to −8, which are attributed to contamination with Archean continental crust (Arndt et al., 1987).

Analyses of Sr isotopic composition were carried out concurrently with the early Nd isotope studies, but with very few exceptions (e.g., Zhuravlev et al., 1987), these studies did not yield useful data, mainly because of the well-documented mobility of both Rb and Sr. Some potentially useful results were obtained by Machado et al. (1986), who applied a rigorous leaching procedure on clinopyroxene separates, but this approach does not seem to have been adopted in later studies. The avenue may now be open for in situ Rb-Sr analyses of pyroxenes using modern high-resolution mass spectrometers. As with Nd and Sr, analyses of stable isotopes were usually carried out as parts of studies that focused on komatiites.

The concentrations of PGE in Archean komatiitic basalts and tholeiites have been reported in several publications (e.g., Puchtel and Humayun, 2000; Puchtel et al., 2016b, 2022a; Puchtel, 2022). The IPGE concentrations are lower in komatiitic basalts than in komatiites, although PPGE abundances are similar. In tholeiites, both IPGE and PPGE are much lower than in komatiites. Due to relatively low Os and high Re abundances, both komatiitic basalts and especially tholeiites are characterized by high Re/Os ratios and radiogenic measured $^{187}Os/^{188}Os$ compositions. As a result of large age corrections for ^{187}Re decay, komatiitic basalts and tholeiites are usually of little use for constraining the initial Os isotopic compositions of their mantle sources. However, when used in combination with komatiites and primary olivine and chromite, these samples can be useful for obtaining precise emplacement ages of komatiite-basalt sequences (e.g., Walker et al., 1999, 2023; Puchtel et al., 2022a; Puchtel, 2022).

Origin of komatiites

Komatiites were most common during the Archean and, during this eon, may have been the second most abundant type of volcanic rock after basalt, comprising as much as 25% of certain volcanic sequences, with an average abundance of ~10% (e.g., Condie, 1975, 1981, 1994; De Wit and Ashwal, 1997). Some of these basalts were derived from komatiites via fractional crystallization, while

others were lower-degree partial melts generated from the same sources as the spatially associated komatiites (Arndt et al., 1977; Campbell et al., 1989; Condie, 2005). The decline in the abundance of komatiites at the Archean-Proterozoic boundary, as well as the decrease in MgO contents of komatiites, have been taken as evidence for significant, up to 300 °C, secular cooling of the mantle over the course of Earth history (e.g., Bickle, 1982, 1986; Nisbet et al., 1993; Herzberg et al., 2007; Herzberg and Gazel, 2009; Campbell and Griffiths, 2014).

The origin of komatiites has been studied for the past half century (e.g., Green, 1975, 1981; Green et al., 1975; Arndt, 1977a; Nesbitt et al., 1979; Allègre, 1982; Arndt et al., 1998, 2008; Parman et al., 2001, 2004; Berry et al., 2008; Sobolev et al., 2016, 2019; Sossi et al., 2016; Asafov et al., 2018). A common interpretation is that the magmas parental to komatiites were produced in unusually hot mantle plumes (e.g., Cawthorn, 1975; Campbell et al., 1989; Griffiths and Campbell, 1990; Richards et al., 1991; Loper, 1991; Herzberg, 1992, 1995; Richard et al., 1996). The initially solid mantle plume material partially melted upon reaching shallower depths as a result of decompression. Based on experimental data, Campbell et al. (1989) argued that komatiites were produced in the hotter plume core or tail which contained mostly materials derived from near the thermal boundary layer, whereas spatially associated basalts were generated in the cooler plume head which, upon arrival near the surface, would have contained a substantial amount of entrained upper mantle material. However, later studies (e.g., Farnetani and Richards, 1995; Jones et al., 2016) argued that such entrainment was unlikely to contribute significantly to the erupted melts. The distribution of komatiites and basalts in the Caribbean oceanic plateau and in Archean greenstone belts provides little support for the "head and tail" model for the formation of the two magma types. The lavas that erupted from the "tails" of the plumes that produced volcanic plateaus such as in the North (Greenland-Iceland) and South Atlantic (Parana-Etendeka) are less magnesian than those in the plateaus themselves suggesting that the distribution of hot and cooler portions of the plume was more complicated than implied by the "head and tail" model.

Dry, damp or wet melting?

Brooks and Hart (1974), Allègre (1982), Grove et al. (1997), and Parman et al. (1997, 2001, 2004) have argued that komatiites in general, and lavas from the Komati Formation in South Africa in particular, were produced in an Archean subduction environment via hydrous melting of the mantle at temperatures similar to, or only slightly higher than, those of the ambient upper mantle. An important initial condition of the hypothesis as advanced by Grove, Parman, and co-authors is the requirement that the Komati komatiites represent intrusive bodies, since only under pressure does water escape outgassing and persist in the magma as it crystallizes (Grove et al., 1997). According to the hydrous komatiite model of Parman et al. (1997, 2001), the presence of water determined both the crystallization sequence and composition of the magmatic minerals of the Komati komatiites. Parman et al. (1997) carried out a detailed experimental study crystallizing material of komatiitic composition under both anhydrous and hydrous conditions, paying particular attention to the composition of the crystallizing pyroxene. Using the pyroxene compositions, these authors estimated that the original Komati komatiite contained between 4 and 6 wt% H_2O. In their follow-up review paper, Grove and Parman (2004) argued that the Archean mantle was only $\leq$100 °C hotter than the modern mantle, offering a view on the thermal evolution of the Earth that contrasts with the assumption of a substantially hotter Archean mantle (e.g., Richter, 1985, 1988; Bickle, 1986; Nisbet et al., 1993; Herzberg et al., 2007, 2010). The wet komatiite hypothesis has since largely fallen out of favor, with most authors recognizing that the measurement of low water contents in melt inclusions (described in the following sections) provides evidence of a near-anhydrous origin for most komatiites.

Studies of komatiitic olivine melt inclusions led Shimizu et al. (2001), Sobolev et al. (2016, 2019) and Asafov et al. (2018) to argue for moderate water contents, between 0.5 and 1.0 wt%, in some komatiite magmas. Berry et al. (2008) also argued, on the basis of $Fe^{3+}/[Fe^{2+}+Fe^{3+}]$ in melt inclusions being around 0.1, that komatiites could not have undergone significant H_2 or H_2O degassing and must have contained much less than 1.5 wt% H_2O, originally. Both Shimizu et al. (2001) and Sobolev and co-authors proposed that water was added to rising, dry plume material from a hydrated layer at the top of the mantle transition zone (MTZ). The existence of a hydrous layer was predicted at 410 km by Bercovici and Karato (2003) in their MTZ water filter model (Fig. 18).

Depth and pressure at the site of melting

Estimates of mantle potential temperatures ($\mathbf{T}_p$°C) for the sources of komatiites, the liquidus temperatures of erupted komatiite lavas ($\mathbf{T}_{liq}$°C) and depths of melting initiation in mantle plumes ($\mathbf{D}_{melt\ init}$), are presented in Table 1, with the details of the calculation algorithm provided in the referenced publications.

The estimated depths of melting initiation range between ~600 and 160 km, while liquidus temperatures vary between 1650 °C and 1460 °C. The apparent depth of melting initiation tends to decrease from 3.6 Ga and 89 Ma. This is also reflected in the ~240 °C decrease in mantle potential temperatures of komatiite sources from 1890 °C to 1650 °C and a corresponding decrease in the MgO contents of emplaced komatiite lavas from ~30 to 20 wt% over the same period. Exceptions are the komatiites from the 3.3 Ga Commondale locality, which are nominated by Wilson (2019) as the world's hottest magmas with ~36 wt% MgO, and the 2.7 Ga Murphy Well komatiite, which contained ~32% MgO and was, thus, hotter than most Early- to Mesoarchean komatiites (Siégel et al., 2014). From 2.7 Ga, the temperatures of komatiites generally decline, and some lavas from the 89 Ma Caribbean oceanic plateau stand out as anomalies. The Gorgona and Tortugal picrites have MgO contents in the emplaced picritic liquids of up to 27 wt% and liquidus temperatures of 1590 °C, values similar to those for late Archean komatiites and ~400 °C higher than

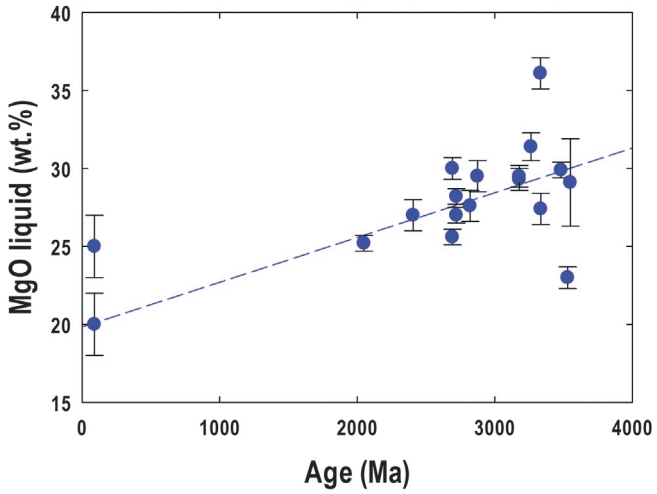

Fig. 18 Variation of the estimates MgO contents of komatiite parental liquids through time. Data from Table 1.

modern ambient mantle (Révillon et al., 2000; Trela et al., 2017). Given the paucity of data in the period between 1.8 Ga and 250 Ma, there is no convincing evidence of an abrupt decline in temperature at the end of the Archean.

A complementary method for estimating conditions and processes at the site of melting is to consider the major and trace element compositions of komatiites. The similarity between the ultramafic composition of komatiites and that of mantle peridotite led many authors to propose that these magmas formed by high degrees of partial melting of their mantle source (e.g., Green et al., 1975; Arndt, 1977a; Nesbitt et al., 1979; Nisbet and Walker, 1982; ; Herzberg and Ohtani, 1988; Herzberg, 1992; Walter, 1998). Quantitative estimates of the degree of melting can be made using trace element concentrations. For example, the concentration of the moderately incompatible element Ti constrains the amount of partial melting because this element is little affected by source enrichment or depletion, nor by garnet fractionation (Hofmann, 1997). At moderate to high degrees of melting, Ti behaves incompatibly and its concentration is inversely correlated with the degree of melting. Assuming a BSE-like mantle source with 0.18 wt% TiO_2 (Hofmann, 1988), we estimate that the degree of partial melting for Al-depleted komatiites was between 30% and 45%. If Al-undepleted komatiites formed by melting of a source with the composition of the Bulk Silicate Earth, the estimated degree of melting ranges from ~30% to an unrealistic 90%. However, if the source was depleted and had a lower TiO_2 content, the estimated degrees of melting would be lower. In the following sections, we propose that fractional melting lowered the concentrations of incompatible elements in the sources of many komatiites.

The ratios of incompatible to compatible elements provide additional constraints. The relative depletion of heavy REE and the low Al_2O_3/TiO_2 ratios of Al-depleted komatiites require that garnet was a residual phase during partial melting. This feature, in combination with their high MgO contents and elevated degrees of partial melting, places the site of melting at a pressure exceeding 10 GPa (~300 km depth) and a temperature close to 2000 °C if the phase relations determined by Herzberg et al. (2010) are used. Sossi et al. (2016) used the melting relations of Walter (1998) to derive somewhat lower (yet still high) pressures between 7 and 9 GPa.

In Al-undepleted komatiites, the relative depletion of the more incompatible elements needs to be taken into account. It is generally accepted that a similar feature in modern N-MORB results from the extraction of a component enriched in incompatible elements leaving a residue depleted in these elements. For modern MORB, this depletion is thought to have happened long in the past, but for Al-undepleted komatiites, there are indications that this event was synchronous with the melting that produced the komatiites themselves, as discussed in the following section.

Fractional versus batch melting; pooling of melts

Estimations of mantle potential temperatures and depths of melting, such as those listed in Table 1, depend on the assumption that the magmas formed either by batch melting or by the accumulation of fractional melts. In the first process, melt is assumed to collect within the source until it reaches a certain level when it escapes in a single pulse; in the second process, the melts escape the source as they form and these melts pool or mix before reaching the surface. Neither process alone is likely to operate during the formation of komatiites, however. Ultramafic melts have very low viscosities, which facilitate their escape once a small melt fraction, probably less than 2%, is attained. To reach the 30% or more of partial melting estimated from the trace element characteristics of komatiites, another process must have facilitated the accumulation of melt within the source, or the source had a more refractory composition, i.e., lower concentrations of incompatible trace elements, in which case the calculated degree of melting would be lower.

Melt versus solid densities

Ohtani (1984), Agee and Walker (1988, 1993), Miller et al. (1991), and Agee (1998) proposed, on the basis of their experimental studies, that silicate melt is more compressible and becomes denser than mantle solids at some depth in the mantle. A postulated negative buoyancy of the melt at depths greater than 8 GPa then formed the basis of models in which certain komatiites are said to have been generated by up to 50% batch melting (e.g., Robin-Popieul et al., 2012; Sossi et al., 2016; Schmeling and Arndt, 2017). More recent experimental work by Suzuki and Ohtani (2003) and Sakamaki et al. (2010) has shown, however, that (a) the pressure interval where the komatiite is denser than olivine shrinks to 13–15 GPa and (b) that the ultramafic melts are never denser than the normal mantle assemblage of olivine and garnet. This result calls into question the notion that komatiites can form as batch melts. Waterton and Arndt (2023) discuss this issue in more detail.

The timing of depletion in the sources of komatiites

The best evidence for the timing of depletion comes from the komatiites and basalts from Gorgona Island. These magmas share similar initial Nd and Hf isotopic compositions indicating that they came from a common source, but they display a large variation in the extent of depletion of incompatible trace elements. Révillon et al. (2000) explained these characteristics using a fractional melting model in which a low-degree enriched melt escapes the source deep in the mantle leaving a depleted residue that subsequently melts to produce first moderately depleted komatiite, then highly depleted picrite (Fig. 19). The fact that these magmas found their way to the surface tells us that they did not pool within the magma conduit or a sub-surface magma chamber, calling into question the notion that these komatiites are accumulated fractional melts.

For Archean Al-undepleted komatiites, a similar process may have operated. Fig. 20 plots the time-integrated $^{147}Sm/^{144}Nd$ ratios of komatiite mantle sources, calculated from the measured $^{143}Nd/^{144}Nd$ composition and the emplacement age of the lavas, as outlined in Fig. 11, against the present-day $^{147}Sm/^{144}Nd$ measured in the emplaced lavas. It can be seen that the calculated time-integrated ratios of the mantle sources vary within a very narrow range, while the measured values are widely dispersed. The explanation is that the wide variation of $^{147}Sm/^{144}Nd$ in the lavas, and the strong depletion in many of them, resulted from extraction of an enriched component synchronous with the generation of the komatiite melts. In other words, a fractional melting process, similar to that proposed for Gorgona (Arndt et al., 1997), probably operated during the generation of Archean komatiites.

A similar process can be advocated for the extremely depleted komatiites such as those from the Commondale or Weltevreden localities. Although it has been suggested that the source of these lavas was depleted peridotite from subcontinental lithosphere, it is difficult to envision how such refractory material could melt without being swamped by more voluminous melts from materials with lower melting temperatures, both within the lithosphere and from underlying asthenosphere or a mantle

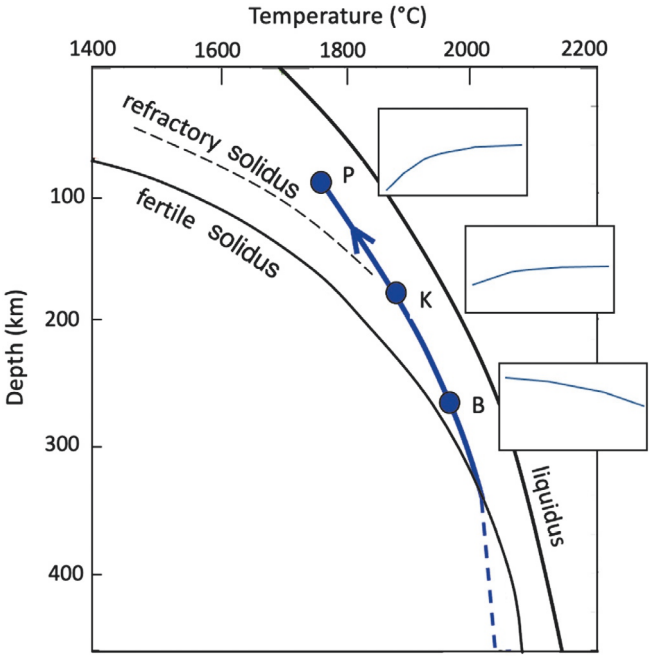

Fig. 19 Diagram illustrating how the fractional melting mechanism can explain the formation of magmas from Gorgona Island. At point B, a low-degree basaltic melt escapes and leaves a refractory residue. This residue melts at point K producing komatiite. The still more refractory residue with its refractory solidus melts again at point P producing picrites with strongly depleted incompatible trace element patterns.

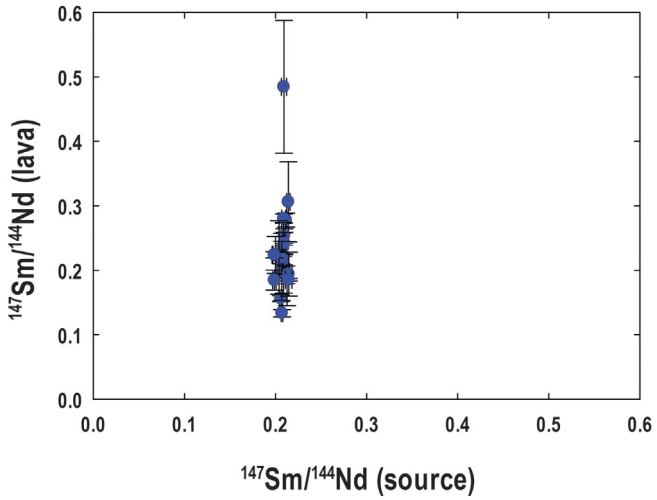

Fig. 20 Calculated time-integrated Sm/Nd ratios in komatiite mantle sources plotted against measured Sm/Nd ratios in emplaced komatiite lavas. Data are from Table 2.

plume. The most likely explanation is that these komatiites were produced by extreme fractional melting. The incompatible elements were removed during the early escape of a small fraction of highly enriched basaltic melt prior to melting of the highly depleted residue that produced the komatiite melt.

Eruption and crystallization

The large range of textures and volcanic structures in komatiites has been linked to the physical properties of komatiitic magmas. These include the high liquidus temperatures and low viscosity of komatiitic liquids, which allowed them to rapidly reach the surface and flow freely, as well as to produce differentiation and layering even in relatively thin flows. Equally important is the wide temperature interval between the liquidus temperature, where olivine, the main liquidus mineral in komatiites, starts to crystallize, and the temperature of the onset of crystallization of the second silicate mineral, usually clinopyroxene. For a komatiite liquid with 30 wt% MgO, this temperature interval is ~400 °C compared to ~50 °C in a typical basalt. This large temperature interval is one of the reasons for the strong internal differentiation commonly exhibited by even relatively thin komatiite lava flows.

The role of superheating (i.e., heating above liquidus temperatures) of the komatiite melt is debated. Donaldson (1979) and Lofgren (1980, 1983) have shown experimentally that a period of superheating strongly influences the subsequent crystallization history of a silicate liquid. The process of heating a silicate melt above its liquidus breaks down the structure of the liquid, destroying the chains and networks that act as nuclei during crystallization on subsequent cooling. A liquid subjected to this process crystallizes quite differently from the one that was never superheated. Superheated liquids display a reluctance to nucleate when cooled, and the crystals that do form tend to be few, large, and skeletal, a process that contributes to the formation of spinifex texture (e.g., Donaldson, 1982). A role of superheating has been questioned by several authors who note the presence of phenocrysts in chilled margins, but Lofgren (1983) has argued that even though phenocrysts may form when a superheated melt is rapidly cooled, textures in the matrix are very different from those resulting from the cooling of non-superheated liquids. Kerr et al. (1996) proposed that the predominance of spinifex texture and the absence of solid olivine grains in the very thin cumulate zones of Gorgona komatiites suggests that these magmas became strongly superheated en route to the surface.

Origin of Archean basalts

Modern basaltic magmas are produced by partial melting of mantle peridotite in four main settings: at mid-ocean ridges, in plume-related settings, such as ocean islands and large igneous provinces, in subduction zones, and in continental rifts and other intraplate settings. In the Archean, the last setting appears to be rare or absent, probably because the products of low-degree melting are overwhelmed by more voluminous high-degree melts from the hotter Archean mantle.

Considerable debate surrounds the question of whether mid-ocean ridge basalts have ever been recognized in the Archean. Many authors (e.g., Kimura et al., 1993; Ohta et al., 1996; Komiya et al., 2002) suggest that they have been, mainly on the basis of a superficial similarity between the compositions of some Archean basalts and modern MORB. While it is true that many Archean tholeiitic basalts have low contents of incompatible trace elements, as expressed by modest depletions in the light REE, the same feature is seen in some basalts from Phanerozoic oceanic plateaus. Furthermore, as discussed in a previous section, there are some notable differences between the compositions of Archean tholeiites and modern MORB that cannot be attributed entirely to a hotter

Archean mantle. Herzberg et al. (2010) proposition that "non-arc" Archean basalts formed through melting of ambient upper mantle at oceanic spreading centers seems unjustified; many of the basalts in their compilation could have formed in oceanic plateaus.

Kusky et al. (2013) have argued that Archean basalts in regions throughout the world formed at mid-ocean ridges. Their interpretation is based on ocean plate stratigraphy, a term used to describe "the sequence of sedimentary and volcanic rocks deposited on oceanic crust substratum from the time it forms at a spreading center, to the time it is incorporated into an accretionary prism at a convergent margin." Kusky et al. (2013) propose criteria that can be used to distinguish the ocean plate stratigraphy of crust formed at a spreading center from that of basalts erupted on oceanic islands and seamounts. The key differences are a transition from shallow- to deeper-water settings of sediments deposited on ocean islands and seamounts and the distinctive geochemical characteristics (e.g., enrichment of incompatible elements) of modern ocean island volcanic rocks. A problem with this approach is that the plate stratigraphy of an oceanic plateau, particularly of those which may have formed near a spreading center, such as Ontong Java, is very similar to that of normal oceanic crust. As discussed in a previous section and emphasized by, e.g., Arndt et al. (1987), Abouchami et al. (1990), Storey et al. (1991), Saunders et al. (1996), and Barnes et al. (2021), the geochemical characteristics of Archean tholeiites are very much like those of Phanerozoic oceanic plateau basalts, and in our opinion, this remains the best analog for the Archean tholeiitic basalts.

The origin of the high-La basalts is also subject to debate. These basalts display enrichment in incompatible trace elements accompanied by negative Nb-Ta anomalies, features that are similar to those of basalts in modern subduction settings. In the Abitibi Belt, basalts with these characteristics are spatially associated with intermediate to felsic volcanic rocks and there is broad, though not universal, agreement that these rocks provide evidence of Archean subduction (e.g., Dostal and Mueller, 1997; Wyman et al., 1998; Polat and Kerrich, 1999, 2001; Sproule et al., 2002).

Chemical features, such as high SiO_2 and Al_2O_3, coupled with low FeO and TiO_2 contents, strong enrichments in highly incompatible lithophile trace elements, and negative HFSE anomalies in the Archean lavas are similar to those commonly found in modern island arcs and convergent margins. The presence of pillow textures, hyaloclastites, and interbedded sedimentary rocks provide clear evidence that most of these rocks erupted subaqueously, but the appearance of pumice and fall deposits toward the tops of lava sequences point to a change from subaqueous to subaerial eruptions.

The association of komatiites and calc-alkaline rocks has raised a debate in the literature on how komatiites, the products of mantle plumes in the opinion of most researchers, became spatially associated with the products of subduction-related magmatism (e.g., Dostal and Mueller, 1997; Hollings et al., 1999; Puchtel et al., 1999; Wyman et al., 2002). In addition, the Archean volcanic rocks have a distinctive bimodal mafic-felsic distribution (e.g., Thurston et al., 1985) characterized by a trough at intermediate compositions, which contrasts with a large range and gradual change of rock composition, from basalt through andesite to dacite or rhyolite, of rocks formed at modern convergent margins.

In the Yilgarn craton, rather than being associated with more evolved volcanic rocks, the high-La basalts are accompanied by komatiites. Many of the komatiites show geochemical and isotopic evidence of contamination with felsic rocks from the continental crust, a process that imparts a geochemical signature resembling that of island arc basalts. On this basis, Barnes et al. (2021) concluded that the majority of high-La basalts in the Yilgarn Craton and elsewhere are the products of crustal contamination of more mafic, possibly komatiitic, parental magmas. A key argument in support of this interpretation is the data plotted in Fig. 17, which reveal a significant difference between the compositions of the Archean and modern basalts, namely, an absence of depletion of incompatible elements (low La/Sm) in the Archean basalts combined with deep negative Nb-Ta anomalies (low Nb/La). Barnes et al. (2021) explained this difference by proposing that Archean basalts formed by crustal contamination of more mafic parental magmas rather than in a subduction setting; we propose instead that they reflect differences in conditions in Archean subduction zones. The depletion of incompatible elements in a modern mantle wedge seems to be linked to the process that extracted these elements from the upper mantle, a process that may be related to growth of the continental crust. Even if a large fraction of continental crust had formed by the end of the Archean (e.g., Sylvester et al., 1997; Campbell, 2003; Dhuime et al., 2012; Korenaga, 2021), to transfer the geochemical signature of this extraction to the mantle wedge requires a lapse of several hundred million years. It is likely, therefore, that the Archean mantle wedge was significantly less depleted than the modern wedge. The absence of deep negative Nb-Ta anomalies may relate to the nature of subducting oceanic crust, which, because of a hotter mantle, was thicker (McKenzie and Bickle, 1988) and probably more hydrated (Arndt and Davaille, 2013; Palin and White, 2016). These conditions may have inhibited preferential transfer of the light REE from crust to wedge, or the retention of residual rutile and/or titanite, the processes that result in negative Nb-Ta anomalies.

Finally, the high Fe contents that accompany many high Nb/La basalts suggest generation from a distinct mantle source (Hanski and Smolkin, 1989; Puchtel et al., 1998b; Polat and Kerrich, 2001). The enrichment of incompatible elements in these basalts may have resulted from relatively low degrees of melting of a metasomatized mantle source.

Conclusions

1. Komatiites are the hottest magmas that have ever formed on Earth. These high temperatures conditioned the manner in which komatiites erupted and crystallized, and imposed tight constraints on how these magmas might have been generated.
2. Komatiites were most common through the Archean and early Proterozoic where they constitute up to 25% of volcanic sequences. Komatiites are virtually absent through the subsequent Earth history. Rare Permian and Cretaceous komatiites are obvious outliers.

3. Major and trace element systematics of komatiites are used to define several types. Of these, the more important are Al-depleted komatiites, characterized by low Al_2O_3/TiO_2 ratios and relatively depleted heavy REE, and Al-undepleted komatiites, which have near-chondritic Al_2O_3/TiO_2 and the heavy REE ratios. The latter commonly show relative depletion of the light REE. Less abundant types are Al-enriched komatiites, some of which display extreme depletions of incompatible trace elements.
4. Al-depleted komatiites are interpreted to form at extreme mantle depths of >300 km, by melting in the presence of garnet. Komatiites with depleted incompatible lithophile trace elements most likely formed via a two-stage process. In the first stage, a basaltic melt enriched in incompatible elements was extracted, leaving a depleted residue that partially melted to produce the komatiite.
5. The isotopic compositions of komatiites provide evidence of sources with a wide range of lithophile trace element depletions, from similar to Bulk Silicate Earth to close to that of modern depleted upper mantle.
6. The highly elevated liquidus temperatures of komatiites, coupled with evidence of melting at extreme depths, require that komatiites formed in unusually hot mantle plumes.
7. Three main types of basalt are recognized in Archean terrains. These include komatiitic basalts, which are genetically related to komatiites, tholeiitic basalts, which resemble their modern counterparts, and calc-alkaline basalts, which form parts of mafic to felsic volcanic suites. The trace element and isotopic compositions of some basalts provide evidence of assimilation of continental crust.
8. The tholeiitic basalts, together with komatiites, erupted in tectonic settings similar to those of recent oceanic plateaus. Calc-alkaline basalts were generated at convergent margins and provide evidence for an early onset of subduction on planet Earth.

Acknowledgments

I.S.P. acknowledges support from the United States National Science Foundation Petrology and Geochemistry grant EAR-2220936. We would like to thank Paolo Sossi for detailed, constructive review of the initial version of this chapter, and Catherine Chauvel for editorial handling.

References

Abbott D (1996) Plumes and hotspots as sources of greenstone belts. *Lithos* 37(2–3): 113–127.
Abbott DH, Burgess L, Longhi J, and Smith WHF (1994) An empirical thermal history of the Earth's upper mantle. *Journal of Geophysical Research* 99(B7): 13835–13850.
Abouchami W, Boher M, Michard A, and Albarède F (1990) A major 2.1 Ga event of mafic magmatism in west Africa—An early stage of crustal accretion. *Journal of Geophysical Research* 95(B11): 17605–17629.
Agee CB (1998) Crystal–liquid density inversions in terrestrial and lunar magmas. *Physics of the Earth and Planetary Interiors* 107: 63–74.
Agee CB and Walker D (1988) Static compression and olivine flotation in ultrabasic silicate liquid. *Journal of Geophysical Research* 93(B4): 3437–3449.
Agee CB and Walker D (1993) Olivine flotation in mantle melt. *Earth and Planetary Science Letters* 114(2–3): 315–324.
Aitken BG and Echeverría LM (1984) Petrology and geochemistry of komatiites and tholeiites from Gorgona Island, Colombia. *Contributions to Mineralogy and Petrology* 86: 94–105.
Alard O, Griffin WL, Lorand J-P, Jackson SE, and O'Reilly SY (2000) Non-chondritic distribution of the highly siderophile elements in mantle sulfides. *Nature* 407(6806): 891–894.
Allègre CJ (1982) Genesis of Archaean komatiites in a wet ultramafic subducted plate. In: Arndt NT and Nisbet EG (eds.) *Komatiites*, pp. 495–500. London: George Allen and Unwin.
Amsellem E, Moynier F, Day JM, Moreira M, Puchtel IS, and Teng F-Z (2018) Stable strontium isotopic composition of OIB, MORB, komatiites and Kilauea Iki lava lake samples. *Chemical Geology* 483: 595–602.
Amsellem E, Moynier F, and Puchtel IS (2019) Evolution of the Ca isotopic composition of the mantle. *Geochimica et Cosmochimica Acta* 258: 195–206.
Arndt NT (1977a) Ultrabasic magmas and high-degree melting of the mantle. *Contributions to Mineralogy and Petrology* 64(2): 205–221.
Arndt NT (1977b) Thick, layered periodotite-gabbro lava flows in Munro Township, Ontario. *Canadian Journal of Earth Sciences* 14: 2620–2637.
Arndt NT (1982) Proterozoic spinifex-textured basalts of Gilmour Island, Hudson Bay. *Geological Survey of Canada Paper* 83-1A: 137–142.
Arndt NT (1986) Differentiation of komatiite flows. *Journal of Petrology* 27: 279–301.
Arndt NT (1999) Why was flood volcanism on submerged continental platforms so common in the Precambrian? *Precambrian Research* 97: 155–164.
Arndt NT and Brooks C (1980) Komatiites—Penrose conference report. *Geology* 8(3): 155–156.
Arndt NT and Davaille A (2013) Episodic earth evolution. *Tectonophysics* 609: 661–674.
Arndt NT and Fleet ME (1979) Stable and metastable pyroxene crystallization in layered komatiite flows. *American Mineralogist* 64: 856–864.
Arndt NT and Jenner GA (1986) Crustally contaminated komatiites and basalts from Kambalda, Western Australia. *Chemical Geology* 56: 229–255.
Arndt NT and Nisbet EG (1982) What is a komatiite? In: Arndt NT and Nisbet EG (eds.) *Komatiites*, pp. 19–28. London: George Allen and Unwin.
Arndt NT, Naldrett AJ, and Pyke DR (1977) Komatiitic and iron-rich tholeiitic lavas of Munro Township, northeast Ontario. *Journal of Petrology* 18: 319–369.
Arndt NT, Brügmann GE, Lehnert K, Chauvel C, and Chappell BW (1987) Geochemistry, petrogenesis, and tectonic environment of Circum-Superior Belt basalts, Canada. In: Pharaoh TC, Beckinsale RD, and Rickard D (eds.) *Geochemistry and Mineralization of Proterozoic Volcanic Suites. Geological Society Special Publication*, Vol. 33, pp. 133–145.
Arndt NT, Teixeira NA, and White WM (1989) Bizarre geochemistry of komatiites from the Crixás greenstone belt, Brazil. *Contributions to Mineralogy and Petrology* 101: 187–197.
Arndt NT, Kerr AC, and Tarney J (1997) Dynamic melting in plume heads: The formation of Gorgona komatiites and basalts. *Earth and Planetary Science Letters* 146(1–2): 289–301.
Arndt NT, Ginibre C, Chauvel C, Albarède F, Cheadle M, Herzberg C, Jenner G, and Lahaye Y (1998) Were komatiites wet? *Geology* 26(8): 739–742.
Arndt NT, Bruzak G, and Reischmann T (2001) The oldest continental and oceanic plateaus: Geochemistry of basalts and komatiites of the Pilbara Craton, Australia. *Geological Society of America Special Paper* 352: 359–387.
Arndt NT, Lesher CM, and Barnes SJ (2008) *Komatiite*. Cambridge, UK: Cambridge University Press. 467 pp.
Asafov EV, Sobolev AV, Gurenko AA, Arndt NT, Batanova VG, Portnyagin MV, Garbe-Schönberg C-D, and Krasheninnikov SP (2018) Belingwe komatiites (2.7 Ga) originate from a plume with moderate water content, as inferred from inclusions in olivine. *Chemical Geology* 478: 39–59.
Ayer JA, Amelin Y, Corfu F, Kamo S, Ketchum J, Kwok K, and Trowell N (2002) Evolution of the southern Abitibi greenstone belt based on U-Pb geochronology: Autochthonous volcanic construction followed by plutonism, regional deformation and sedimentation. *Precambrian Research* 115(1–4): 63–95.

Barley ME (1986) Incompatible-element enrichment in Archean basalts: A consequence of contamination by older sialic crust rather than mantle heterogeneity. *Geology* 14(11): 947–950.
Barnes SJ (1986) The distribution of chromium among orthopyroxene, spinel and silicate liquid at atmospheric pressure. *Geochimica et Cosmochimica Acta* 50(9): 1889–1909.
Barnes SJ (1998) Chromite in komatiites, I. Magmatic controls on crystallization and composition. *Journal of Petrology* 39(10): 1689–1720.
Barnes SJ (2000) Chromite in komatiites, II. Modification during greenschist to mid-amphibolite facies metamorphism. *Journal of Petrology* 41(3): 387–409.
Barnes SJ (2006) Komatiites: Petrology, volcanology, metamorphism, and geochemistry. *Society of Economic Geologists Special Publication* 13: 13–49.
Barnes SJ and Arndt NT (2019) Distribution and geochemistry of komatiites and basalts through the Archean. In: Van Kranendonk MJ, Bennett VC, and Hoffmann E (eds.) *Earth's Oldest Rocks*, Second Edition, pp. 103–132. Amsterdam: Elsevier.
Barnes S-J and Often M (1990) Ti-rich komatiites from Northern Norway. *Contributions to Mineralogy and Petrology* 105(1): 42–54.
Barnes SJ and Roeder PL (2001) The range of spinel compositions in terrestrial mafic and ultramafic rocks. *Journal of Petrology* 42(12): 2279–2302.
Barnes S-J, Naldrett AJ, and Gorton MP (1985) The origin of the fractionation of platinum-group elements in terrestrial magmas. *Chemical Geology* 53(3–4): 303–323.
Barnes SJ, Hill RET, and Gole MJ (1988) The Perseverance ultramafic complex, Western Australia: The product of a komatiite lava river. *Journal of Petrology* 29(2): 305–331.
Barnes SJ, Fiorentini M, Duuring P, Perring C, and Grguric B (2011) The perseverance and Mount Keith Ni deposits of the Agnew-Wiluna Belt, Yilgarn Craton, Western Australia. *Reviews in Economic Geology* 17: 51–88.
Barnes SJ, Williams M, Smithies RH, Hanski E, and Lowrey JR (2021) Trace element contents of mantle-derived magmas through time. *Journal of Petrology* 62(6): 1–38.
Barrie CT and Shirey SB (1991) Nd- and Sr-isotope systematics for the Kamiskotia–Montcalm area: Implications for the formation of late Archean crust in the western Abitibi Subprovince, Canada. *Canadian Journal of Earth Sciences* 28(1): 58–76.
Barrie CT, Cousens B, Hannington MD, Bleeker W, and Gibson H (1999) Lead and neodymium isotope systematics of the Kidd Creek Mine stratigraphic sequence and ore, Abitibi Subprovince Canada. *Economic Geology Monographs* 10: 497–510.
Bavinton OA (1981) The nature of sulfidic metasediments at Kambalda and their broad relationships with associated ultramafic rocks and nickel ores. *Economic Geology* 76: 1606–1628.
Beaty DW and Taylor HP (1982) The oxygen isotope geochemistry of komatiites: Evidence for water-rock interaction. In: Arndt NT and Nisbet EG (eds.) *Komatiites*, pp. 267–280. London: George Allen and Unwin.
Becker H, Horan MF, Walker RJ, Gao S, Lorand J-P, and Rudnick RL (2006) Highly siderophile element composition of the Earth's primitive upper mantle: Constraints from new data on peridotite massifs and xenoliths. *Geochimica et Cosmochimica Acta* 70(17): 4528–4550.
Bekker A, Barley ME, Fiorentini ML, Rouxel OJ, Rumble D, and Beresford SW (2009) Atmospheric sulfur in Archean komatiite-hosted nickel deposits. *Science* 326: 1086–1089.
Bercovici D and Karato S (2003) Whole-mantle convection and the transition-zone water filter. *Nature* 425(6953): 39–44.
Berry AJ, Danyushevsky LV, O'Neill HSC, Newville M, and Sutton SR (2008) Oxidation state of iron in komatiitic melt inclusions indicates hot Archaean mantle. *Nature* 455(7215): 960–963.
Bickle MJ (1982) The magnesium contents of komatiitic liqiuds. In: Arndt NT and Nisbet EG (eds.) *Komatiites*, pp. 479–494. London: George Allen and Unwin.
Bickle MJ (1986) Implications of melting for stabilisation of lithosphere and heat loss in the Archaean. *Earth and Planetary Science Letters* 80(3–4): 314–324.
Bickle MJ and Nisbet EG (1993) *The Geology of the Belingwe Greenstone Belt*, p. 239. Balkema, Rotterdam: Zimbabwe.
Bickle MJ, Arndt NT, Nisbet EG, Orpen JL, Martin A, Keays RR, and Renner R (1993) Geochemistry of the igneous rocks of the Belingwe Greenstone Belt: Alteration, contamination and petrogenesis. In: Bickle MJ and Nisbet EG (eds.) *The Geology of the Belingwe Greenstone Belt, Zimbabwe. A Study of the Evolution of Archaean Continental Crust*, pp. 175–213. Geological Society of Zimbabwe Special Publication 2.
Bickle MJ, Nisbet EG, and Martin A (1994) Archean greenstone belts are not oceanic crust. *Journal of Geology* 102(2): 121–138.
Blichert-Toft J and Arndt NT (1999) Hf isotope compositions of komatiites. *Earth and Planetary Science Letters* 171(3): 439–451.
Blichert-Toft J and Puchtel IS (2010) Depleted mantle sources through time: Evidence from Lu-Hf and Sm-Nd isotope systematics of Archean komatiites. *Earth and Planetary Science Letters* 297(3–4): 598–606.
Blichert-Toft J, Arndt NT, Wilson A, and Coetzee G (2015) Hf and Nd isotope systematics of early Archean komatiites from surface sampling and ICDP drilling in the Barberton Greenstone Belt, South Africa. *American Mineralogist* 100: 2396–2411.
Bouvier A, Vervoort JD, and Patchett PJ (2008) The Lu-Hf and Sm-Nd isotopic composition of CHUR: Constraints from unequilibrated chondrites and implications for the bulk composition of terrestrial planets. *Earth and Planetary Science Letters* 273(1–2): 48–57.
Boyet M and Carlson RW (2005) ^{142}Nd evidence for early (>4.53 Ga) global differentiation of the silicate Earth. *Science* 309(5734): 576–581.
Boyet M and Carlson RW (2006) A new geochemical model for the Earth's mantle inferred from ^{146}Sm-^{142}Nd systematics. *Earth and Planetary Science Letters* 250(1–2): 254–268.
Boyet M, Blichert-Toft J, Rosing M, Storey M, Télouk P, and Albarède F (2003) ^{142}Nd evidence for early Earth differentiation. *Earth and Planetary Science Letters* 214(3–4): 427–442.
Boyet M, Garçon M, Arndt NT, Carlson RW, and Konc Z (2021) Residual liquid from deep magma ocean crystallization in the source of komatiites from the ICDP drill core in the Barberton Greenstone Belt. *Geochimica et Cosmochimica Acta* 304: 141–159.
Brandon AD, Walker RJ, Puchtel IS, Becker H, Humayun M, and Révillon S (2003) ^{186}Os-^{187}Os systematics of Gorgona Island komatiites: Implications for early growth of the inner core. *Earth and Planetary Science Letters* 206(3–4): 411–426.
Brandon AD, Humayun M, Puchtel IS, and Zolensky M (2005) Re-Os isotopic systematics and platinum group element composition of the Tagish Lake carbonaceous chondrite. *Geochimica et Cosmochimica Acta* 69(6): 1619–1631.
Brandon AD, Walker RJ, and Puchtel IS (2006) Platinum-osmium isotope evolution of the Earth's mantle: Constraints from chondrites and Os-rich alloys. *Geochimica et Cosmochimica Acta* 70(8): 2093–2103.
Brévart O, Dupré B, and Allègre CJ (1986) Lead-lead age of komatiitic lavas and limitations on the structure and evolution of the Precambrian mantle. *Earth and Planetary Science Letters* 77(3–4): 293–302.
Brooks C and Hart SR (1974) On the significance of komatiite. *Geology* 2(2): 107–110.
Brügman GE, Arndt NT, Hofmann AW, and Tobschall HJ (1987) Noble metal abundances in komatiite suites from Alexo, Ontario, and Gorgona Island, Colombia. *Geochimica et Cosmochimica Acta* 51(8): 2159–2170.
Byerly BL, Kareem K, Bao H, and Byerly GR (2017) Early Earth mantle heterogeneity revealed by light oxygen isotopes of Archaean komatiites. *Nature Geoscience* 10: 871–876.
Cameron WE and Nisbet EG (1982) Phanerozoic analogues of komatiitic basalts. In: Arndt NT and Nisbet EG (eds.) *Komatiites*, pp. 29–50. London: George Allen and Unwin.
Campbell IH (2003) Constraints on continental growth models from Nb/U ratios in the 3.5 Ga Barberton and other Archaean basalt-komatiite suites. *American Journal of Science* 303(4): 319–351.
Campbell IH and Griffiths RW (2014) Did the formation of D″ cause the Archaean-Proterozoic transition? *Earth and Planetary Science Letters* 388: 1–8.
Campbell IH, Griffiths RW, and Hill RI (1989) Melting in an Archaean mantle plume: Head it's basalts, tails it's komatiites. *Nature* 339(6227): 697–699.
Canil D (1997) Vanadium partitioning and the oxidation state of Archaean komatiite magmas. *Nature* 389(6653): 842–845.
Canil D (1999) Vanadium partitioning between orthopyroxene, spinel and silicate melt and the redox states of mantle source regions for primary magmas. *Geochimica et Cosmochimica Acta* 63(3–4): 557–572.
Canil D (2002) Vanadium in peridotites, mantle redox and tectonic environments: Archean to present. *Earth and Planetary Science Letters* 195(1–2): 75–90.
Canil D and Fedortchouk Y (2001) Olivine-liquid partitioning of vanadium and other trace elements, with applications to modern and ancient picrites. *Canadian Mineralogist* 39: 319–330.
Capdevila R, Arndt NT, Letendre J, and Sauvage J-F (1999) Diamonds in volcaniclastic komatiite from French Guiana. *Nature* 399: 456–458.

Card KD (1990) A review of the Superior province of the Canadian Shield, a product of Archean accretion. *Precambrian Research* 48(1–2): 99–156.
Carignan J, Machado N, and Gariépy C (1995) U-Pb isotopic geochemistry of komatiites and pyroxenes from the southern Abitibi greenstone belt, Canada. *Chemical Geology* 126(1): 17–27.
Caro G, Bourdon B, Birck J-L, and Moorbath S (2003) ^{146}Sm-^{142}Nd evidence from Isua metamorphosed sediments for early differentiation of the Earth's mantle. *Nature* 423(6938): 428–432.
Caro G, Bourdon B, Wood BJ, and Corgne A (2005) Trace-element fractionation in Hadean mantle generated by melt segregation from a magma ocean. *Nature* 436(7048): 246–249.
Caro G, Bourdon B, Birck J-L, and Moorbath S (2006) High-precision ^{142}Nd/^{144}Nd measurements in terrestrial rocks: Constraints on the early differentiation of the Earth's mantle. *Geochimica et Cosmochimica Acta* 70(1): 164–191.
Cattell A (1987) Enriched komatiitic basalts from Newton Township, Ontario: Their genesis by crustal contamination of depleted komatiite magma. *Geological Magazine* 124(4): 303–309.
Cattell A, Krough TE, and Arndt NT (1984) Conflicting Sm-Nd whole rock and U-Pb zircon ages for Archean lavas from Newton Township, Abitibi belt, Ontario. *Earth and Planetary Science Letters* 70(2): 280–290.
Cawthorn RG (1975) Degrees of melting in mantle diapirs and the origin of ultrabasic liquids. *Earth and Planetary Science Letters* 27(1): 113–120.
Chauvel C, Dupre B, and Jenner GA (1985) The Sm-Nd age of Kambalda volcanics is 500 Ma too old! *Earth and Planetary Science Letters* 74(4): 315–324.
Chauvel C, Dupré B, and Arndt NT (1993) Pb and Nd isotopic correlation in Belingwe komatiites and basalts. In: Bickle MJ and Nisbet EG (eds.) *The Geology of the Belingwe Greenstone Belt, Zimbabwe. A Study of the Evolution of Archaean Continental Crust*, pp. 167–174. A.A. Balkema, Rotterdam/Brookfield.
Chavagnac V (2004) A geochemical and Nd isotopic study of Barberton komatiites (South Africa): Implication for the Archean mantle. *Lithos* 75: 253–281.
Claoué-Long JC, Thirlwall MF, and Nesbitt RW (1984) Revised Sm-Nd systematics of Kambalda greenstones, Western Australia. *Nature* 307(5953): 697–701.
Claoué-Long JC, Compston W, and Cowden A (1988) The age of the Kambalda greenstones resolved by ion microprobe: Implications for Archaean dating methods. *Earth and Planetary Science Letters* 89(2): 239–259.
Cloete M (1999) Aspects of volcanism and metamorphism of the Onverwacht Group lava in the southwestern portion of the Barberton Greenstone Belt. *Geological Survey of South Africa Memoir* 84. 232 pp.
Coffin MF and Eldholm O (1993) Scratching the surface: Estimating dimensions of large igneous provinces. *Geology* 21(6): 515–518.
Coffin MF and Gahagan LM (1995) Ontong Java and Kerguelen plateaux: Cretaceous Icelands. *Journal of the Geological Society of London* 152(6): 1047–1052.
Compston W, Williams IS, Campbell IH, and Gresham JJ (1986) Zircon xenocrysts from the Kambalda volcanics: Age constraints and direct evidence for older continental crust below the Kambalda-Norseman greenstones. *Earth and Planetary Science Letters* 76(3–4): 299–311.
Condie KC (1975) Mantle-plume model for the origin of Archaean greenstone belts based on trace element distributions. *Nature* 258(5534): 413–414.
Condie KC (1981) *Archaean Greenstone Belts*, p. 434. Amsterdam: Elsevier.
Condie KC (1994) Greenstones through time. In: Condie KC (ed.) *Archean Crustal Evolution*, pp. 85–120. Amsterdam: Elsevier.
Condie KC (2005) High field strength element ratios in Archean basalts: A window to evolving sources of mantle plumes? *Lithos* 79(3–4): 491–504.
Connolly BD, Puchtel IS, Walker RJ, Arevalo R Jr, Piccoli PM, Byerly GR, Robin-Popieul C, and Arndt NT (2011) Highly Siderophile Element systematics of the 3.3 Ga Weltevreden komatiites, South Africa: Implications for early Earth history. *Earth and Planetary Science Letters* 311(3–4): 253–263.
Courtillot V, Jaupart C, Manighetti I, Tapponnier P, and Besse J (1999) On casual links between flood basalts and continenetal breakup. *Earth and Planetary Science Letters* 166(3–4): 177–195.
Cowden A (1988) Emplacement of komatiite lava flows and associated nickel sulfides at Kambalda, Western Australia. *Economic Geology* 83(2): 436–442.
Crocket JH, Fleet ME, and Stone WE (1997) Implications of composition for experimental partitioning of platinum-group elements and gold between sulfide liquid and basalt melt: The significance of nickel content. *Geochimica et Cosmochimica Acta* 61(19): 4139–4149.
Dann JC (2000) The 3.5 Ga Komati Formation, Barberton Greenstone Belt, South Africa, Part I: New maps and magmatic architecture. *South African Journal of Geology* 103: 47–68.
Dann JC (2001) Vesicular komatiites, 3.5-Ga Komati Formation, Barberton Greenstone Belt, South Africa: Inflation of submarine lavas and origin of spinifex zones. *Bulletin of Volcanology* 63(7): 462–481.
Dauphas N, Teng F-Z, and Arndt NT (2010) Magnesium and iron isotopes in 2.7 Ga Alexo komatiites: Mantle signatures, no evidence for Soret diffusion, and identification of diffusive transport in zoned olivine. *Geochimica et Cosmochimica Acta* 74: 3274–3291.
Davies DR, Rawlinson N, Iaffaldano G, and Campbell IH (2015) Lithospheric controls on magma composition along Earth's longest continental hotspot track. *Nature* 525(7570): 511–514.
De Rosen-Spence AF, Provost G, Dimroth E, Gochnauer K, and Owen V (1980) Archean subaqueous felsic flows, Rouyn-Nornada, Quebec, Canada, and their Quaternary equivalents. *Precambrian Research* 12(1): 43–77.
De Wit MJ and Ashwal LD (1997) *Greenstone Belts*, p. 809. Oxford: Clarendon Press.
Debaille V, O'Neill C, Brandon AD, Haenecour P, Yin Q-Z, Mattielli N, and Treiman AH (2013) Stagnant-lid tectonics in early Earth revealed by ^{142}Nd variations in late Archean rocks. *Earth and Planetary Science Letters* 373: 83–92.
DePaolo DJ and Wasserburg GJ (1979) Sm-Nd age of the Stillwater Complex and the mantle evolution curve for neodimium. *Geochimica et Cosmochimica Acta* 43(7): 999–1008.
Desrochers J-P, Hubert C, Ludden JN, and Pilote P (1993) Accretion of Archaean oceanic plateau fragments in the Abitibi greenstone belt, Canada. *Geology* 21(5): 451–454.
Dhuime B, Hawkesworth CJ, Cawood PA, and Storey CD (2012) A change in the geodynamics of continental growth 3 billion years ago. *Science* 335: 1334–1336.
Dimroth E, Cousineau P, Leduc M, and Sanschagrin Y (1978) Structure and organization of Archean subaqueous basalt flows, Rouyn-Noranda area, Quebec, Canada. *Canadian Journal of Earth Sciences* 15(6): 902–918.
Dimroth E, Imreh L, Rocheleau M, and Goulet N (1982) Evolution of the south-central part of the Archaean Abitibi belt, Quebec. Part I: Stratigraphy and paleogeographic model. *Canadian Journal of Earth Sciences* 19(9): 1729–1758.
Dimroth E, Imreh L, Cousineau P, Leduc M, and Sanschagrin Y (1985) Paleogeographic analysis of mafic submarine flows and its use in the exploration for massive sulphide deposits. In: Ayres LD, Thurston PC, Card KD, and Weber W (eds.) *Evolution of Archean Supracrustal Sequences. Geological Association of Canada Special Paper*, Vol. 28, pp. 203–222. Ottawa: Geological Society of Canada.
Donaldson CH (1979) An experimental investigation of the delay in nucleation of olivine in mafic magmas. *Contributions to Mineralogy and Petrology* 69(1): 21–32.
Donaldson CH (1982) Spinifex textured komatiites: A review of textures, compositions, and layering. In: Arndt NT and Nisbet EG (eds.) *Komatiites*, pp. 213–244. London: George Allen and Unwin.
Dostal J and Mueller WU (1997) Komatiite flooding of a rifted Archean rhyolite arc complex: Geochemical signature and tectonic significance of the Stoughton-Roquemaure Group, Abitibi greenstone belt, Canada. *Journal of Geology* 105(5): 545–563.
Dupré B and Arndt NT (1990) Pb isotopic composition of Archean komatiites and sulfides. *Chemical Geology* 85(1–2): 35–56.
Dupré B, Chauvel C, and Arndt NT (1984) Pb and Nd isotopic study of two Archean komatiitic flows from Alexo, Ontario. *Geochimica et Cosmochimica Acta* 48(10): 1965–1972.
Echeverria LM (1980) Tertiary or Mesozoic komatiites from Gorgona Island, Colombia: Field relations and geochemistry. *Contributions to Mineralogy and Petrology* 73: 253–266.
Echeverria LM and Aitken B (1986) Pyroclastic rocks: another manifestation of ultramafic volcanism of Gorgona Island, Colombia. *Contributions to Mineralogy and Petrology* 92(4): 428–436.
Ernst RE and Bleeker W (2010) Large igneous provinces (LIPs), giant dyke swarms, and mantle plumes: Significance for breakup events within Canada and adjacent regions from 2.5 Ga to the present. *Canadian Journal of Earth Sciences* 47(5): 695–739.
Farnetani CG and Richards MA (1995) Thermal entrainment and melting in mantle plumes. *Earth and Planetary Science Letters* 136(4): 251–267.

Farquhar J and Wing BA (2003) Multiple sulfur isotopes and the evolution of the atmosphere. *Earth and Planetary Science Letters* 213: 1–13.
Farquhar J, Bao H, and Thiemens M (2000) Atmospheric influence of Earth's earliest sulfur cycle. *Science* 289: 756–758.
Faure F, Trolliard G, Nicollet C, and Montel J-M (2003) A developmental model of olivine morphology as a function of the cooling rate and the degree of undercooling. *Contributions to Mineralogy and Petrology* 145(2): 151–163.
Faure F, Arndt NT, and Libourel G (2006) Formation of spinifex texture in komatiite: An experimental study. *Journal of Petrology* 47: 1591–1610.
Fiorentini M, Beresford S, Barley M, Duuring P, Bekker A, Rosengren N, Cas R, and Hronsky J (2012) District to camp controls on the genesis of komatiite-hosted nickel sulfide deposits, agnew-wiluna greenstone belt, Western Australia: Insights from the multiple sulfur isotopes. *Economic Geology* 107: 781–796.
Fischer-Gödde M, Becker H, and Wombacher F (2010) Rhodium, gold and other highly siderophile element abundances in chondritic meteorites. *Geochimica et Cosmochimica Acta* 74(1): 356–379.
Fleet ME, Crocket JH, and Stone WE (1996) Partitioning of platinum-group elements (Os, Ir, Ru, Pt, Pd) and gold between sulfide liquid and basalt melt. *Geochimica et Cosmochimica Acta* 60(13): 2397–2412.
Foley SF, Barth MG, and Jenner GA (2000) Rutile/melt partition coefficients for trace elements and an assessment of the influence of rutile on the trace element characteristics of subduction zone magmas. *Geochimica et Cosmochimica Acta* 64(5): 933–938.
Fonseca ROC, Mallmann G, O'Neill HSC, Campbell IH, and Laurenz V (2011) Solubility of Os and Ir in sulfide melt: Implications for Re/Os fractionation during mantle melting. *Earth and Planetary Science Letters* 311(3–4): 339–350.
Fonseca ROC, Laurenz V, Mallmann G, Luguet A, Hoehne N, and Jochum KP (2012) New constraints on the genesis and long-term stability of Os-rich alloys in the Earth's mantle. *Geochimica et Cosmochimica Acta* 87: 227–242.
Francis DM and Hynes AJ (1979) Komatiite-derived tholeiites in the Proterozoic of New Quebec. *Earth and Planetary Science* 44(3): 473–481.
Gangopadhyay A and Walker RJ (2003) Re-Os systematics of the ca. 2.7 Ga komatiites from Alexo, Ontario, Canada. *Chemical Geology* 196(1–4): 147–162.
Gangopadhyay A, Walker RJ, Hanski E, and Solheid P (2006) Origin of Paleoproterozoic komatiites at Jeesiörova, Kittilä greenstone complex, Finnish Lapland. *Journal of Petrology* 47(4): 773–789.
Gélinas L and Brooks C (1974) Archean quench-texture tholeiites. *Canadian Journal of Earth Sciences* 11(2): 234–240.
Gélinas L, Lajoie J, and Brooks C (1977) Origin and significance of Archean ultramafic volcaniclastics from Spinifex Ridge, La Motte Township, Québec. In: Baragar WRA, Coleman LC, and Hall JM (eds.) *Volcanic Regimes in Canada. Geological Association of Canada, Special Paper*, 16, pp. 297–309.
Goldstein SL and Galer SJG (1992) On the trail of early mantle differentiation: $^{142}Nd/^{144}Nd$ ratios of early Archean rocks. *Eos* 73(30): 323.
Goldstein SL, O'Nions RK, and Hamilton PJ (1984) A Sm-Nd isotopic study of atmospheric dusts and particulates from major river systems. *Earth and Planetary Science Letters* 70(2): 221–236.
Greber ND, Puchtel IS, Nägler TF, and Mezger K (2015) Komatiites constrain molybdenum isotope composition of the Earth's mantle. *Earth and Planetary Science Letters* 421: 129–138.
Greber ND, Dauphas N, Puchtel IS, Hofmann BA, and Arndt NT (2017) Titanium stable isotopic variations in chondrites, achondrites and lunar rocks. *Geochimica et Cosmochimica Acta* 213: 534–552.
Green DH (1975) Genesis of Archean peridotitic magmas and constraints on Archean geothermal gradients and tectonics. *Geology* 3(1): 15–18.
Green DH (1981) Petrogenesis of Archean ultramafic magmas and implications for Archean tectonics. In: Kröner A (ed.) *Precambrian Plate Tectonics*, pp. 469–480. Amsterdam: Elsevier.
Green DH, Nicholls IA, Viljoen MJ, and Viljoen RP (1975) Experimental demonstration of the existence of peridotitic liquids in earliest Archean magmatism. *Geology* 3(1): 11–15.
Greene AR, Scoates JS, Weis D, Katvala EC, Israel S, and Nixon GT (2010) The architecture of oceanic plateaus revealed by the volcanic stratigraphy of the accreted Wrangellia oceanic plateau. *Geosphere* 6(1): 47–73.
Gresham JJ and Loftus-Hills GD (1981) The geology of the Kambalda nickel field, Western Australia. *Economic Geology* 76(6): 1373–1416.
Griffiths RW and Campbell IH (1990) Stirring and structure in mantle starting plumes. *Earth and Planetary Science Letters* 99(1–2): 66–78.
Grove TL and Parman SW (2004) Thermal evolution of the Earth as recorded by komatiites. *Earth and Planetary Science Letters* 219(3–4): 173–187.
Grove TL, de Wit MJ, and Dann J (1997) Komatiites from the Komati type section, Barberton, South Africa. In: de Wit MJ and Ashwal LD (eds.) *Greenstone Belts*, pp. 422–437. Oxford: Oxford Science Publications.
Gruau G, Tourpin S, Fourcade S, and Blais S (1992) Loss of isotopic (Nd, O) and chemical (REE) memory during metamorphism of komatiites: New evidence from Eastern Finland. *Contributions to Mineralogy and Petrology* 112(1): 66–82.
Gruau G, Rosing M, Bridgwater D, and Gill RCO (1996) Resetting of Sm-Nd systematics during metamorphism of >3.7-Ga rocks: Implications for isotopic models of early Earth differentiation. *Chemical Geology* 133(1–4): 225–240.
Gurenko AA, Kamenetsky VS, and Kerr AC (2016) Oxygen isotopes and volatile contents of the Gorgona komatiites, Colombia: A confirmation of the deep mantle origin of H_2O. *Earth and Planetary Science Letters* 454: 154–165.
Hallberg JA (1972) Geochemistry of the Archean volcanic rocks in the Eastern Goldfields region of Western Australia. *Journal of Petrology* 13: 45–56.
Hamilton PJ, O'Nions RK, and Evensen NM (1977) Sm-Nd dating of Archaean basic and ultrabasic volcanics. *Earth and Planetary Science Letters* 36(2): 263–268.
Hamilton PJ, O'Nions RK, Evensen NM, Bridgwater D, and Allaart JH (1978) Sm-Nd isotopic investigations of Isua supracrustals and implications for mantle evolution. *Nature* 272: 41–43.
Hamilton PJ, Evensen NM, O'Nions RK, Smith HS, and Erlank AJ (1979) Sm-Nd dating of Onverwacht Group volcanics, Southern Africa. *Nature* 279: 298–300.
Hamilton PJ, O'Nions RK, Bridgwater D, and Nutman AP (1983) Sm-Nd studies of Archaean metasediments and metavolcanics from West Greenland and their implications for the Earth's early history. *Earth and Planetary Science Letters* 62(2): 263–272.
Hanski EJ (1980) Komatiitic and tholeiitic metavolcanics of the Siivikkovaara area in the Archean Kuhmo greenstone belt, eastern Finland. *Bulletin of the Geological Society of Finland* 52: 67–100.
Hanski EJ and Smolkin VF (1989) Pechenga ferropicrites and other early Proterozoic picrites in the eastern part of the Baltic Shield. *Precambrian Research* 45: 63–82.
Hanski E, Huhma H, Rastas P, and Kamenetsky VS (2001) The Palaeoproterozoic komatiite-picrite association of Finnish Lapland. *Journal of Petrology* 42(5): 855–876.
Hanski E, Walker RJ, Huhma H, Polyakov GV, Balykin PA, Hoa TT, and Phuong NT (2004) Origin of the Permian-Triassic komatiites, northwestern Vietnam. *Contributions to Mineralogy and Petrology* 147(4): 453–469.
Hargreaves R and Ayres LD (1979) Morphology of Archean metabasalt flows, Utik Lake, Manitoba. *Canadian Journal of Earth Sciences* 16(7): 1452–1466.
Harper CL and Jacobsen SB (1992) Evidence from coupled ^{147}Sm-^{143}Nd and ^{146}Sm-^{142}Nd systematics for very early (4.5-Gyr) differentiation of the Earth's mantle. *Nature* 360(6406): 728–732.
Hart SR and Davis KE (1978) Nickel partitioning between olivine and silicate melt. *Earth and Planetary Science Letters* 40(2): 203–219.
Herzberg CT (1992) Depth and degree of melting of komatiites. *Journal of Geophysical Research* 97(B4): 4521–4540.
Herzberg CT (1995) Generation of plume magmas through time: An experimental perspective. *Chemical Geology* 126(1): 1–16.
Herzberg C and Asimow PD (2008) Petrology of some oceanic island basalts: PRIMELT2.XLS software for primary magma calculation. *Geochemistry, Geophysics, Geosystems* 9(9): Q09001.
Herzberg C and Gazel E (2009) Petrological evidence for secular cooling in mantle plumes. *Nature* 458(7238): 619–622.
Herzberg C and O'Hara MJ (2002) Plume-associated ultramafic magmas of Phanerozoic age. *Journal of Petrology* 43(10): 1857–1883.
Herzberg CT and Ohtani E (1988) Origin of komatiite at high pressures. *Earth and Planetary Science Letters* 88(3–4): 321–329.

Herzberg C, Asimow PD, Arndt NT, Niu YL, Lesher CM, Fitton JG, Cheadle MJ, and Saunders AD (2007) Temperatures in ambient mantle and plumes: Constraints from basalts, picrites, and komatiites. *Geochemistry, Geophysics, Geosystems* 8: Q02006.
Herzberg C, Condie K, and Korenaga J (2010) Thermal history of the Earth and its petrological expression. *Earth and Planetary Science Letters* 292(1–2): 79–88.
Hibbert KEJ, Williams HM, Kerr AC, and Puchtel IS (2012) Iron isotopes in ancient and modern komatiites: Evidence in support of an oxidized mantle from Archean to present. *Earth and Planetary Science Letters* 321–322: 198–207.
Hiebert RS, Bekker A, Houlé MG, Wing BA, and Rouxel OJ (2016) Tracing sources of crustal contamination using multiple S and Fe isotopes in the Hart komatiite associated Ni–Cu–PGE sulfide deposit, Abitibi greenstone belt, Ontario, Canada. *Mineralium Deposita* 51: 919–935.
Hill RET (2001) Komatiite volcanology, volcanological setting, and primary geochemical properties of komatiite-associated nickel deposits. *Geochemistry: Exploration, Environment, Analysis* 1: 365–381.
Hill RET, Barnes SJ, Gole MJ, and Dowling SE (1995) The volcanology of komatiites as deduced from field relationships in the Norseman-Wiluna greenstone belt, Western Australia. *Lithos* 34: 159–188.
Hill RET, Barnes SJ, Dowling SE, and Thordarson T (2004) Komatiites and nickel sulphide orebodies of the Black Swan area, Yilgarn Craton, Western Australia. 1. Petrology and volcanology of host rocks. *Mineralium Deposita* 39(7): 684–706.
Hoefs J and Binns RA (1978) Oxygen isotope compositions in Archaean rocks from Western Australia, with special reference to komatiites. In: Zartman RE (ed.) , *Fourth International Conference, Geochronology, Cosmochronology, Isotope Geology*, pp. 180–182. Boulder: United States Geological Survey.
Hoffmann JE and Wilson AH (2017) The origin of highly radiogenic Hf isotope compositions in 3.33 Ga Commondale komatiite lavas (South Africa). *Chemical Geology* 455: 6–21.
Hofmann AW (1988) Chemical differentiation of the Earth: The relationship between mantle, continental crust and oceanic crust. *Earth and Planetary Science Letters* 90(3): 297–314.
Hofmann AW (1997) Mantle geochemistry: the message from oceanic volcanism. *Nature* 385: 219–229.
Hofmann AW, Jochum KP, Seufert M, and White WM (1986) Nb and Pb in oceanic basalts: New constraints on mantle evolution. *Earth and Planetary Science Letters* 79(1–2): 33–45.
Hofmann A, Anhaeusser CR, and Li XH (2021) Layered ultramafic complexes of the Barberton Greenstone Belt—Age constraints and tectonic implications. *South African Journal of Geology* 124(1): 7–16.
Hollings P, Wyman D, and Kerrich R (1999) Komatiite-basalt-rhyolite volcanic associations in Northern Superior Province greenstone belts: Significance of plume-arc interaction in the generation of the protocontinental Superior Province. *Lithos* 46(1): 137–161.
Horan MF, Walker RJ, Morgan JW, Grossman JN, and Rubin AE (2003) Highly siderophile elements in chondrites. *Chemical Geology* 196(1–4): 5–20.
Houlé M, Lesher CM, Gibson HL, Fowler AD, and Sproule RA (2001) *Project unit 99-021. Physical volcanology of komatiites in the Abitibi greenstone belt*, pp. 13.1–13.7. Ontario Geological Survey. OFR 6070.
Huppert HE and Sparks RSJ (1985) Cooling and contamination of mafic and ultramafic magmas during ascent through continental crust. *Earth and Planetary Science Letters* 74(4): 371–386.
Huppert HE, Sparks RSJ, Turner JS, and Arndt NT (1984) Emplacement and cooling of komatiite lavas. *Nature* 309(5963): 19–22.
Jacobsen SB and Wasserburg GJ (1980) Sm-Nd isotopic evolution of chondrites. *Earth and Planetary Science Letters* 50(1): 139–155.
Jahn B-M, Gruau G, and Glikson AY (1982) Komatiites of the Onverwacht Group, South Africa: REE geochemistry, Sm-Nd age and mantle evolution. *Contributions to Mineralogy and Petrology* 80(1): 25–40.
Jerram M, Bonnand P, Kerr AC, Nisbet EG, Puchtel IS, and Halliday AN (2020) The δ^{53}Cr isotope composition of komatiite flows and implications for the composition of the BSE. *Chemical Geology* 551: 119761.
Jochum KP, Arndt NT, and Hofmann AW (1991) Nb-Th-La in komatiites and basalts: Constraints on komatiite petrogenesis and mantle evolution. *Earth and Planetary Science Letters* 107(2): 272–289.
Jolly WT (1982) Progressive metamorphism of komatiites and related Archaean lavas of the Abitibi area, Canada. In: Arndt NT and Nisbet EG (eds.) *Komatiites*, pp. 247–266. London: George Allen and Unwin.
Jones TD, Davies DR, Campbell IH, Wilson CR, and Kramer SC (2016) Do mantle plumes preserve the heterogeneous structure of their deep-mantle source? *Earth and Planetary Science Letters* 434: 10–17.
Kareem K (2005) *Komatiites of the Weltevreden Formation, Barberton Greenstone Belt, South Africa: Implications for the chemistry and temperature of the Archean mantle*. Baton Rouge, LA, USA: Louisiana State University. Ph.D. Thesis, 233 pp.
Keays RR (1995) The role of komatiitic and picritic magmatism and S-saturation in the formation of ore deposits. *Lithos* 34(1–3): 1–18.
Kennish MJ and Lutz RA (1998) Morphology and distribution of lava flows on mid-ocean ridges: A review. *Earth-Science Reviews* 43(3): 63–90.
Kent RW, Hardarson BS, Saunders AD, and Storey M (1996) Plateaux ancient and modern: Geochemical and sedimentological perspectives on Archaean oceanic magmatism. *Lithos* 37(2–3): 129–142.
Kerr AC and Arndt NT (2001) A note on the IUGS reclassification of the high-Mg and picritic volcanic rocks. *Journal of Petrology* 42(11): 2169–2171.
Kerr AC, Marriner GF, Arndt NT, Tarney J, Nivia A, Saunders AD, and Duncan RA (1996) The petrogenesis of komatiites, picrites and basalts from the Isle of Gorgona, Colombia; new field, petrographic and geochemical constraints. *Lithos* 37: 245–260.
Kerr AC, Tarney J, Marriner GF, Nivia A, and Saunders AD (1997) The Caribbean-Colombian cretaceous igneous province: The internal anatomy of an oceanic plateau. In: Mahoney JJ and Coffin M (eds.) *Large Igneous Provinces: Continental, Oceanic, and Planetary Flood Volcanism. AGU Geophysical Monograph*, Vol. 100, pp. 123–144.
Kimura G, Ludden JN, Desroshers J-P, and Hori R (1993) A model of ocean-crust accretion for the Superior province, Canada. *Lithos* 30(3–4): 337–355.
Kinzler RJ and Grove TL (1985) Crystallization and differentiation of Archean komatiite lavas from northeast Ontario: Phase equilibrium and kinetic studies. *American Mineralogist* 70(1–2): 40–51.
Kinzler RJ, Grove TL, and Recca SI (1990) An experimental study on the effect of temperature and melt composition on the partitioning of nickel between olivine and silicate melt. *Geochimica et Cosmochimica Acta* 54(5): 1255–1265.
Kiseeva ES, Fonseca ROC, and Smythe DJ (2017) Chalcophile elements and sulfides in the upper mantle. *Elements* 113: 111–116.
Klein EM and Langmuir CH (1987) Global correlations of ocean ridge basalt chemistry with axial depth and crustal thickness. *Journal of Geophysical Research* 92(B8): 8089–8115.
Komiya T, Maruyama S, Hirata T, and Yurimoto H (2002) Petrology and geochemistry of MORB and OIB in the mid-Archean North Pole region, Pilbara craton, Western Australia: Implications for the composition and temperature of the upper mantle at 3.5 Ga. *International Geology Review* 44(11): 988–1016.
Korenaga J (2021) Hadean geodynamics and the nature of early continental crust. *Precambrian Research* 359: 106178.
Kubota Y, Matsu'ura F, Shimizu K, Ishikawa A, and Ueno Y (2022) Sulfur in Archean komatiite implies early subduction of oceanic lithosphere. *Earth and Planetary Science Letters* 598: 117826.
Kusky TM and Kidd WSF (1992) Remnants of an Archean oceanic plateau, Belingwe greenstone belt, Zimbabwe. *Geology* 20(1): 43–46.
Kusky TM, Windley BF, Safonova I, Wakita K, Wakabayashi J, Polat A, and Santosh M (2013) Recognition of ocean plate stratigraphy in accretionary orogens through Earth history: A record of 3.8 billion years of sea floor spreading, subduction, and accretion. *Gondwana Research* 24: 501–547.
Lahaye Y and Arndt NT (1996) Alteration of a komatiitic flow: Alexo, Ontario, Canada. *Journal of Petrology* 37: 1261–1284.
Lahaye Y, Barnes S-J, Frick LR, and Lambert DD (2001) Re-Os isotopic study of komatiitic volcanism and magmatic sulfide formation in the southern Abitibi greenstone belt, Ontario, Canada. *Canadian Mineralogist* 39(2): 473–490.
Lassiter JC, DePaolo DJ, and Mahoney JJ (1995) Geochemistry of the Wrangellia flood basalt province: Implications for the role of continental and oceanic lithosphere in flood basalt genesis. *Journal of Petrology* 36: 983–1009.
Le Bas MJ (2000) IUGS reclassification of the high-Mg and picritic volcanic rocks. *Journal of Petrology* 41: 1467–1470.
Lesher CM (1989) Komatiite-associated nickel sulfide deposits. *Review of Economic Geology* 4: 44–101.

Lesher CM and Arndt NT (1995) REE and Nd isotope geochemistry, petrogenesis and volcanic evolution of contaminated komatiites at Kambalda, Western Australia. *Lithos* 34: 127–157.
Lesher CM and Keays RR (2002) Komatiite-associated Ni–Cu–(PGE) deposits: Geology, mineralogy, geochemistry and genesis. In: Louis JC (ed.) *The Geology, Geochemistry, Mineralogy and Mineral Benefication of Platinum-Group Elements. Canadian Institute for Mining and Metallurgy, Special Volume 54*, pp. 579–619.
Lesher CM, Arndt NT, and Groves DI (1984) Genesis of komatiite-associated nickel sulfide deposits at Kambalda, Western Australia: A distal volcanic model. In: Buchanan DL and Jones MJ (eds.) *Sulfide Deposits in Mafic and Ultramafic Rocks*, pp. 70–80. London: Inst. For Mining and Metallurgy.
Libourel G (1999) Systematics of calcium partitioning between olivine and silicate melt: Implications for melt structure and calcium content of magmatic olivines. *Contributions to Mineralogy and Petrology* 136(1): 63–80.
Lightfoot PC, Naldrett AJ, Gorbachev NS, Doherty W, and Fedorenko VA (1990) Geochemistry of the Siberian Trap of the Noril'sk area, USSR, with implications for the relative contributions of crust and mantle to flood basalt magmatism. *Contributions to Mineralogy and Petrology* 104(6): 631–644.
Lofgren GE (1980) Experimental studies on the dynamic crystallization of silicate melts. In: Hargraves RB (ed.) *Physics of Magmatic Processes*, pp. 487–552. Princeton: Princeton University Press.
Lofgren GE (1983) Effect of heterogeneous nucleation on basaltic textures: A dynamic crystallization study. *Journal of Petrology* 24(3): 229–255.
Loper DE (1991) Mantle plumes. *Tectonophysics* 187(4): 373–384.
Lorand J-P and Alard O (2001) Platinum-group element abundances in the upper mantle: new constraints from in situ and whole-rock analyses of Massif Central xenoliths (France). *Geochimica et Cosmochimica Acta* 65(16): 2789–2806.
Lowrey JR, Ivanic TJ, Wyman DA, and Roberts MP (2017) Platy pyroxene: New insights into spinifex texture. *Journal of Petrology* 58(9): 1671–1700.
Luguet A, Shirey SB, Lorand J-P, Horan MF, and Carlson RW (2007) Residual platinum-group minerals from highly depleted harzburgites of the Lherz massif (France) and their role in HSE fractionation of the mantle. *Geochimica et Cosmochimica Acta* 71(12): 3082–3097.
Machado N, Brooks C, and Hart SR (1986) Determination of initial $^{87}Sr/^{86}Sr$ and $^{143}Nd/^{144}Nd$ in primary minerals from mafic and ultramafic rocks: Experimental procedure and implications for the isotopic characteristics of the Archean mantle under the Abitibi greenstone belt, Canada. *Geochimica et Cosmochimica Acta* 50(10): 2335–2348.
Maier WD, Barnes SJ, Campbell IH, Fiorentini ML, Peltonen P, Barnes S-J, and Smithies RH (2009) Progressive mixing of meteoritic veneer into the early Earth's deep mantle. *Nature* 460(7255): 620–623.
Mallmann G and O'Neill HSC (2009) The crystal/melt partitioning of V during mantle melting as a function of oxygen fugacity compared with some other elements (Al, P, Ca, Sc, Ti, Cr, Fe, Ga, Y, Zr and Nb). *Journal of Petrology* 50(9): 1765–1794.
Matsumoto T, Seta A, Matsuda J, Takebe M, Chen Y, and Araid S (2002) Helium in the Archean komatiites revisited: Significantly high $^{3}He/^{4}He$ ratios revealed by fractional crushing gas extraction. *Earth and Planetary Science Letters* 196: 213–225.
Matzen AK, Baker MB, Beckett JR, and Stolper EM (2013) The temperature and pressure dependence of nickel partitioning between olivine and silicate melt. *Journal of Petrology* 54(12): 2521–2545.
McCulloch MT and Bennett VC (1993) Evolution of the early Earth: Constraints from ^{143}Nd-^{142}Nd isotopic systematics. *Lithos* 30(3–4): 237–255.
McCulloch MT and Compston W (1981) Sm-Nd age of Kambalda and Kanowna greenstones and heterogeneity in the Archaean mantle. *Nature* 294(5839): 322–327.
McKenzie D and Bickle MJ (1988) The volume and composition of melt generated by extension of the lithosphere. *Journal of Petrology* 29(3): 625–679.
Meisel T, Walker RJ, Irving AJ, and Lorand J-P (2001) Osmium isotopic compositions of mantle xenoliths: A global perspective. *Geochimica et Cosmochimica Acta* 65(8): 1311–1323.
Miller GH, Stolper EM, and Ahrens TJ (1991) The equation of state of a molten komatiite. 2. Application to komatiite petrogenesis and the Hadean mantle. *Journal of Geophysical Research* 96(B7): 11849–11864.
Moilanen M, Hanski E, Konnunaho J, Yang S-H, Törmänen T, Li C, and Zhou LM (2019) Re-Os isotope geochemistry of komatiite-hosted Ni-Cu-PGE deposits in Finland. *Ore Geology Reviews* 105: 102–122.
Mueller WU and Mortensen JK (2002) Age constraints and characteristics of subaqueous volcanic construction, the Archean Hunter Mine Group, Abitibi greenstone belt. *Precambrian Research* 115: 119–152.
Mungall JE and Naldrett AJ (2008) Ore deposits of the platinum-group elements. *Elements* 4(4): 253–258.
Murck BW and Campbell IH (1986) The effects of temperature, oxygen fugacity and melt composition on the behavior of chromium in basic and ultrabasic melts. *Geochimica et Cosmochimica Acta* 50(9): 1871–1888.
Nakanishi N, Puchtel IS, Walker RJ, and Nabelek PI (2023) Dissipation of Tungsten-182 anomalies in the Archean upper mantle: Evidence from the Black Hills, South Dakota, USA. *Chemical Geology* 617: 121255.
Naldrett AJ (2010) Secular variation of magmatic sulfide deposits and their source magmas. *Economic Geology* 105(3): 669–688.
Naldrett AJ and Turner AR (1977) The geology and petrogenesis of a greenstone belt and related nickel sulfide mineralization at Yakabindie, Western Australia. *Precambrian Research* 5(1): 43–103.
Neal CR, Mahoney JJ, Kroenke LW, Duncan RA, and Petterson MG (1997) The Ontong Java plateau. In: Mahoney JJ and Coffin M (eds.) *Large Igneous Provinces; Continental, Oceanic and Planetary Flood Volcanism. Geophysical Monograph*, Vol. 100, pp. 183–216. American Geophysical Union.
Nesbitt RW (1971) Skeletal crystal forms in the ultramafic rocks of the Yilgarn Block, Western Australia: Evidence for an Archaean ultramafic liquid. *Geological Society of Australia Special Publication* 3: 331–347.
Nesbitt RW and Sun S-S (1976) Geochemistry of Archaean spinifex-textured peridotites and magnesian and low-magnesian tholeiites. *Earth and Planetary Science Letters* 31: 433–453.
Nesbitt RW, Sun SS, and Purvis AC (1979) Komatiites: Geochemistry and genesis. *Canadian Mineralogist* 17(2): 165–186.
Nicklas RW, Puchtel IS, and Ash RD (2018) The redox evolution of the Archean mantle: Evidence from komatiites. *Geochimica et Cosmochimica Acta* 222: 447–466.
Nicklas RW, Puchtel IS, Ash RD, Piccoli PM, Hanski E, Nisbet EG, Waterton P, Pearson DG, and Anbar AD (2019) Secular mantle oxidation across the Archean-Proterozoic boundary: Evidence from V partitioning in komatiites and picrites. *Geochimica et Cosmochimica Acta* 250: 49–75.
Nisbet EG and Chinner GA (1981) Controls of the eruption of mafic and ultramafic lavas, Ruth Well nickel-copper prospect, West Pilbara. *Economic Geology* 76(6): 1729–1735.
Nisbet EG, Bickle MJ, and Martin A (1977) The mafic and ultramafic lavas of the Belingwe greenstone belt, Rhodesia. *Journal of Petrology* 18: 521–566.
Nisbet EG, Arndt NT, Bickle MJ, Cameron WE, Chauvel C, Cheadle M, Hegner E, Kyser TK, Martin A, Renner R, and Roedder E (1987) Uniquely fresh 2.7 Ga komatiites from the Belingwe greenstone belt, Zimbabwe. *Geology* 5(12): 1147–1150.
Nisbet EG, Cheadle MJ, Arndt NT, and Bickle MJ (1993) Constraining the potential temperature of the Archaean mantle: A review of the evidence from komatiites. *Lithos* 30: 291–307.
O'Neill HSC, Dingwell DB, Borisov A, Spettel B, and Palme H (1995) Experimental petrochemistry of some highly siderophile elements at high temperatures, and some implications for core formation and the mantle's early history. *Chemical Geology* 120(3–4): 255–273.
Nisbet EG and Walker D (1982) Komatiites and the structure of the Archaean mantle. *Earth and Planetary Science Letters* 60(1): 105–113.
Ohta H, Maruyama S, Takahashi E, Watannabe Y, and Kato Y (1996) Field occurrence, geochemistry and petrogenesis of the Archean Mid-Oceanic Ridge Basalts (AMORBs) of the Cleaverville area, Pilbara Craton, Western Australia. *Lithos* 37(2–3): 199–221.
Ohtani E (1984) Generation of komatiite magma and gravitational differentiation in the deep upper mantle. *Earth and Planetary Science Letters* 67(2): 261–272.
Palin R and White R (2016) Emergence of blueschists on Earth linked to secular changes in oceanic crust composition. *Nature Geoscience* 9: 60–64.
Parman SW, Dann JC, Grove TL, and de Wit MJ (1997) Emplacement conditions of komatiite magmas from the 3.49 Ga Komati Formation, Barberton greenstone belt, South Africa. *Earth and Planetary Science Letters* 150(3–4): 303–323.
Parman SW, Grove TL, and Dann JC (2001) The production of Barberton komatiites in an Archean subduction zone. *Geophysical Research Letters* 28(13): 2513–2516.
Parman SW, Grove TL, Dann JC, and de Wit MJ (2004) A subduction origin for komatiites and cratonic lithospheric mantle. *South African Journal of Geology* 107(1–2): 107–118.

Peach CL, Mathez EA, Keays RR, and Reeves SJ (1994) Experimentally determined sulfide melt-silicate melt partition coefficients for iridium and palladium. *Chemical Geology* 117(1–4): 361–377.
Perring CS, Barnes SJ, and Hill RET (1995) The physical volcanology of Archaean komatiite sequences from Forrestania, Southern Cross Province, Western Australia. *Lithos* 34(1–3): 189–208.
Polat A and Kerrich R (1999) Formation of an Archean tectonic mélange in the Schreiber-Hemlo greenstone belt, Superior Province, Canada: Implications for Archean subduction-accretion process. *Tectonics* 18(5): 733–755.
Polat A and Kerrich R (2001) Magnesian andesites, Nb-enriched basalt-andesites, and adakites from late-Archean 2.7 Ga Wawa greenstone belts, Superior Province, Canada: implications for late Archean subduction zone petrogenetic processes. *Contributions to Mineralogy and Petrology* 141(1): 36–52.
Polat A and Kerrich R (2002) Nd-isotope systematics of ~2.7 Ga adakites, magnesian andesites, and arc basalts, Superior Province: evidence for shallow crustal recycling at Archean subduction zones. *Earth and Planetary Science Letters* 202(2): 345–360.
Prendergast MD (2003) The nickeliferous Late Archean Reliance komatiitic event in the Zimbabwe craton—Magmatic architecture, physical volcanology, and ore genesis. *Economic Geology* 98(5): 865–891.
Puchtel IS (2022) Re-Os isotope and HSE abundance systematics of the 2.9 Ga komatiites and basalts from the Sumozero-Kenozero greenstone belt, SE Fennoscandian Shield: Implications for the mixing rates of the mantle. *Petrology* 30(6): 548–566.
Puchtel IS and Humayun M (2000) Platinum group elements in Kostomuksha komatiites and basalts: Implications for oceanic crust recycling and core-mantle interaction. *Geochimica et Cosmochimica Acta* 64(24): 4227–4242.
Puchtel IS and Humayun M (2001) Platinum group element fractionation in a komatiitic basalt lava lake. *Geochimica et Cosmochimica Acta* 17(65): 2979–2993.
Puchtel IS and Humayun M (2005) Highly siderophile element geochemistry of ^{187}Os-enriched 2.8-Ga Kostomuksha komatiites, Baltic Shield. *Geochimica et Cosmochimica Acta* 69(6): 1607–1618.
Puchtel IS and Zhuravlev DZ (1993) Petrology of mafic-ultramafic metavolcanics and related rocks from the Olondo greenstone belt, Aldan Shield. *Petrology* 1(3): 263–299.
Puchtel IS, Hofmann AW, Mezger K, Shchipansky AA, Kulikov VS, and Kulikova VV (1996) Petrology of a 2.41 Ga remarkably fresh komatiitic basalt lava lake in Lion Hills, Central Vetreny Belt, Baltic Shield. *Contributions to Mineralogy and Petrology* 124: 273–290.
Puchtel IS, Haase KM, Hofmann AW, Chauvel C, Kulikov VS, Garbe-Schönberg C-D, and Nemchin AA (1997) Petrology and geochemistry of crustally contaminated komatiitic basalts from the Vetreny Belt, southeastern Baltic Shield: Evidence for an early Proterozoic mantle plume beneath rifted Archean continental lithosphere. *Geochimica et Cosmochimica Acta* 61(6): 1205–1222.
Puchtel IS, Hofmann AW, Mezger K, Jochum KP, Shchipansky AA, and Samsonov AV (1998a) Oceanic plateau model for continental crustal growth in the Archaean: A case study from the Kostomuksha greenstone belt, NW Baltic Shield. *Earth and Planetary Science Letters* 155(1–2): 57–74.
Puchtel IS, Arndt NT, Hofmann AW, Haase KM, Kröner A, Kulikov VS, Kulikova VV, Garbe-Schönberg C-D, and Nemchin AA (1998b) Petrology of mafic lavas within the Onega plateau, central Karelia: Evidence for 2.0 Ga plume-related continental crustal growth in the Baltic Shield. *Contributions to Mineralogy and Petrology* 130(2): 134–153.
Puchtel IS, Hofmann AW, Amelin YV, Garbe-Schönberg C-D, Samsonov AV, and Shchipansky AA (1999) Combined mantle plume—Island arc model for the formation of the 2.9 Ga Sumozero-Kenozero greenstone belt, SE Baltic Shield: Isotope and trace element constraints. *Geochimica et Cosmochimica Acta* 63(21): 3579–3595.
Puchtel IS, Brügmann GE, Hofmann AW, Kulikov VS, and Kulikova VV (2001) Os isotope systematics of komatiitic basalts from the Vetreny belt, Baltic Shield: Evidence for a chondritic source of a 2.45 Ga plume. *Contributions to Mineralogy and Petrology* 140: 588–599.
Puchtel IS, Brandon AD, and Humayun M (2004a) Precise Pt-Re-Os isotope systematics of the mantle from 2.7-Ga komatiites. *Earth and Planetary Science Letters* 224(1–2): 157–174.
Puchtel IS, Humayun M, Campbell A, Sproule R, and Lesher CM (2004b) Platinum group element geochemistry of komatiites from the Alexo and Pyke Hill areas, Ontario, Canada. *Geochimica et Cosmochimica Acta* 68(6): 1361–1383.
Puchtel IS, Brandon AD, Humayun M, and Walker RJ (2005) Evidence for the early differentiation of the core from Pt-Re-Os isotope systematics of 2.8-Ga komatiites. *Earth and Planetary Science Letters* 237(1–2): 118–134.
Puchtel IS, Walker RJ, Brandon AD, and Nisbet EG (2009a) Pt-Re-Os and Sm-Nd isotope and HSE and REE systematics of the 2.7 Ga Belingwe and Abitibi komatiites. *Geochimica et Cosmochimica Acta* 73(20): 6367–6389.
Puchtel IS, Walker RJ, Anhaeusser CR, and Gruau G (2009b) Re-Os isotope systematics and HSE abundances of the 3.5 Ga Schapenburg komatiites, South Africa: Hydrous melting or prolonged survival of primordial heterogeneities in the mantle? *Chemical Geology* 262(3–4): 355–369.
Puchtel IS, Blichert-Toft J, Touboul M, Walker RJ, Byerly G, Nisbet EG, and Anhaeusser CR (2013) Insights into early Earth from Barberton komatiites: Evidence from lithophile isotope and trace element systematics. *Geochimica et Cosmochimica Acta* 108: 63–90.
Puchtel IS, Walker RJ, Touboul M, Nisbet EG, and Byerly GR (2014) Insights into early Earth from the Pt-Re-Os isotope and highly siderophile element abundance systematics of Barberton komatiites. *Geochimica et Cosmochimica Acta* 125: 394–413.
Puchtel IS, Blichert-Toft J, Touboul M, Horan MF, and Walker RJ (2016a) The coupled ^{182}W-^{142}Nd record of early terrestrial mantle differentiation. *Geochemistry, Geophysics, Geosystems* 17(6): 2168–2193.
Puchtel IS, Touboul M, Blichert-Toft J, Walker RJ, Brandon AD, Nicklas RW, Kulikov VS, and Samsonov AV (2016b) Lithophile and siderophile element systematics of the mantle at the Archean-Proterozoic boundary: Evidence from 2.4 Ga komatiites. *Geochimica et Cosmochimica Acta* 180: 227–255.
Puchtel IS, Blichert-Toft J, Touboul M, and Walker RJ (2018) ^{182}W and HSE constraints from 2.7 Ga komatiites on the heterogeneous nature of the Archean mantle. *Geochimica et Cosmochimica Acta* 228: 1–26.
Puchtel IS, Mundl-Petermeier A, Horan M, Hanski EJ, Blichert-Toft J, and Walker RJ (2020) Ultra-depleted 2.05 Ga komatiites of Finnish Lapland: Products of grainy late accretion or core-mantle interaction? *Chemical Geology* 554: 119801.
Puchtel IS, Nicklas RW, Slagle J, Horan M, Walker RJ, Nisbet EG, and Locmelis M (2022a) Early global mantle chemical and isotope heterogeneity revealed by the komatiite-basalt record: The Western Australia connection. *Geochimica et Cosmochimica Acta* 320: 238–278.
Puchtel IS, Blichert-Toft J, Horan M, Touboul M, and Walker RJ (2022b) The komatiite testimony to ancient mantle heterogeneity. *Chemical Geology* 594: 120776. Invited Review Article.
Pyke DR, Naldrett AJ, and Eckstrand OR (1973) Archean ultramafic flows in Munro Township, Ontario. *Geological Society of America Bulletin* 84: 955–978.
Rehkämper M, Halliday AN, Fitton JG, Lee D-C, Wieneke M, and Arndt NT (1999) Ir, Ru, Pt and Pd in basalts and komatiites: New constraints for the geochemical behavior of the platinum group elements in the mantle. *Geochimica et Cosmochimica Acta* 63(22): 3915–3934.
Renner R, Nisbet EG, Cheadle MJ, Arndt NT, Bickle MJ, and Cameron WE (1994) Komatiite flows from the Reliance Formation, Belingwe Belt, Zimbabwe: I. Petrography and mineralogy. *Journal of Petrology* 35(2): 361–400.
Révillon S, Arndt NT, Chauvel C, and Hallot E (2000) Geochemical study of ultramafic volcanic and plutonic rocks from Gorgona Island, Colombia: The plumbing system of an oceanic plateau. *Journal of Petrology* 41(1): 1127–1153.
Révillon S, Chauvel C, Arndt NT, Pik R, Martineau F, Fourcade S, and Marty B (2002) Heterogeneity of the Caribbean plateau mantle source: Sr, O and He isotopic compositions of olivine and clinopyroxene from Gorgona Island. *Earth and Planetary Science Letters* 205(1): 95–106.
Richard D, Marty B, Chaussidon M, and Arndt NT (1996) Helium isotopic evidence for a lower mantle component in depleted Archean komatiite. *Science* 273(5271): 93–95.
Richards MA, Jones DL, Duncan RA, and DePaolo DJ (1991) A mantle plume initiation model for the Wrangellia flood basalt and other oceanic plateaus. *Science* 254(5029): 263–265.
Richter FM (1985) Models for the Archean thermal regime. *Earth and Planetary Science Letters* 73(2–4): 350–360.
Richter FM (1988) A major change in the thermal state of the Earth at the Archean-Proterozoic boundary: Consequences for the nature and preservation of continental lithosphere. *Journal of Petrology*: 39–52. Special Lithosphere Issue.

Righter K and Drake MJ (1997) Metal-silicate equilibrium in a homogeneously accreting earth: New results for Re. *Earth and Planetary Science Letters* 146(3–4): 541–553.
Rizo H, Boyet M, Blichert-Toft J, and Rosing M (2011) Combined Nd and Hf isotope evidence for deep-seated source of Isua lavas. *Earth and Planetary Science Letters* 312(3–4): 267–279.
Robin-Popieul C, Arndt NT, Chauvel C, Byerly G, Sobolev AV, and Wilson A (2012) A new model for Barberton komatiites: Deep critical melting with high melt retention. *Journal of Petrology* 53: 2191–2229.
Rosas JC and Korenaga J (2021) Archaean seafloors shallowed with age due to radiogenic heating in the mantle. *Nature Geoscience* 14(1): 51–56.
Rosengren NM, Beresford SW, Grguric BA, and Cas RAF (2005) An intrusive origin for the komatiitic dunite-hosted Mount Keith disseminated nickel sulfide deposit, Western Australia. *Economic Geology* 100(1): 149–156.
Rosing MT (1990) The theoretical effect of metasomatism on Sm-Nd isotopic systems. *Geochimica et Cosmochimica Acta* 54(5): 1337–1341.
Rudnick RL and Gao S (2014) Composition of the continental crust. *Treatise on Geochemistry*: 1–51.
Rudnick RL, Barth M, Horn I, and McDonough WF (2000) Rutile-bearing refractory eclogites: Missing link between continents and depleted mantle. *Science* 287(5451): 278–281.
Sakamaki T, Ohtani E, Urakawa S, Suzuki A, and Katayama Y (2010) Density of dry peridotite magma at high pressure using an X-ray absorption method. *American Mineralogist* 95: 144–147.
Saunders AD, Tarney J, Kerr AC, and Kent RW (1996) The formation and fate of large oceanic igneous provinces. *Lithos* 37: 81–95.
Savage PS, Moynier F, Chen H, Shofner G, Siebert J, Badro J, and Puchtel IS (2015) Isotopic evidence for large-scale sulfide fractionation during Earth's differentiation. *Geochemical Perspectives Letters* 1: 53–64.
Saverikko M (1985) The pyroclastic komatiite complex at Sattasvaara in northern Finland. *Bulletin of the Geological Society of Finland* 57(1–2): 55–87.
Schaefer SJ and Morton P (1991) Two komatiitic pyroclastic units, Superior Province, northwestern Ontario: Their geology, petrography, and correlation. *Canadian Journal of Earth Sciences* 28(9): 1455–1470.
Schmeling H and Arndt NT (2017) Modelling komatiitic melt accumulation and segregation in the transition zone. *Earth and Planetary Science Letters* 472: 95–106.
Sharma M, Papanastassiou DA, Wasserburg GJ, and Dymek RF (1996) The issue of the terrestrial record of ^{146}Sm. *Geochimica et Cosmochimica Acta* 60(11): 2037–2047.
Shejwalkar A and Coogan LA (2013) Experimental calibration of the roles of temperature and composition in the Ca-in-olivine geothermometer at 0.1 MPa. *Lithos* 177: 54–60.
Shimizu K, Komiya T, Hirose K, Shimizu N, and Maruyama S (2001) Cr-spinel, an excellent micro-container for retaining primitive melts—Implications for a hydrous plume origin for komatiites. *Earth and Planetary Science Letters* 189: 177–188.
Shimizu K, Nakamura E, Kobayashi K, and Maruyama S (2004) Discovery of Archean continental and mantle fragments inferred from xenocrysts in komatiites, the Belingwe greenstone belt, Zimbabwe. *Geology* 32(4): 285–288.
Shirey SB and Hanson GN (1986) Mantle heterogeneity and crustal recycling in Archean granite-greenstone belts: Evidence from Nd isotopes and trace elements in the Rainy Lake area, Superior Province, Ontario, Canada. *Geochimica et Cosmochimica Acta* 50(12): 2631–2651.
Shore M and Fowler D (1999) The origin of spinifex texture in komatiites. *Nature* 397(6721): 691–694.
Siégel C, Arndt NT, Barnes S, Henriot A-L, Haenecour P, Debaille V, and Mattielli N (2014) Fred's Flow (Canada) and Murphy Well (Australia): Thick komatiitic lava flows with contrasting compositions, emplacement mechanisms, and water contents. *Contributions to Mineralogy and Petrology* 168(6): 1–17.
Sleep NH and Windley BF (1982) Archean plate tectonics: Constraints and inferences. *Journal of Geology* 90(4): 363–379.
Smith HS and Erlank AJ (1982) Geochemistry and petrogenesis of komatiites from the Barberton greenstone belt, South Africa. In: Arndt NT and Nisbet EG (eds.) *Komatiites*, pp. 347–398. London: George Allen and Unwin.
Smith AD and Ludden JN (1989) Nd isotopic evolution of the Precambrian mantle. *Earth and Planetary Science Letters* 93(1): 14–22.
Smith HS, Erlank AJ, and Duncan AR (1980) Geochemistry of some ultramafic komatiite lava flows from the Barberton Mountain Land. *South Africa. Precambrian Research* 11(3–4): 399–415.
Smith HS, O'Neil JR, and Erlank AJ (1984) Oxygen isotope compositions of minerals and rocks and chemical alteration patterns in pillow lavas from the Barberton greenstone belt, South Africa. In: Kröner A, Hanson GN, and Goodwin AM (eds.) *Archaean Geochemistry*, pp. 115–138. Berlin: Springer-Verlag.
Smithies RH, Champion DC, Van Kranendonk MJ, and Hickman AH (2007) Geochemistry of volcanic rocks of the northern Pilbara Craton, Western Australia. *Geological Survey of Western Australia*. Report 104. Perth, 47 pp.
Sobolev AV, Asafov EV, Gurenko AA, Arndt NT, Batanova VG, Portnyagin MV, Garbe-Schönberg D, and Krasheninnikov SP (2016) Komatiites reveal a hydrous Archaean deep-mantle reservoir. *Nature* 531(7596): 628–632.
Sobolev AV, Asafov EV, Gurenko AA, Arndt NT, Batanova VG, Portnyagin MV, Garbe-Schönberg D, Wilson AH, and Byerly GR (2019) Deep hydrous mantle reservoir provides evidence for crustal recycling before 3.3 billion years ago. *Nature* 571(7766): 555–559.
Sossi PA and O'Neill HSC (2016) Liquidus temperatures of komatiites and the effect of cooling rate on element partitioning between olivine and komatiitic melt. *Contributions to Mineralogy and Petrology* 171(5): 49–74.
Sossi PA, Eggins SM, Nesbitt RW, Nebel O, Hergt JM, Campbell IH, O'Neill HSC, Van Kranendonk M, and Davies DR (2016) Petrogenesis and geochemistry of Archean komatiites. *Journal of Petrology* 57(1): 147–184.
Sossi P, Nebel O, O'Neill HSC, and Moynier F (2018) Zinc isotope composition of the Earth and its behaviour during planetary accretion. *Chemical Geology* 477: 73–84.
Sproule RA, Lesher CM, Ayer JA, Thurston PC, and Herzberg CT (2002) Spatial and temporal variations in the geochemistry of komatiites and komatiitic basalts in the Abitibi greenstone belt. *Precambrian Research* 115(1–4): 153–186.
Stepanova AV, Samsonov AV, Salnikova EB, Puchtel IS, Larionova YO, Larionov AN, Stepanov VS, Shapovalov YB, and Egorova SV (2014) Palaeoproterozoic Continental MORB-type Tholeiites in the Karelian Craton: Petrology, Geochronology, and Tectonic Setting. *Journal of Petrology* 55(9): 1719–1751.
Stepanova AV, Salnikova EB, Samsonov AV, Egorova SV, Larionova YO, and Stepanov VS (2015) The 2.31 Ga mafic dykes in the Karelian Craton, eastern Fennoscandian shield: U-Pb age, source characteristics and implications for continental break-up processes. *Precambrian Research* 259: 43–57.
Stiegler MT, Cooper M, Byerly GR, and Lowe DR (2012) Geochemistry and petrology of komatiites of the Pioneer Ultramafic Complex of the 3.3 Ga Weltevreden Formation, Barberton greenstone belt, South Africa. *Precambrian Geology* 212: 1–12.
Stone WE, Jensen LS, and Church WR (1987) Petrography and geochemistry of an unusual Fe-rich basaltic komatiite from Boston Township, Northeastern Ontario. *Canadian Journal of Earth Sciences* 24(12): 2537–2550.
Storey M, Mahoney JJ, Kroenke LW, and Saunders AD (1991) Are oceanic plateaus sites of komatiite formation? *Geology* 19(4): 376–379.
Sumino H, Shimizu K, and Komiya T (2023) Noble gas isotope and halogen analyses of Cr-spinels within beach sand from Gorgona Island to constrain the origin of volatiles in the youngest komatiite magmatism on the Earth. In: *V. M. Goldschmidt Conference, Lyon, France*.
Sun S-S (1984) Geochemical characteristics of Archean ultramafic and mafic volcanic rocks: Implications for mantle composition and evolution. In: Kröner A, Hanson GM, and Googwin AM (eds.) *Archaean Geochemistry*, pp. 25–47. Berlin: Springer-Verlag.
Sun S-S and Nesbitt RW (1978) Petrogenesis of Archean ultrabasic and basic volcanics: Evidence from the rare earth elements. *Contributions to Mineralogy and Petrology* 65: 301–325.
Sun S-S, Nesbitt RW, and McCulloch T (1989) Geochemistry and petrogenesis of Archean and early Proterozoic siliceous high-magnesian basalts. In: Crawford AJ (ed.) *Boninites and Related Rocks*, pp. 148–173. London: George Allen and Unwin.
Suzuki A and Ohtani E (2003) Density of peridotite melts at high pressure. *Physics and Chemistry of Minerals* 30(8): 449–456.
Sylvester PJ, Campbell IH, and Bowyer DA (1997) Nb/U evidence for early formation of the continental crust. *Science* 275(5299): 521–523.
Takahashi E (1990) Speculations on the Archean mantle: Missing link between komatiite and depleted garnet peridotite. *Journal of Geophysical Research* 95(B10): 15941–15954.
Thompson PME, Kempton PD, White RV, Kerr AC, Tarney J, Saunders AD, Fitton JG, and McBirney A (2003) Hf-Nd isotope constraints on the origin of the Cretaceous Caribbean plateau and its relationship to the Galapagos plume. *Earth and Planetary Science Letters* 217(1–2): 59–75.

Thurston PC, Ayres LD, Edwards GR, Gelinas L, Ludden JN, and Verpaelst P (1985) Archean bimodal volcanism. *Geological Association of Canada Special Paper* 28: 7–21.
Thurston PC, Ayer JA, Goutier J, and Hamilton MA (2008) Depositional gaps in abitibi greenstone belt stratigraphy: A key to exploration for syngenetic mineralization. *Economic Geology* 103: 1097–1134.
Tian S, Moynier F, Inglis EC, Creech JB, Bizzarro M, Siebert J, Day JMD, and Puchtel IS (2020) Zirconium isotopic composition of the mantle through time. *Geochemical Perspectives Letters* 15: 40–43.
Touboul M, Puchtel IS, and Walker RJ (2012) ^{182}W Evidence for long-term preservation of early mantle differentiation products. *Science* 335: 1065–1069.
Tourpin S, Gruau G, Blais S, and Fourcade S (1991) Resetting of REE, and Nd and Sr isotopes during carbonatization of a komatiite flow from Finland. *Chemical Geology* 90(1–2): 15–29.
Trela J, Gazel E, Sobolev AV, Moore L, Bizimis M, Jicha B, and Batanova VG (2017) The hottest lavas of the Phanerozoic and the survival of deep Archaean reservoirs. *Nature Geoscience* 10: 451–456.
Turner JS, Huppert HE, and Sparks RSJ (1986) Komatiites II: Experimental and theoretical investigations of post-emplacement cooling and crystallization. *Journal of Petrology* 27: 397–437.
Tusch J, Münker C, Hasenstab E, Jansen M, Marien CS, Kurzweil F, Van Kranendonk MJ, Smithies H, Maier W, and Garbe-Schönberg D (2021) Convective isolation of Hadean mantle reservoirs through Archean time. *Proceedings of the National Academy of Sciences of the United States of America* 118(2): e2012626118.
Tusch J, Hoffmann JE, Hasenstab E, Fischer-Gödde M, Marien CS, Wilson AH, and Münker C (2022) Long-term preservation of Hadean protocrust in Earth's mantle. *Proceedings of the National Academy of Sciences of the United States of America* 119(18): e2120241119.
Tympel JF, Hergt JM, Maas R, Woodhead JD, Greig A, Bolhar R, and Powell R (2021) Mantle-like Hf-Nd isotope signatures in ~3.5 Ga greenstones: No evidence for Hadean crust beneath the East Pilbara Craton. *Chemical Geology* 576: 120273.
Vervoort JD and Blichert-Toft J (1999) Evolution of the depleted mantle: Hf isotope evidence from juvenile rocks through time. *Geochimica et Cosmochimica Acta* 63(3–4): 533–556.
Vervoort JD, White WM, and Thorp RI (1994) Nd and Pb isotope ratios of the Abitibi greenstone belt: New evidence for very early differentiation of the Earth. *Earth and Planetary Science Letters* 128(3–4): 215–229.
Viljoen MJ and Viljoen RP (1969) The geology and geochemistry of the Lower Ultramafic Unit of the Onverwacht Group and a proposed new class of igneous rocks. *Geological Society of South Africa Special Publication* 2: 55–86.
Viljoen M, Viljoen R, Smith HS, and Erlank AJ (1983) Geological, textural and geochemical features of komatiitic flows from the Komati formation. In: Anhaeusser CR (ed.) *Contributions to the Geology of the Barberton Mountain Land. Geological Survey of South Africa*, pp. 1–20.
Wagner LJ, Kleinhanns IC, Weber N, Babechuk MG, Hofmann A, and Schoenberg R (2021) Coupled stable chromium and iron isotopic fractionation tracing magmatic mineral crystallization in Archean komatiite-tholeiite suites. *Chemical Geology* 576: 120121.
Walker RJ, Mundl-Petermeier A, Puchtel IS, Nicklas RW, Hellmann JL, Echeverría LM, Ludwig KD, Bermingham KR, Gazel E, Devitre CL, Jackson MG, and Chauvel C (2023) ^{182}W and ^{187}Os constraints on the origin of siderophile isotopic heterogeneity in the mantle. *Geochimica et Cosmochimica Acta* 363: 15–39.
Walker RJ, Shirey SB, and Stecher O (1988) Comparative Re-Os, Sm-Nd and Rb-Sr isotope and trace element systematics for Archean komatiite flows from Munro Township, Abitibi belt, Ontario. *Earth and Planetary Science Letters* 87(1–2): 1–12.
Walker RJ, Echeverria LM, Shirey SB, and Horan MF (1991) Re-Os isotopic constraints on the origin of volcanic rocks, Gorgona Island, Colombia: Os-isotopic evidence for ancient heterogeneities in the mantle. *Contributions to Mineralogy and Petrology* 107(2): 150–162.
Walker RJ, Storey M, Kerr AC, Tarney J, and Arndt NT (1999) Implications of ^{187}Os isotopic heterogeneities in a mantle plume: Evidence from Gorgona Island and Curaçao. *Geochimica et Cosmochimica Acta* 63(5): 713–728.
Walker RJ, Horan MF, Morgan JW, Becker H, Grossman JN, and Rubin AE (2002) Comparative ^{187}Re-^{187}Os systematics of chondrites: Implications regarding early solar system processes. *Geochimica et Cosmochimica Acta* 66(23): 4187–4201.
Walter MJ (1998) Melting of garnet peridotite and the origin of komatiite and depleted lithosphere. *Journal of Petrology* 39(1): 29–60.
Wang H, Wilson A, Yang J, Li Q, Tang G, Feng L, and Jia L (2023) No ^{18}O-depleted mantle source for Archean komatiite. *Science Bulletin* 68(1): 53–55.
Waterton P and Arndt NT (2023) Komatiites: Their geochemistry and origins. In: Homann M (ed.) *The Archaean Earth: Tempos and Events (2nd Edition of The Precambrian Earth)*. Elsevier.
Waterton P, Pearson DG, Kjarsgaard B, Hulbert L, Locock A, Parman S, and Davis B (2017) Age, origin, and thermal evolution of the ultra-fresh ~1.9 Ga Winnipegosis komatiites, Manitoba, Canada. *Lithos* 268-271: 114–130.
Waterton P, Pearson DG, Mertzman SA, Mertzman KR, and Kjarsgaard BA (2020) A fractional crystallisation link between komatiites, basalts, and dunites of the Palaeoproterozoic Winnipegosis Komatiite Belt, Manitoba, Canada. *Journal of Petrology* 61(5): egaa052.
Wells G, Bryan WB, and Pearce TH (1979) Comparative morphology of ancient and modern pillow lavas. *Journal of Geology* 87(4): 427–440.
Wilson AH (2019) The late-Paleoarchean ultra-depleted Commondale komatiites: Earth's hottest lavas and consequences for eruption. *Journal of Petrology* 60: 1575–1620.
Wilson AH and Bolhar R (2022) Olivine in komatiite records origin and travel from the deep upper mantle. *Geology* 50(3): 351–355.
Wilson AH and Carlson RW (1989) A Sm-Nd and Pb isotope study of Archaean greenstone belts in the southern Kaapvaal Craton, South Africa. *Earth and Planetary Science Letters* 96(1–2): 89–105.
Wilson AH, Shirey SB, and Carlson RW (2003) Archaean ultra-depleted komatiites formed by hydrous melting of cratonic mantle. *Nature* 423: 858–860.
Wyman DA, Bleeker W, and Kerrich R (1998) A 2.7 Ga komatiite, low/Ti tholeiite, arc tholeiite transition, and inferred proto-arc geodynamic setting of the Kidd Creek deposit: Evidence from precise trace element data. *Economic Geology Monographs* 10. 511 pp.
Wyman DA, Kerrich R, and Polat A (2002) Assembly of Archean cratonic mantle lithosphere and crust: Plume-arc interaction in the Abitibi-Wawa subduction-accretion complex. *Precambrian Research* 115: 37–62.
Xie Q, Kerrich R, and Fan J (1993) HFSE/REE fractionations recorded in three komatiite-basalt sequences, Archean Abitibi greenstone belt: Implications for multiple plume sources and depths. *Geochimica et Cosmochimica Acta* 57: 4111–4118.
Zakharov DO and Bindeman IN (2019) Triple oxygen and hydrogen isotopic study of hydrothermally altered rocks from the 2.43–2.41 Ga Vetreny belt, Russia: An insight into the early Paleoproterozoic seawater. *Geochimica et Cosmochimica Acta* 248: 185–209.
Zhuravlev DZ, Puchtel IS, Samsonov AV, and Simon AK (1987) Sm-Nd and Rb-Sr age of metavolcanics from the Sura greenstone belt (Middle Cis-Dneeper region). *Transactions of the USSR Academy of Sciences* 295(3): 703–707.
Zhuravlev DZ, Puchtel IS, and Samsonov AV (1989) Sm-Nd age and geochemistry of metavolcanics from the Olondo greenstone belt, Aldan Shield. *International Geology Review* 2: 39–49.
Zindler A (1982) Nd and Sr isotopic studies of komatiites and related rocks. In: Arndt NT and Nisbet EG (eds.) *Komatiites*, pp. 399–420. London: George Allen and Unwin.